State of Oregon
Oregon Department of Geology and Mineral Industries
Brad Avy, State Geologist

OPEN-FILE REPORT O-20-08

COOS BAY TSUNAMI MODELING: TOWARD IMPROVED MARITIME PLANNING RESPONSE

by Jonathan C. Allan[1], Joseph Zhang[2], Fletcher E. O'Brien[3], and Laura L. S. Gabel[1]

2020

[1]Oregon Department of Geology and Mineral Industries, Coastal Field Office, P.O. Box 1033, Newport, OR 97365
[2]Virginia Institute of Marine Science, College of William & Mary, Center for Coastal Resource Management, 1375 Greate Road, Gloucester Point, VA 23062
[3]Oregon Department of Geology and Mineral Industries, 800 NE Oregon Street, Suite 965, Portland, OR 97232

DISCLAIMER

This product is for informational purposes and may not have been prepared for or be suitable for legal, engineering, or surveying purposes. Users of this information should review or consult the primary data and information sources to ascertain the usability of the information. This publication cannot substitute for site-specific investigations by qualified practitioners. Site-specific data may give results that differ from the results shown in the publication.

WHAT'S IN THIS REPORT?

This study evaluates new tsunami modeling results completed for both distant and local tsunamis for the Coos estuary. The goal is to examine the interaction of tsunamis with fluctuating (dynamic) tides (as opposed to modeling using a fixed tidal elevation such as mean higher high water), different riverine flow regimes, and friction to provide an improved understanding of tsunami effects at Coos Bay. These data are then used to develop maritime tsunami guidance to assist ships, commercial and recreational vessels operating offshore the mouth of Coos Bay and within the estuary.

Cover photo: View looking south over the Southwest Oregon Regional Airport, Coos Bay estuary, and navigation channel. Photo taken by J. Allan, August 2011.

Oregon Department of Geology and Mineral Industries Open File Report O-20-08
Published in conformance with ORS 516.030

DOGAMI Administrative Offices
800 NE Oregon Street, Suite 965
Portland, OR 97232
Telephone (971) 673-1555
https://www.oregongeology.org/
https://www.oregon.gov/DOGAMI/

TABLE OF CONTENTS

LIST OF FIGURES

LIST OF TABLES

EXECUTIVE SUMMARY

Recent tsunamis affecting the West Coast of the United States have resulted in significant damage to ports and harbors as well as to recreational and commercial vessels attempting to escape the tsunami. Although local tsunamis will strike the coast within minutes after the start of earthquake shaking, providing little response time to evacuate, distant tsunamis are expected to arrive some 4 to 12 hours after the event, providing more time to respond. This study evaluates new tsunami modeling results completed for both distant and local tsunamis for the Coos estuary. The goal is to examine the interaction of tsunamis with dynamic tides (as opposed to modeling using a fixed tidal elevation such as mean higher high water), different riverine flow regimes, and friction to provide an improved understanding of tsunami effects on maritime traffic operating offshore the mouth of Coos Bay (MCB) and within the estuary. This was accomplished by evaluating a suite of tsunami simulations (19 in total) for Coos Bay focused on two distant earthquake scenarios: the 1964 Anchorage, Alaska (AK64) earthquake and a maximum considered eastern Aleutian Island (AKMax) earthquake, and two local Cascadia subduction zone (CSZ) scenarios: Large1 (L1) and Extra-extra-large1 (XXL1).

Our modeling indicates that for a maximum considered eastern Aleutian Island (AKMax) earthquake, the tsunami would arrive at the MCB ~4 hours after the start of the earthquake. From the mouth of Coos Bay the tsunami takes an additional 13 minutes to reach its maxima inundating the community of Barview; 15 minutes to reach Empire; 27 minutes to reach Jordon Point; and ~41 minutes to reach the town of Coos Bay; total travel time to the town of Coos Bay is 4 hours 41 minutes. The largest tsunami waves are concentrated at the MCB, where the AKMax tsunami reaches ~5.6 m (19 ft) in height. Maximum water levels remain high for much of the channel before decreasing substantially upriver of Jordon Point, where the tsunami waves expand out into the broader upper Coos estuary, and where bathymetric shallowing effectively disburses much of the energy. Strongest currents are observed at the MCB, while large parts of the estuary would be affected by currents >2.0 m/s [>4 knots], which are capable of causing significant damage to facilities located adjacent to the ports and harbors as well as to any vessels that may be moored.

For a maximum considered distant tsunami, we recommend that ***vessels seaward of the MCB proceed to a staging area greater than 46 m (25 fathoms/150 ft) (located ~2.5 nautical miles northwest of the mouth of Coos Bay [2.4 nautical miles north of the Cape Arago lighthouse]).*** Dangerous currents > 2.6 m/s [5 knots] are expected to occur at depths shallower than 27 m (15 fathoms/90 ft). Offshore maritime evacuation may be feasible for some vessels operating out of Charleston harbor, or in the navigation channel downstream of Jordon Point. Seaward evacuation for vessels in the upper Coos estuary is not advised because those vessels might be transiting the mouth at the time when a tsunami arrives.

For a maximum considered locally generated CSZ tsunami, we find that the tsunami reaches the MCB in as little as 7 minutes and takes an additional 18 minutes to reach Jordon Point; the XXL1 local tsunami arrives at the town of Coos Bay ~39 minutes after the start of earthquake shaking. Maximum water levels exceeding 17 m (56 ft) will be observed at the MCB, decreasing to 10 to 13 m (~33 to 43 ft) in the navigation channel downriver of Jordon Point. Extreme currents exceeding 6 m/s [12 knots] will be observed across the entire estuary. Damage is expected to be devastating for ports and harbors in the lower estuary.

Due to the speed at which a CSZ tsunami reaches the MCB, ***there is insufficient time for mariners in ports to respond to this event other than to evacuate by foot to high ground***. Vessels operating on the ocean west of the MCB should immediately evacuate toward deeper water. ***We recommend a Coos Bay maritime evacuation zone for a local tsunami hazard zone beginning at ~128 m depth (70 fathoms)***

and extending westward to depths > 274 m (150 fathoms). Mariners should prepare to remain offshore for potentially days as the MCB is unlikely to be navigable following a CSZ tsunami. As a result, plans to evacuate to potentially safe ports located south of Cape Mendocino on the California coast should be developed. For vessels in the Coos estuary, the only course of action is to head vessels toward the nearest point of high ground and evacuate uphill out of the tsunami inundation zone.

1.0 INTRODUCTION

The objective of this study is to evaluate new modeling results completed for both distant and local tsunamis at Coos Bay, Coos County, Oregon (**Figure 1**). The goal here is to provide an improved understanding of tsunamis and their effect on maritime traffic operating offshore the mouth of Coos Bay, within the estuary, and upriver toward the Port of Coos Bay (**Figure 1**).

Figure 1. Location map of the Coos Bay system showing key place names, model domain (map view), and Charleston tide gauge station. Note: gray shaded region defines the XXL1 (local) tsunami inundation zone.

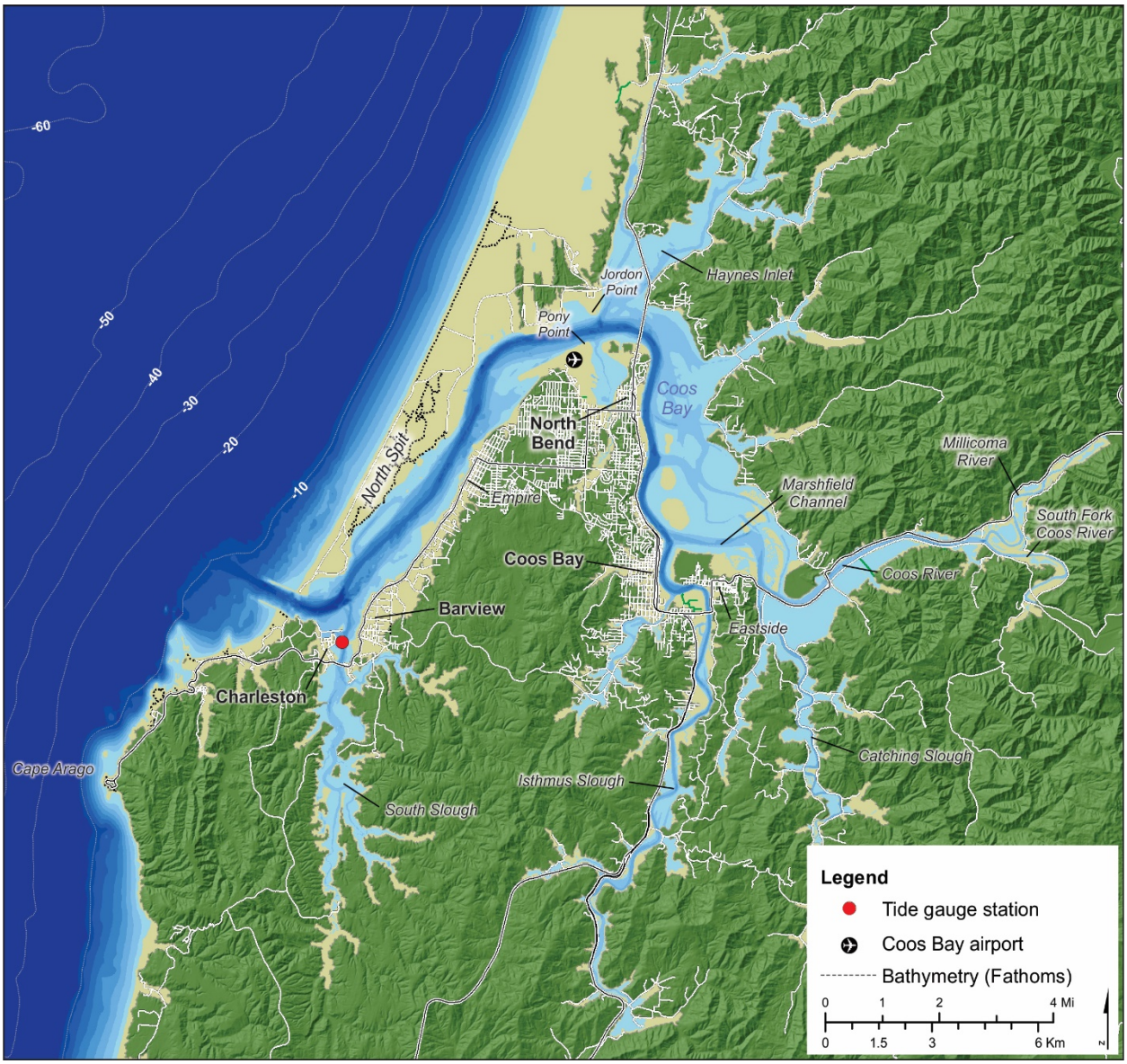

The coast of Oregon and its many estuaries are exposed to significant risk from tsunamis generated locally due to great (~ Mw 8-9) earthquakes on the Cascadia subduction zone (CSZ) (Atwater and others, 1995; Satake and others, 2003; Witter and others, 2003; Atwater and others, 2005; Nelson and others, 2006; Priest and others, 2009; Witter and others, 2012), as well as from distant tsunamis generated elsewhere in the Pacific basin (Allan and others, 2018). Local tsunamis generated on the CSZ are estimated to occur on the order of 220 to 350 years (Goldfinger and others, 2017). Conversely, similar magnitude events from distant sources have historically had only a modest impact on the Oregon coast but occur much more frequently than local tsunamis (Lander and others, 1993; Priest and others, 2009). Although local tsunamis will strike the coast within minutes after the start of earthquake shaking, providing little response time to evacuate, distant tsunamis are expected to arrive some 4 to 12 hours after the event, providing more time to respond. These differences are important not just for land-based tsunami evacuation but also for maritime evacuation for vessels operating offshore the coast and potentially within ports and harbors.

Coos Bay is the second largest estuary (after the Columbia River estuary) on the Oregon coast and is regarded as the best natural harbor between San Francisco Bay and Puget Sound[1]. The estuary is a drowned river valley, formed from sea-level rise during the last 10,000 years (Hickey and Banas, 2003). The entrance to the estuary is flanked by jetties, and in the estuary the dredged main channel connects to multiple shallower tributaries before terminating in Isthmus Slough (**Figure 1**). The navigation channel is ~20 m (65 ft) deep at the mouth and decreases to ~13–15 m (42–49 ft) in the channel. From its mouth, the river extends some 20 km (12.5 mi) upriver to the town of Coos Bay; distance from the mouth to the end of Isthmus Slough (**Figure 1**) is ~ 39 km (24.3 mi), while the mouth to the upper Coos River is ~38 km (23.6 mi) in length. The estuary is mesotidal (mean tidal range of ~1.7 m) and experiences highly variable seasonal river flows with typical discharge events of 50–500 m^3/s and background winter flows of 10–50 m^3/s; summer flows are on the order of ~1-2 m^3/s (Conroy and others, 2020). The wet surface area of the estuary at mean sea level is around 34 km^2 (Hyde, 2007) and is tidally influenced some 12–15 km up the estuary (Hickey and Banas, 2003). The estuary may be broadly divided into two zones:

- A wave- and current-dominated entrance that includes portions of Charleston and Barview (**Figure 1**); and,
- The estuary, which extends upriver beyond about Eastside (located just east of Coos Bay, **Figure 1**).

The estuary experiences significant maritime traffic to and from the Pacific Ocean and the Charleston Marina and farther upriver to the Port of Coos Bay (**Figure 1**). The bulk of the traffic between Charleston and the Pacific Ocean is commercial and recreational fishing boats, while the Port of Coos Bay is the largest forest products shipper in the world; fishing and timber are the foundation of the economy of Coos County[2]. According to the Port of Coos Bay[3], more than 1.5 million tons of cargo cross the bar annually, making the Coos Bay harbor the busiest seaport in Oregon. Furthermore, forecasts suggest that the number of vessels traversing the estuary could increase in the next decade in response to plans to develop a new LNG terminal on the North Spit as well as future plans to build an international container terminal. Coincident with an increase in maritime traffic would be an increase in supporting infrastructure needed to service these vessels, along with enhancements and expansion to moorage facilities. Due to the proximity of such facilities to the estuary and their location relative to the tsunami inundation zone, such

[1] https://www.coastalatlas.net/?option=com_jumi&view=application&fileid=8&e=14&Itemid=107
[2] https://www.coastalatlas.net/index.php/learn/places/6-estuaries
[3] https://www.portofcoosbay.com/maritime-commerce

facilities are potentially at risk from damage and destruction by both local and distant tsunamis. Although there is time for maritime operators to respond to a distant tsunami event, the current modeling suggests there is little time to respond for a local tsunami event (Allan and others, 2018). Determining where maritime safety zones may be found offshore the Coos estuary is a major objective of this study.

To facilitate this work, new tsunami modeling has been completed for Coos Bay, extending from offshore along the coast to upriver to include Isthmus Slough, the Coos River, and Haynes Inlet (**Figure 1**). The specific tasks associated with this modeling included the following:

1) Quality assessment (QA) modeling of the 1964 Alaska tsunami to compare model results with dynamic (varying) tides versus a fixed (e.g., mean higher high water) tidal elevation;
2) New tsunami modeling based around three specific scenarios drawn from Priest and others (2013):
    a. AKMax (maximum-considered distant tsunami event);
    b. Large1 (L1), which has an estimated recurrence rate of ~2,500–3,333 years; and
    c. Extra-extra-large1 (XXL1), which has an estimated recurrence rate of >10,000 years (used by the state of Oregon to model its tsunami evacuation zone).

    Each of these scenarios was used to evaluate the sensitivity of peak tsunami currents, maximum water levels, vorticity, and minimum water depths to various tidal and riverine flow effects in different parts of the estuary. These data provide important insights into the role of dynamic tides and riverine flows in modifying tsunami waves. In addition, these data have been used to refine our understanding of timing of tsunamis at various points in the estuary system; and
3) Produce this technical report documenting the overall modeling approach and results, as well as key information that can be incorporated into needed maritime guidance information (e.g. Allan, 2020).

2.0 METHODS

2.1 Background

Between 2009 and 2013, the Oregon Department of Geology and Mineral Industries (DOGAMI) initiated a comprehensive effort to model and map tsunami inundation zones for the entire Oregon coast (Priest and others, 2010; Witter and others, 2011; Priest and others, 2013; Witter and others, 2013). Modeling of possible earthquake scenarios settled on two Gulf of Alaska distant source scenarios and five locally generated earthquake scenarios occurring on the CSZ. The local earthquake source parameters were guided by data that describe the geometry and tectonic behavior of the CSZ (Mitchell and others, 1994; Hyndman and Wang, 1995; McCrory and others, 2004; McCaffrey and others, 2007) and by knowledge of the size and frequency of earthquakes identified from offshore turbidite records that are inferred to record the occurrence of 42 tsunamigenic CSZ earthquakes over the last 10,000 years (Goldfinger and others, 2012). Here we briefly define the characteristics of the various earthquake source parameters before describing the hydrodynamic model used to simulate tsunami inundation.

2.1.1 Distant earthquake sources

Over the past 160 years, 29 distant (far-field) earthquake events have produced transoceanic tsunamis that struck the Oregon coast (Allan and others, 2018). The majority (19) of the tsunamis were small (maximum water level heights of < 0.2 m [0.7 ft]), which resulted in little to no impact to ports and harbors along the Oregon coast. Five events produced water level heights in the range of 0.2 to 0.6 m (0.7 to 2 ft),

and the remaining five generated maximum water level heights exceeding 0.6 m (2 ft) (NGDC, 2017). The latter five occurred in:

- 1873, from northern California;
- 1946, from Unimak, Alaska;
- 1960, from Chile;
- 1964, from the Gulf of Alaska; and
- 2011, from Tōhoku, Japan.

Of these, the 1964 Alaska tsunami produced the largest observed water levels, with estuarine water levels between ~2.5 and 3.7 m (8 and 12 ft) (Schatz and others, 1964; Zhang and others, 2011) but higher wave heights at the open coast based on only a few observations proximal to the beaches: ~5 m (16 ft) in northern Oregon at Cannon Beach (Witter, 2008) and Seaside (Tsunami Pilot Study Working Group [TPSWG], 2006, Appendix C) and > 3.7 m (12 ft) at Sunset Beach, near Coos Bay in southern Oregon (Zhang and others, 2011). The Alaska tsunami caused significant damage to infrastructure in the coastal communities of Seaside and Cannon Beach (Witter, 2008) and killed four people camping along Beverly Beach near Newport on the central Oregon coast; no damage was reported for Coos Bay. Other notable water levels produced by distant tsunamis include 3.05 m (10 ft) in 1873 at Port Orford, 1.8 m (6 ft) in 1946 at Clatsop Spit, and 1.5 m (5 ft) in 1960 at Seaside. Each of these previous events exceeded the effects of the March 11, 2011, Japan tsunami and, by inference, had greater potential to cause damage to ports and harbors along the Oregon coast.

The March 11, 2011, Japan earthquake provided scientists with the most comprehensive set of modern observations of a major distant tsunami. The magnitude (Mw) 9.0 earthquake took place 129 km offshore from the coast of Sendai, northeast Honshu, Japan (Mori and Takahashi, 2012), triggering a catastrophic tsunami that within minutes inundated the northeast coast of Japan, sweeping far inland and killing ~18,000 people (Mori and others, 2011; Suppasri and others, 2013). In addition to loss of life, over 28,000 boats (including 26 ships) and 319 ports (Suppasri and others, 2013) were damaged or destroyed. Economic losses due to port closures were estimated at $3.4 billion per day (Wiśniewski and Wolski, 2012).

The 2011 tsunami propagated eastward across the Pacific Ocean, impacting coastal communities in Hawaii and along the west coast of the continental United States, including Oregon. Along the Oregon coast the tsunami was relatively small, reaching heights ~0.7–3.4 m (2.3–11.2 ft) at tide gauges near the open coast (Allan and others, 2012); at Coos Bay, the maximum wave reached 1.75 m (5.74 ft). Damage in Oregon was entirely confined to harbors, including the ports of Depoe Bay, Coos Bay, and at Brookings; the majority of ports were unaffected. Fortunately for Oregon, the tsunami impact was moderated because the highest waves arrived during a low tide (Allan and others, 2012)—had the tsunami arrived at high tide, the local impact could have been much worse. At Brookings on the southern Oregon coast, 12 fishing vessels put to sea at about 6 am, prior to the arrival of the tsunami waves. However, the *Hilda*, a 220-ton fishing boat and the largest remaining in the harbor, broke loose under the forces of the wave-induced currents and sank several other boats as it washed around the harbor. The tsunami destroyed much of the commercial part of the harbor and about one third of the sports basin; the total damage was estimated at about $10 million. At Crescent City in California where offshore bathymetry amplifies all tsunami waves relative to the Oregon coast, the tsunami was 4.2 m high in the local harbor (Allan and others, 2012). The tsunami damaged the entire open-coast breakwater, destroyed all of the docks in the Inner Boat Basin, and sank or damaged numerous vessels. The estimated damage associated with the event for Crescent City harbor was ~$20 million (Wilson and others, 2013). Accordingly, even modest distant tsunamis like

the one in 2011 pose a significant risk to Oregon ports and harbors and to the safety of commercial and recreational fishermen who operate offshore of the coast.

For the purposes of our simulations for a distant tsunami affecting Coos Bay, Priest and others (2013) and Witter and others (2011) defined two far-field earthquake sources (Mw ~9.2) for maximum-considered tsunamis originating on the eastern part of the Alaska-Aleutian subduction zone. The first scenario, termed AK64, reflects the historical 1964 Prince William Sound earthquake, which produced the largest distant tsunami to reach the Oregon coast in the written historical record. Simulations of this event were used to provide quality control against known observations of water levels and tsunami wave runup identified along the Oregon coast, enabling validation of the hydrodynamic model, Semi-implicit Eulerian-Lagrangian Finite Element model (SELFE), used to simulate tsunami inundation (Priest and others, 2010).

A hypothetical maximum-considered event originating in the Gulf of Alaska was also simulated. This second scenario, termed AKMax, is identified as "Source 3" in Table 1 of González and others (2009); more detailed information describing the earthquake parameters is provided by TPSWG (2006). The AKMax fault model reflects a distributed slip source on 12 subfaults, with each subfault assigned an individual slip value of 15, 20, 25, and 30 m (49, 66, 82, and 98 ft). These extreme parameters result in maximum seafloor uplift that is nearly twice as large as the uplift produced by the 1964 Prince William Sound earthquake estimated by Johnson and others (1996). Examination of the simulated tsunami amplitudes for this source indicates beams of high energy directed more efficiently toward the Oregon coast (González and others, 2009; Allan and others, 2018), when compared with other Alaska-Aleutian subduction zone sources. Accordingly, the hypothetical Gulf of Alaska scenario was used by the State of Oregon as the maximum-considered distant tsunami source for modeling a far-field tsunami for the Oregon coast. Priest and others (2013) noted that testing the geological plausibility of the AKMax scenario and the possibility of other potential sources with better directivity toward the Oregon coast was beyond the scope of the Witter and others (2011) and Priest and others (2009, 2010) studies.

2.1.2 Local earthquake sources

Guided by CSZ geometry and tectonic behavior (Mitchell and others, 1994; Hyndman and Wang, 1995; McCrory and others, 2004; McCaffrey and others, 2007), Priest and others (2010) and Witter and others (2013) described the range of plausible CSZ earthquake sources for the Oregon coast. These data were calibrated against coastal paleoseismic records that document the impacts of as many as 13 major subduction zone earthquakes and associated tsunamis over the past ~7,000 years (Witter and others, 2003; Kelsey and others, 2005; Witter and others, 2010), while recent studies of turbidite records within sediment cores collected in deep water at the heads of Cascadia submarine canyons provide evidence for at least 19 full-margin ruptures and accompanying tsunamis over the past ~10,200 years (Goldfinger and others, 2003, 2012, 2017). Peak fault slip was assumed to be approximately equal to the plate convergence rate (i.e., coupling ratio = 1.0), while the variations in the time intervals between offshore turbidites were determined to be representative of variations in coseismic slip (Priest and others, 2010).

The earthquake scenarios that were ultimately used to model tsunami inundation for the Oregon coast reflect a full-length rupture of the Cascadia megathrust and the corresponding surface deformation used for tsunami simulations (Witter and others, 2013). This was necessary because the primary purpose of that effort was to develop regional tsunami inundation maps. For the purposes of that effort, representative slip models were defined and tested, including slip partitioned to a hypothetical splay fault in the accretionary wedge and models that varied the updip limit of slip on the megathrust. Each tsunami scenario was then weighted using a logic tree, and the results summarized on maps depicting the percent confidence that the local CSZ tsunami will reach no farther inland than each inundation line. Inter-event

time intervals inferred to separate the 19 sandy turbidites range from as little as ~110 years to as long as ~1,150 years (Table 1 from Witter and others, 2011). From these data, four time intervals (mean values rounded to the nearest quarter century) were defined as representative of four general earthquake scenarios, or size classes: small (S), medium (M), large (L), and extra-large (XL). Respectively, these events have a mean inter-event time of 300 years (range = ~110 to 480 years, 5 events), 525 years (range = ~310 to 660 years, 10 events), 800 years (range = ~680 to 1,000 years, 3 events), and 1,150 years (1 event), rounded to 1,200 years. The mean inter-event time interval multiplied by the CSZ plate convergence rate at each latitude equals the peak slip deficit released in each scenario earthquake. Slip was tapered to zero up and down dip from the peak value (Priest and others, 2010). Slip was also reduced progressively from north to south on the CSZ to account for evidence in the paleoseismic record of increasing numbers of partial CSZ ruptures from north to south (Goldfinger and others, 2012; Witter and others, 2013). A fifth scenario, termed extra-extra-large (XXL), simulated a maximum-considered tsunami, which would be used to guide evacuation planning (Witter and others, 2013). This last hypothetical scenario assumes 1,200 years of slip deficit release but without any reduction of slip from north to south. According to Witter and others (2013), these size classes correspond to approximate recurrence rates as follows: S, 1/2,000 yr; M, 1/1,000 yr; L, 1/3,333 yr; and XL, < 1/10,000 yr. Recurrence for the maximum-considered XXL event is not known.

2.2 Tsunami Simulation

Vertical components of seabed deformation from the earthquake rupture were used to set up the initial water surface for tsunami simulations as well as the initial velocity, assuming a short (10 s) initial constant acceleration of the seafloor. Simulations of tsunami propagation and inundation used the hydrodynamic finite element model SCHISM (Semi-implicit Cross-scale Hydroscience Integrated System Model, schism.wiki) (Zhang and others, 2016a), which is derived from the model SELFE (Semi-implicit Eulerian-Lagrangian Finite Element model) (Zhang and Baptista, 2008; Priest and others, 2009; Zhang and others, 2011; Witter and others, 2012). Algorithms used to solve the Navier-Stokes equations in these models are computationally efficient and stable. SELFE passed all standard tsunami benchmark tests (Zhang and Baptista, 2008; Zhang and others, 2011) and closely reproduced observed inundation and flow depths of the 1964 Alaska tsunami in a trial at Cannon Beach (Priest and others, 2009). More recently, SCHISM successfully passed a suite of standardized tsunami current benchmark tests (Zhang and others, 2016b; Lynett and others, 2017), indicating that the original SELFE model results are acceptable for simulating tsunami currents used in maritime evacuation planning.

The unstructured finite element mesh used in our Coos Bay modeling was constructed by first compiling digital elevation models (DEMs) covering the model domain and then retrieving from the DEM elevations at a series of points defining a triangular irregular network (TIN). The DEM for the tsunami simulations was derived from a combined bathymetric/topographic seamless digital surface model created by Dr. David Sutherland, Department of Earth Sciences, University of Oregon. These data were originally compiled to support hydraulic modeling efforts undertaken in Coos Bay (Conroy and others, 2020; Eidam and others, 2020). The DEM comprises a variety of data sources, including a NOAA tsunami grid, water-penetrating airborne lidar survey gridded at 1-m spacing (https://coast.noaa.gov/htdata/lidar1_z/geoid12b/data/4905/), complemented by single-beam sonar collected from a Coastal Profiling System (Ruggiero and others, 2000), and channel surveys from the U.S. Army Corps of Engineers (Conroy and others, 2020). In areas of dry land, the data were supplemented with 2009 lidar data collected by DOGAMI.

The completed tsunami model domain is shown in **Figure 1** for Coos Bay and extends ~40 km (25 mi) offshore from the coast. The size of the unstructured grid consisted of ~1.75 million nodes and ~3.5 million triangular elements in the horizontal dimension. The nominal resolution is ~10 m (33 ft) in the river channel and ~10–13 m (15–42 ft) on land in areas adjacent to the estuary and river channel. The DEM was further refined by adding finer-resolution detail in areas adjacent to the Coos jetties, the breakwaters at the port of Charleston, along the Coos Bay harbor wharf and along various levees.

A second grid that included adjustments specific to the navigation channel was developed. This grid reflects a proposal to deepen the navigation channel to allow for larger vessels to enter the estuary and travel up the channel. The goal here was to understand potential hydrodynamic changes in the tsunami as it interacted with the deeper channel. To account for the deeper channel we modified the grid based on the information included in **Table 1**. In general, the revised grid included an increase to the channel depth of 3.3 m (10 ft) near the mouth to a fixed depth of 17.4 m (57 ft), while the rest of the channel was deepened by ~2.4 m (8 ft) to a fixed depth of 13.7 m (45 ft) (Oregon International Port of Coos Bay, 2019).

Table 1. Modified navigation channel depths based on existing and proposed future configurations. RM is river mile. MLLW is mean lower low water.

	Original (m, MLLW)	New Depth (m, MLLW)
Offshore Limit of Navigation Channel (~RM-1) to RM 0.3	−14.3 (−47 ft)	−17.4 (−57 ft)
Entrance Range RM 0.3 to 1.0	−14.3 (−47 ft) at RM 0.3 decreasing to −11.3 (−37 ft) at RM 1	−17.4 (−57 ft) at RM 0.3 decreasing to −13.7 (−45 ft) at RM 1
Entrance Range and Turn RM 1.0 to 2.0	−11.3 (−37 ft)	−13.7 (−45 ft)
Inside Range RM 2.0 to 2.5	−11.3 (−37 ft)	−13.7 (−45 ft)
Coos Bay Range RM 2.5 to 4.3	−11.3 (−37 ft)	−13.7 (−45 ft)
Empire Range RM 4.3 to 5.9	−11.3 (−37 ft)	−13.7 (−45 ft)
Lower Jarvis Range RM 5.9 to 6.8	−11.3 (−37 ft)	−13.7 (−45 ft)
Jarvis Turn RM 6.8 to 7.3	−11.3 (−37 ft)	−13.7 (−45 ft)
Upper Jarvis Range RM 7.3 to 8.2	−11.3 (−37 ft)	−13.7 (−45 ft)
Turning Basin RM 7.3 to 7.8	None	−11.3 (−37 ft)

We use only one layer in the vertical, so the model is effectively 2D depth averaged. This is consistent with the majority of existing tsunami inundation maritime modeling efforts presently being implemented; incorporation of fully 3D modeling is left for future study. Ideally, SCHISM 3D would provide better results, especially in terms of resolving the density-driven currents that are important (Burla and others, 2010). However, the effects of the density flow (on the order of 1 m/s [1.9 knot]) are arguably minor compared to those from the tsunami event (on the order of 5 m/s [9.7 knot]). Furthermore, a fully 3D model with the required very fine resolution needed for tsunami simulations is too costly at present.

Each simulation was run for 24 hours, providing sufficient time for the tsunami to run its course; the simulation time step is 1 second for distant and 2 seconds for local sources; the data output was established at 40-second intervals. The model is fully parallelized with hybrid openMP[4] and MPI[5] and runs ~7 times faster[6] than real time on 500 Intel® Xeon® cores using this higher-resolution grid.

The tsunami simulations were run using both static (i.e., fixed tidal elevation) and dynamic tides (tide elevation varies over time), as well as different river discharge levels. The complete suite of simulations is summarized in **Table 2**. For static tidal runs, we used mean higher high water (MHHW) and mean high water (MHW) determined at the Charleston tide gauge station (**Figure 2**), respectively 2.32 m (7.6 ft) and 2.12 m (7.0 ft). For dynamic tide runs, the tsunami was timed to arrive at Charleston at the following tide stages: flood, ebb, flood slack, and ebb slack (**Table 2, Figure 2**). Tidal forcing at the ocean boundary was calculated from the WEBTIDE package (http://www.bio.gc.ca/science/research-recherche/ocean/webtide/index-en.php). Coos River discharge information was provided by Dr. David Sutherland, Department of Earth Sciences, University of Oregon (Sutherland, unpub. data, December 2018). We focused on two river flow regimes (**Figure 3**, **Table 2**): average and high flow scenarios.

Figure 2. Tidal stages defined for the Charleston tide gauge.

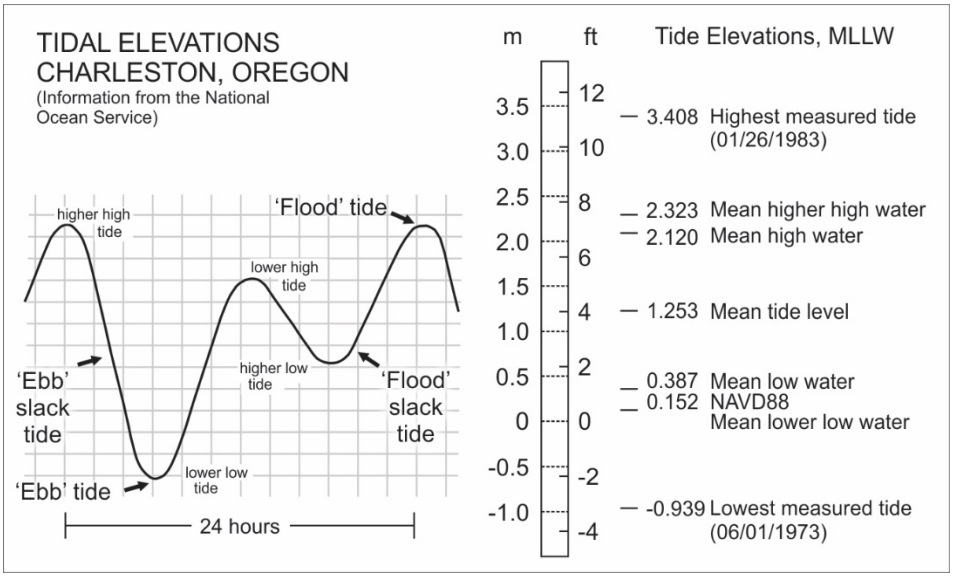

The bottom drag coefficient (*Cd*) or friction used in tsunami modeling is specified from Manning-*n*, which is known to be a function of land cover type (USACE, 2008). The Coos estuary is characterized by a wide range of land cover types, including open water, developed space, pastures, shrubs, wetlands, evergreen forest, and woodland, which are captured in the USGS 2011 National Land Cover Data (Homer and others, 2015). Values of Manning-*n* are estimated for each land cover type based on published values provided by Bunya and others (2010) and provided in **Table 3.** This process is accomplished using a look-up table script that assigns the Manning-*n* value based on the local land cover data. The spatial dataset of

[4] openMP: share memory parallelism (MP=multi-processing)
[5] MPI: message passing protocol (for distributed parallelism)
[6] 24/7=3.4 hours to finish one simulation day

friction is then used in the model simulations. The friction generally increases landward, thus helping to dissipate the tsunami wave energy. For the subaqueous portion of the DEM, we used Manning-*n* = 0.02.

Table 2. Coos Bay simulated tsunami scenarios. See text for scenario definitions.

Group Number	Scenario	Tidal Phase*	Spring/ Neap	River Flow (m^3/sec) (Q)**	Bottom Friction***	Run Name
1	AK64	event	event	estimated	landscape	Run03c-1964
2	XXL1	static (MHHW)	N/A	0	0	Run01a-XXL1 ***(2012 grid)*** Run01b-XXL1 ***(2019 grid)***
3	AKMax/L1/XXL1	dynamic (MSL), flood	spring	average	landscape	XXL1 = Run05a L1 = Run05a-L1 AKMax = Run05a-pmel01
4	AKMax/L1/XXL1	dynamic (MSL), ebb	spring	average	landscape	XXL1 = Run06a L1 = Run06a-L1 AKMax = Run06a-pmel01
5	AKMax/L1/XXL1	dynamic (MSL), flood slack	spring	average	landscape	XXL1 = Run07a L1 = Run07a-L1 AKMax = Run07a-pmel01
6	AKMax/L1/XXL1	dynamic (MSL), ebb slack	spring	average	landscape	XXL1 = Run08a L1 = Run08a-L1 AKMax = Run08a-pmel01
7	AKMax/L1/XXL1	dynamic (MSL), flood	spring	high	landscape	XXL1 = Run04a L1 = Run04a-L1 AKMax = Run04a-pmel01
8	L1	dynamic (MSL), flood	spring	average	landscape	L1 = Run05c-L1 (reflects modified deeper navigation channel)

Notes: Static means a fixed tidal elevation, and dynamic means the tide varies over time. MSL is mean sea level.

*Vertical station datums according to the Charleston tide gauge. MHHW = 3.469 m (11.38 ft); MSL = 2.390 m (7.84 ft); NAVD88 = 1.298 m (4.26 ft).

**Average spring "freshet" (spring thaw resulting from snowmelt) flows = January 24, 2008 conditions.

**High flow = January 9, 2012 event.

***Nodal Manning-*n* coefficients are spatially assigned using land-cover definitions from the USGS National Land Cover Data (NLCD) for Oregon and Washington (see **Table 3**). For the ocean bottom we used Manning-*n* = 0.02.

Figure 3.Time history of Coos River discharge, 2002–2008. Data provided by Dr. David Sutherland, University of Oregon (unpub. data, December 2018).

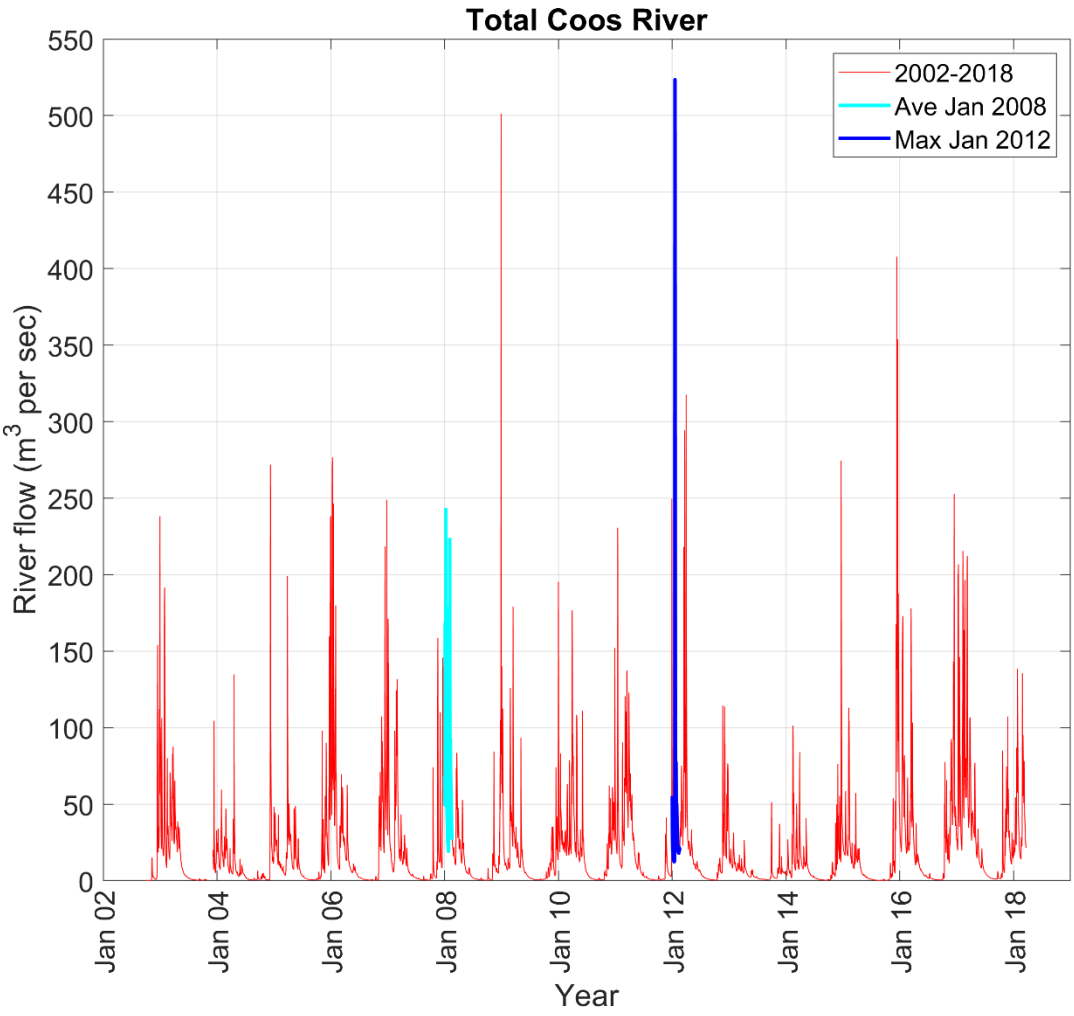

Table 3. Manning-*n* values for various landform types (from Bunya and others, 2010, Tables 4 and 5).

Description	Manning-*n* Value
Open water	0.020
Sand beach, bare ground, recreational grass	0.030
Fallow, transportation	0.032
Pasture	0.033
Grassland, farmed wetlands, urban grassy pasture, herbaceous wetland	0.035
Agriculture, bare rock	0.040
Low-density urban/commercial	0.050
Shrub land	0.070
Transitional, orchard, vineyard	0.100
Medium-density urban	0.120
Woody wetland	0.140
High-density urban	0.150
Deciduous forest	0.160
Mixed forest	0.170
Evergreen forest	0.180

Multiple model runs were undertaken to simulate the effects of tides, river flow, and tsunamis before these were compared across all "dynamic-tide" runs. **Table 2** shows summary information for each of the model runs completed for this study. In this report we will focus initially on comparisons between static- and dynamic-tide run results to illustrate the importance of incorporating tides in tsunami simulations for this high-energy system. For dynamic-tide simulations, the effects of spring[7]/neap[8] tides, tidal phases, and river flow conditions are examined. Most of the simulations are done for 1 day under an average spring freshet[9] condition as observed in 2008 (**Figure 3**). Longer simulations (12 to 24 days) are done for tidal runs.

Finally, **Figure 4** presents a map identifying the locations where time series information has been extracted from the simulations in order to generate plots of tsunami currents and water levels. These data are useful for better understanding of the complex nonlinear responses of the tsunamis as they interact with tides and riverine flows.

[7] Spring tides occur twice each lunar month when the Earth, sun and moon are nearly in alignment, producing high tides that are a little higher than normal.

[8] Neap tides occur seven days after the spring tide occurring when the sun and moon are at right angles to each other. This results in high tides that are slightly lower than normal.

[9] A term used to describe a spring thaw resulting from snowmelt.

Figure 4. Map showing the locations of virtual water level stations in the Coos estuary used to observe tsunami currents and water level time series information. Inset example shows the simulated XXL1 water levels for Run05a (flood tide) and Run06a (ebb tide) at station 7 located at the mouth of Coos Bay. Blue to yellow shading defines the offshore bathymetry and subaerial topography.

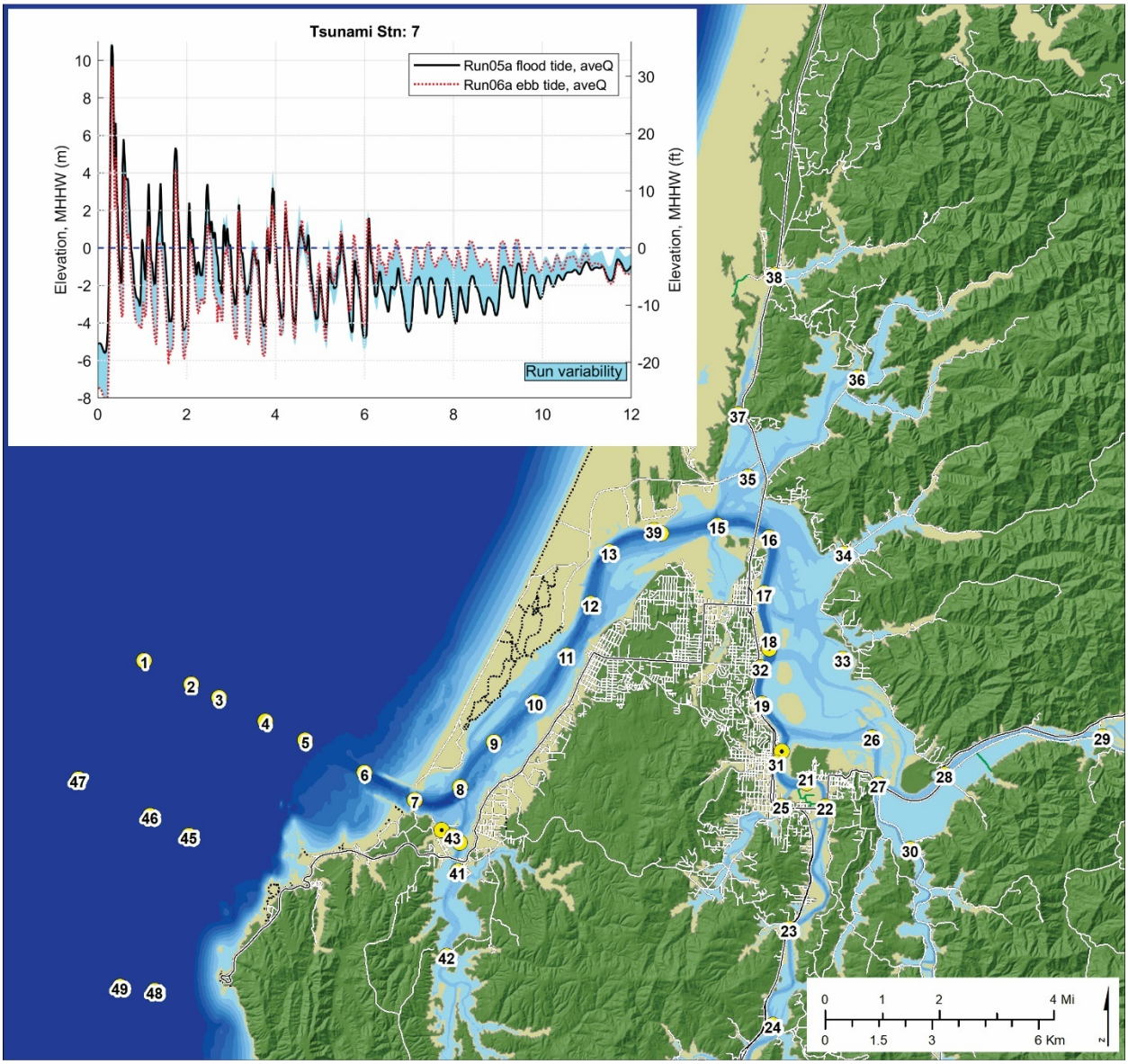

3.0 MODEL VALIDATIONS

3.1 Tides

We first validate the model for tidal elevations. We used a high river flow event on January 9, 2012 to evaluate the tidal modeling. **Figure 5** provides a comparison between the measured tides at the Charleston tide gauge (its location is included in **Figure 1**) with the model results determined by SCHISM. As can be seen in **Figure 5**, our 2D model replicates the measured data well, while some of the mismatch may be explained by our omission of wind effects in the simulation. Besides including wind, better accuracy may be achieved with the 3D version of SCHISM, especially when using 3D baroclinic SCHISM (Burla and others, 2010).

All dynamic-tide runs discussed in this report consist of three separate runs:

- A tidal run (with river flow) that starts ~10 days before the tsunami event and ends 1 day after the event;
- A static-tide run with tsunami only (with no river flow or tides); and
- A final dynamic-tide run that is initiated from the tidal run at the start of the earthquake event and uses the information at the ocean boundary from the other two runs as well as bed deformation inside the domain. Comparison of results from this run and the sum of the other two runs reveals nonlinearity due to tide-river-tsunami interaction.

Figure 5. Comparison of modeled and observed tidal elevations at the Charleston tide gauge station operating near the mouth of Coos Bay.

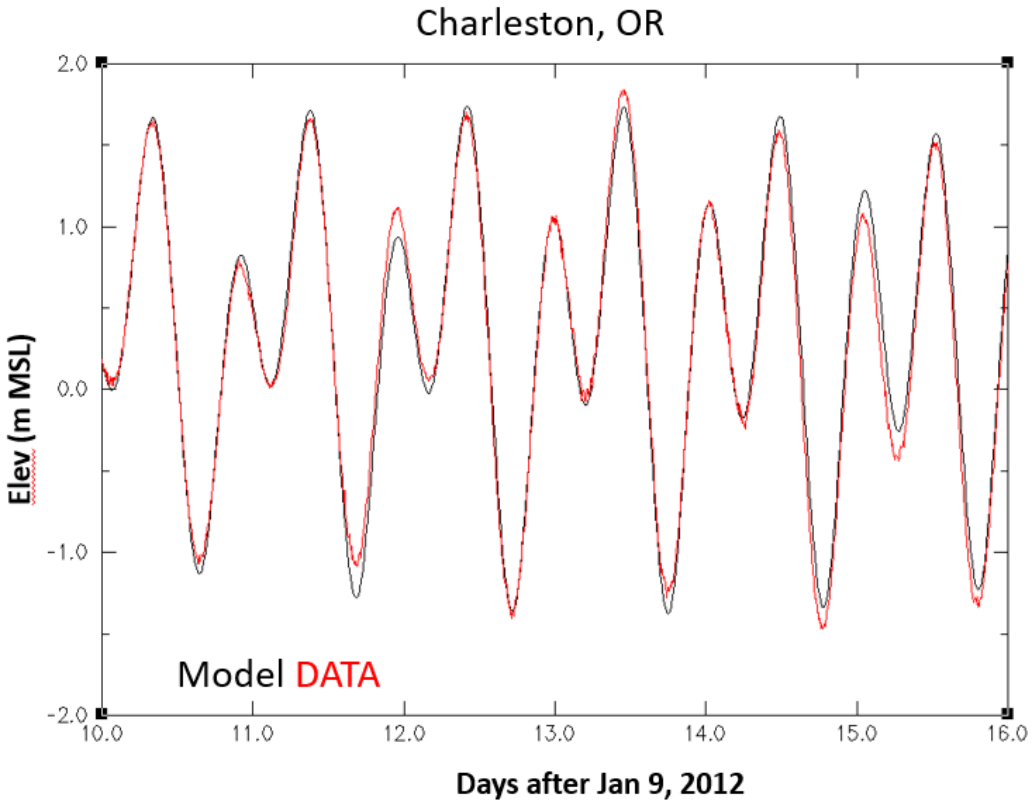

3.2 1964 Great Alaska Tsunami

The great Alaska 1964 earthquake and tsunami were previously validated using SELFE and a grid that covers a large region from Alaska to the U.S. west coast, while the modeling accounted for both tsunami waves and the dynamic tides (Zhang and others, 2011). Schatz and others (1964) reported that the initial tsunami wave at Coos Bay was about 3 m [10 ft] above mean high water (MHW). The tsunami dissipated rapidly up the Coos Channel due to the wide tidal flats and was negligible in height by the time it reached Pony Point, about 7 miles up the channel. Lander and others (1993) noted that the maximum range of water levels observed reached ~4.3 m [14 ft]. At Coos Bay, damage from the tsunami was minimal, estimated at ~$20,000 (Wilson and Torum, 1968). Here we re-validate the model using higher-resolution DEM data developed for the Coos estuary.

The static-tide run uses MHHW as the vertical datum (3.469 m [11.38 ft] based on the Charleston tide gauge station datum) while the other two runs (tidal and dynamic-tide runs) use mean sea level (MSL) (2.39 m [7.84 ft]). For the 1964 event, we initiated the tide model from March 10, 1964. The model was then restarted at 03:36 GMT on March 28, 1964 (19:36 pm PDT on March 27, 1964), when the earthquake occurred, with the 1964 tsunami wave signal added at the ocean boundary. These latter data were calculated from a previous large-domain run undertaken by Priest and others (2013). The first waves of tsunami arrived at Coos Bay approximately 4 hours 4 minutes later (23:40 pm PDT on March 27, 1964). Unfortunately, we are unable to directly compare model results with observed water levels as the Charleston tide gauge station was not operational at the time of the event. Nevertheless, modeling by Zhang and others (2011) and analyses here indicate that the maximum tsunami height of ~2.5 m [8.2 ft] (**Figure 6**) is achieved near Coos Bay, consistent with the observations of Schatz and others (1964) and (Lander and others, 1993). The tsunami waves coincided with a spring flood tide, which further exacerbated local impacts (Zhang and others, 2011). The tsunami waves are visible during the subsequent ebb and flood and persisted more than one day after the earthquake (**Figure 6**).

Overall, SCHISM did a reasonable job in capturing this complex interaction between tsunami waves and tides. Moreover, the model also captured the wave runup processes inside the estuary. There are field estimates of the tsunami runup at one site up the navigation channel near Empire, where the maximum wave runup was estimated to be 2.1 m [6.9 ft] (Lander and others, 1993). This value compares reasonably well with the peak wave observed in our virtual water level station (**Figure 6**). In addition, although the longitude-latitude coordinates of the observation site were not precisely given (the coordinates place it in the navigation channel), we can still estimate the tsunami runup height at the nearest dryland locations, which is 1.96 m at the dryland point nearest to Empire, and 2.09 m on the North Spit (**Figure 7**). These comparisons suggest that the model is sufficiently accurate to be used in the study of tsunami-tide interaction.

Because the Alaska 1964 event remains the largest far-field tsunami to strike the Oregon coast in the last century, these data are useful for assisting with the development of maritime tsunami guidance for Coos Bay. **Figure 8** and **Figure 9** present the simulated maximum water levels and current velocities generated for the Alaska 1964 tsunami. For tsunami currents (**Figure 9**) we use the same binning approach as proposed by Lynett and others (2014, **Table 4**), after finding a strong relationship between current velocity and damage caused by the 2011 Tōhoku tsunami on ports and harbors on the California coast. In general, Lynett and others found that for velocities ranging from 1.5 to 3 m/s [3 to 6 knots], moderate tsunami damage tended to occur to port facilities and moored vessels. When the current velocities increased to ~3–4.5 m/s [6–9 knots], ports and docks were subject to major damage. Extreme damage occurred when current velocities exceeded 4.5 m/s [9 knots].

Figure 6. Simulated water level elevations near Empire during the 1964 event from the dynamic tide simulation; the virtual station is approximately 5 miles from the mouth of Coos Bay.

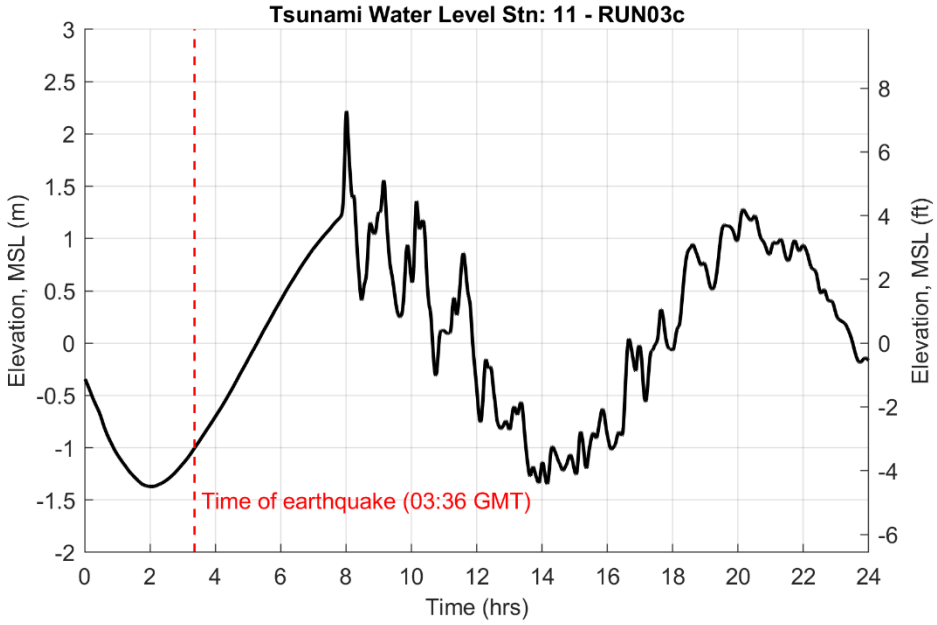

Figure 7. Method used to calculate the maximum runup near Empire, Coos Bay. The yellow dash line is used to intersect with the nearest dryland location observed on the North Spit and at Empire, based on the coordinates of the observation point near the center of the navigation channel.

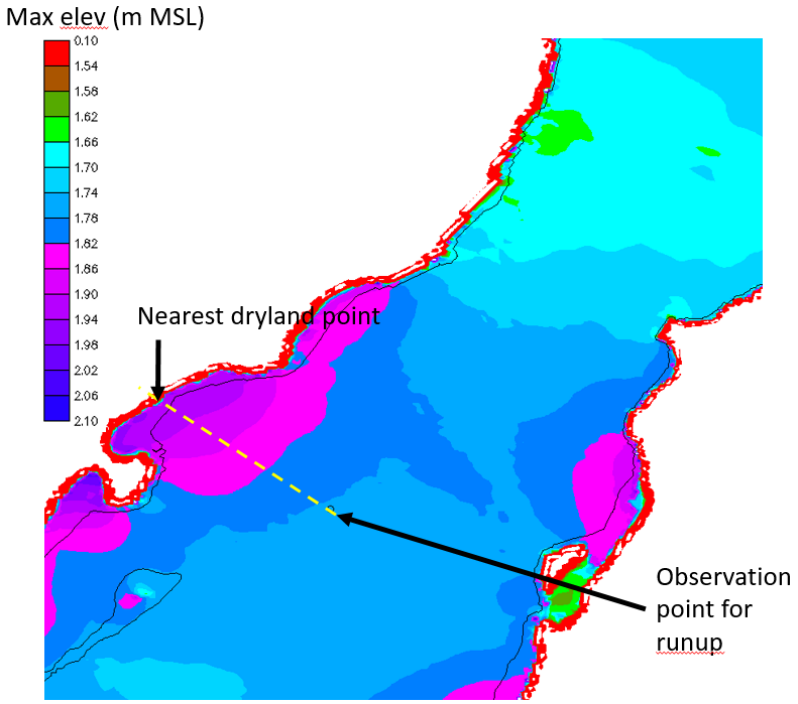

Table 4. Damage index and corresponding damage type (after Lynett and others, 2014).

Damage Index	Associated Current Velocity	Damage Type
0		no damage/impacts
1	< 1.5 m/s [< 3 knots]	small buoys moved
2	1.5–3 m/s [3–6 knots]	1-2 docks/small boast damaged and/or large buoys moved
3		moderate dock/boat damage (< 25% of docks/vessels damaged and/or midsized vessels off moorings)
4	3–4.5 m/s [6–9 knots]	major dock/boat damage (< 50% of docks/vessels damaged and/or midsized vessels off moorings)
5	> 4.5 m/s [> 9 knots]	extreme/complete damage (> 50% of docks/vessels damaged)

As can be seen in **Figure 8**, maximum water levels range from 1 to 1.4 m (3.3 to 4.6 ft) adjacent to the mouth of Coos Bay. Water levels reached ~1.3 m (4.3 ft) at Barview, within the Charleston harbor, and in the vicinity of Empire. In the northeast, near the Southwest Oregon Regional Airport (referred to as Coos airport herein), localized runup levels peaked at ~1.8 m (5.9 ft). However, for much of the navigation channel between the mouth and Pony Point, the water levels remained ~1 m (3 ft). Upriver from Pony Point, water levels remain ~0.6 m (2 ft), including ship-mooring sites near the Port of Coos Bay. On the open coast, water levels are highest along the North Spit and south of the Coos Bay mouth, where they reached ~2.0 m (6.6 ft).

Evident from **Figure 9**, the modeled currents are generally low throughout the lower Coos estuary. Strongest currents (>6 knots) are observed at the mouth of the estuary near river mile 1 (RM1). Strong currents [3–6 knots] are also observed along the navigation channel downstream of Jordon Point. Elsewhere in the estuary the tsunami current velocities are generally below the 3 knot threshold (**Figure 9**). According to Lander and others (1993, p. 100) damage from the tsunami was "done by the first two waves and the sucking action of the surge." The latter action was probably associated with outgoing tsunami currents following the peak wave arrival (**Figure 6**). Lander and others (1993, p. 100) further noted that "Charleston Hanson's Landing and the Charleston small boat basin took the brunt of the damage. Hansen's large charter boat was torn from its mooring, flipped over and sunk. The boat was salvaged but damage to the boat and floating dock was estimated at $21,500. In the small boat basin several boats were torn from their moorings. Nineteen pilings were damaged, four 40 foot floats, six pontoons (4 x 4 x 12 feet) and ten fenders were ripped out. Damage here was estimated at about $17,000. A fishing boat was tipped over and sank north of the bridge."

Figure 8. Simulated maximum water levels for the Alaska 1964 tsunami using dynamic tides. White circles and numbers are U.S. Army Corps of Engineers river mile locations and values. Star denotes the approximate location of an observed runup.

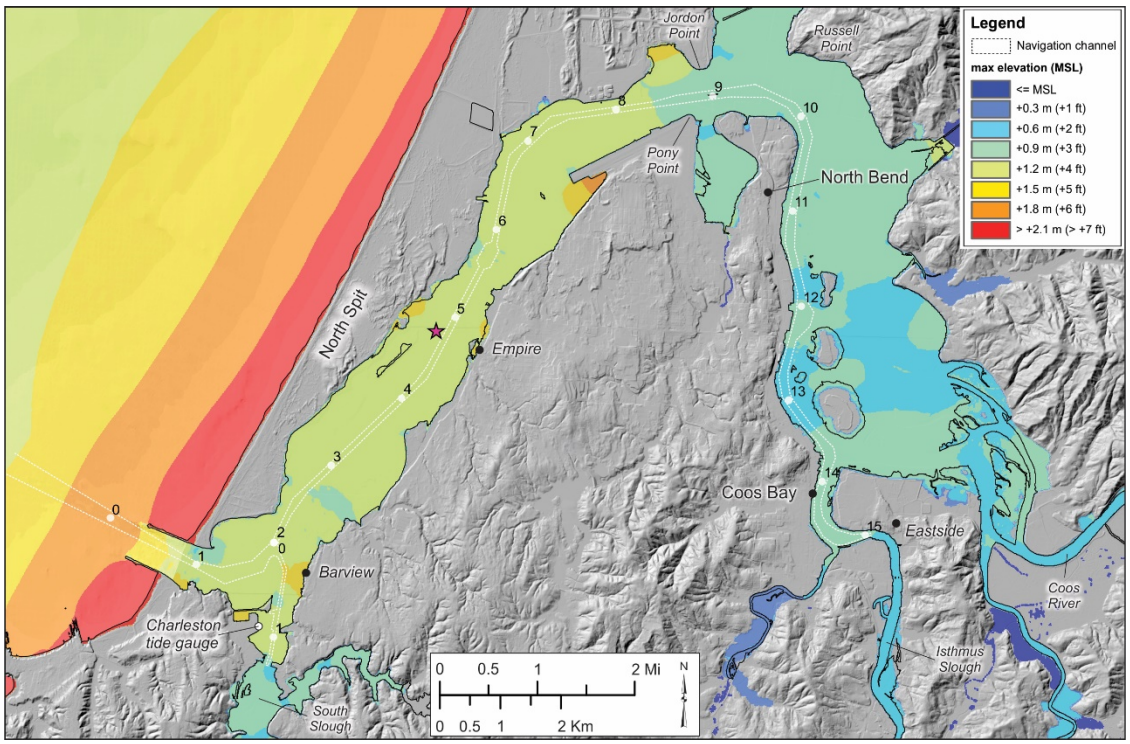

Figure 9. Simulated maximum currents for the Alaska 1964 tsunami using dynamic tides. White circles and numbers are U.S. Army Corps of Engineers river mile locations and values.

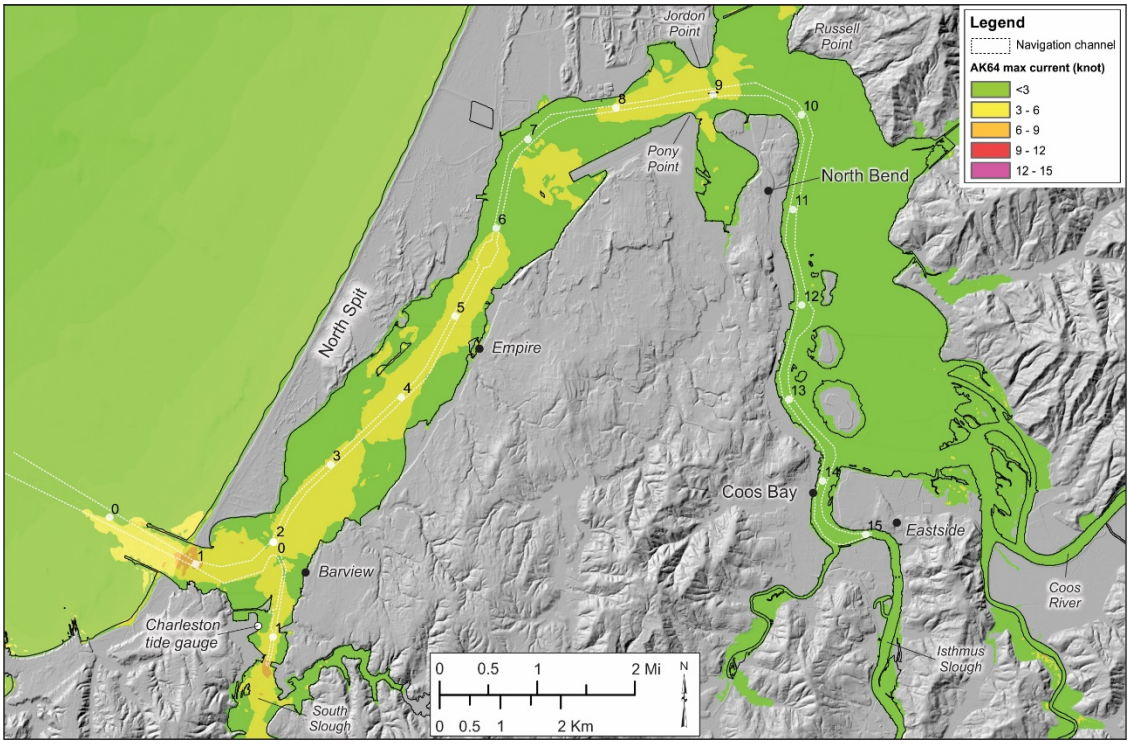

4.0 STATIC AND DYNAMIC TSUNAMI SIMULATIONS

4.1 Static-Tide Results

Simulations involving static-tide modeling were implemented for only the XXL1 local CSZ scenario. As a reminder, these runs do not include river flow and use a frictionless bottom (**Table 2**, group 2), making them consistent with previous modeling efforts undertaken for the Oregon coast from 2009 to 2013 (Priest and others, 2009; Witter and others, 2011; Priest and others, 2013). The vertical datum used in our static run modeling is MHHW defined at the Charleston tide gauge.

The major difference between the latest simulation and the previous modeling effort is the adoption of an updated digital elevation model (**Figure 10**, *top*) that includes bathymetric improvements to areas seaward of the North Spit (bright yellow in **Figure 10**), in the nearshore, as well as changes to the navigation channel (dark blues), and inter-tidal areas within the estuary.

Comparisons of the inundation extents produced from our latest simulation versus modeling undertaken in 2013 (Priest and others, 2013) indicate that for most areas within the estuary, differences between the two modeling efforts are relatively minor (yellow). Overall, we find several small areas nearest the coast that are now removed from the XXL1 tsunami inundation zone (rose color). These include areas west of Charleston and east of Barview (**Figure 10**, *bottom*). Conversely, areas now flooded are confined largely to the distal ends of the estuary, such as up the South Slough, near Eastside, and up the Coos River. Several new areas near Empire are also flooded in the new simulation (**Figure 10**, *bottom*).

As can be seen in **Figure 11** (*top*, maximum water levels; *bottom*, currents), the entire Coos North Spit is overtopped under the maximum considered XXL1 scenario. Because the Coos estuary geometry serves as an effective dissipater of short-wavelength tsunami waves, the greatest impact caused by an XXL1 tsunami (**Figure 11**, *top*; hot colors) is in the estuary between the MCB and Jordon Point. Both modeled tsunami water levels and current velocities can be expected to yield catastrophic results throughout this area, with the communities of Charleston, Barview, and Empire severely impacted. With respect to the maximum water levels, our modeling indicates several additional "hotspot" areas upriver of the Coos airport, including near Jordon Point, northeast of the Conde B. McCullough Memorial Bridge (near RM10), east of RM11, and in the south near Eastside. Although tsunami energy will be concentrated in these "hotspot" areas, significant inundation and impacts will also occur in low-lying areas near North Bend and in much of downtown Coos Bay. Flow depths in these areas are projected to exceed 2 m (> 6.6 ft). Finally, strong tsunami currents exceeding 12 knots will impact the entire estuary (**Figure 11**, *bottom*; red-brown-purple colors), contributing to the destruction of buildings located in the inundation zone.

To further highlight the transformation in the tsunami (Run01b) as it propagates up along the Coos navigation channel, we define the maximum tsunami water level along the length of the navigation channel, which extends from offshore the mouth of Coos Bay, upriver and past downtown Coos Bay, and up along Isthmus Slough (**Figure 12**); **Figure 12** also includes simulation results based on the original DEM. The maximum water level is defined as:

$$\max \text{wl} = FD - d \tag{1}$$

where FD is the flow depth and d is the elevation of the ground or bathymetric surface after subsidence.

Figure 10. ***(top)*** **Bathymetric (DEM) changes defined for 2019 compared with original 2013 DEM. Hot colors indicate bathymetry is shallower relative to 2013 DEM, while darker blue colors indicate deeper conditions.** ***(bottom)*** **2019 static (MHHW) run modeling compared with results from 2013. Rose color denotes those areas now removed from inundation, while cyan color indicates areas now flooded; yellow color indicates no change. Numbers on map are U.S. Army Corps of Engineers river mile locations.**

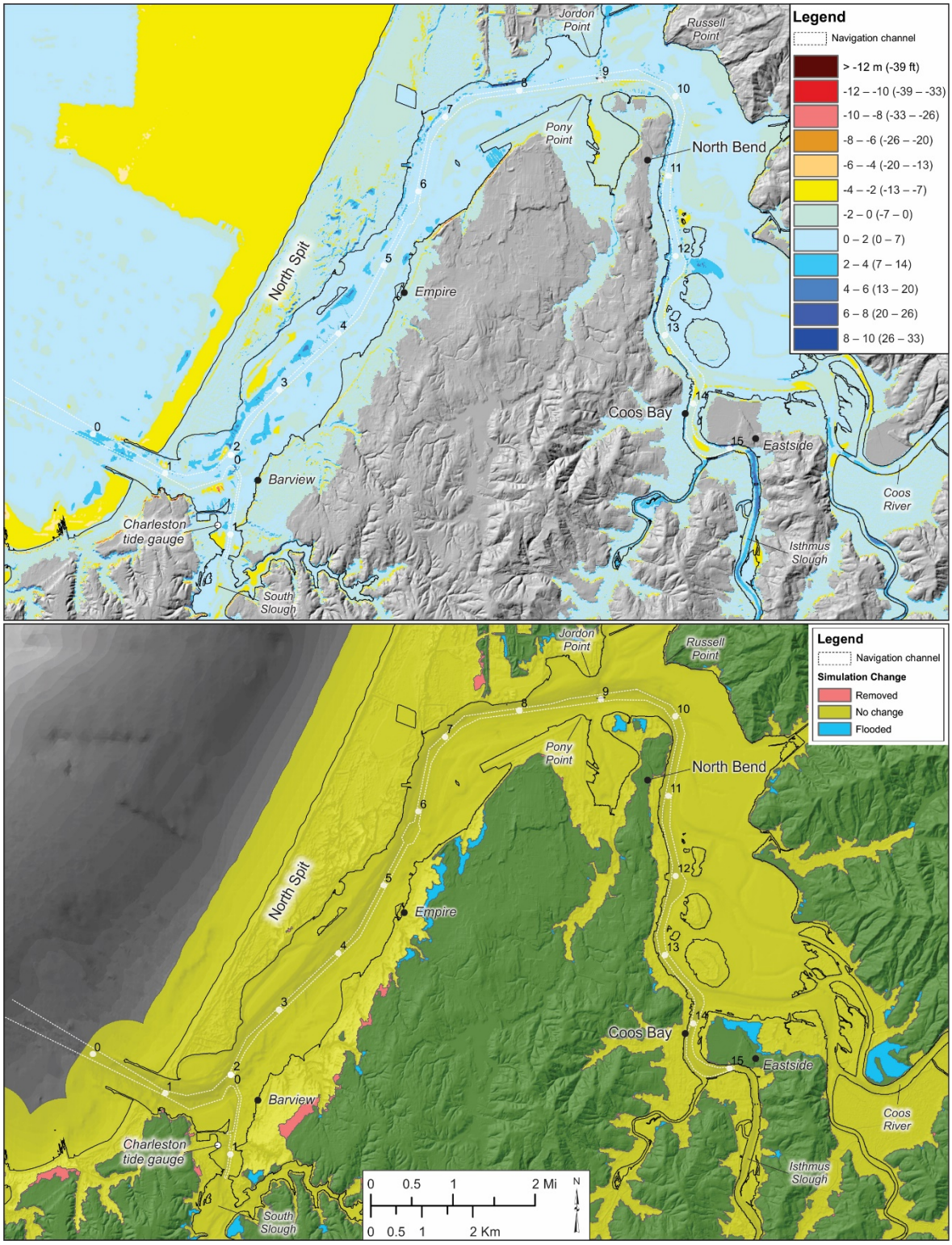

Figure 11. ***(top)*** **Maximum tsunami elevation and** ***(bottom)*** **current velocities, in knots, generated for the XXL1 (Run01b) simulation, modeled using MHHW, no river flow, and a frictionless landscape. Numbers on map are U.S. Army Corps of Engineers river mile locations.**

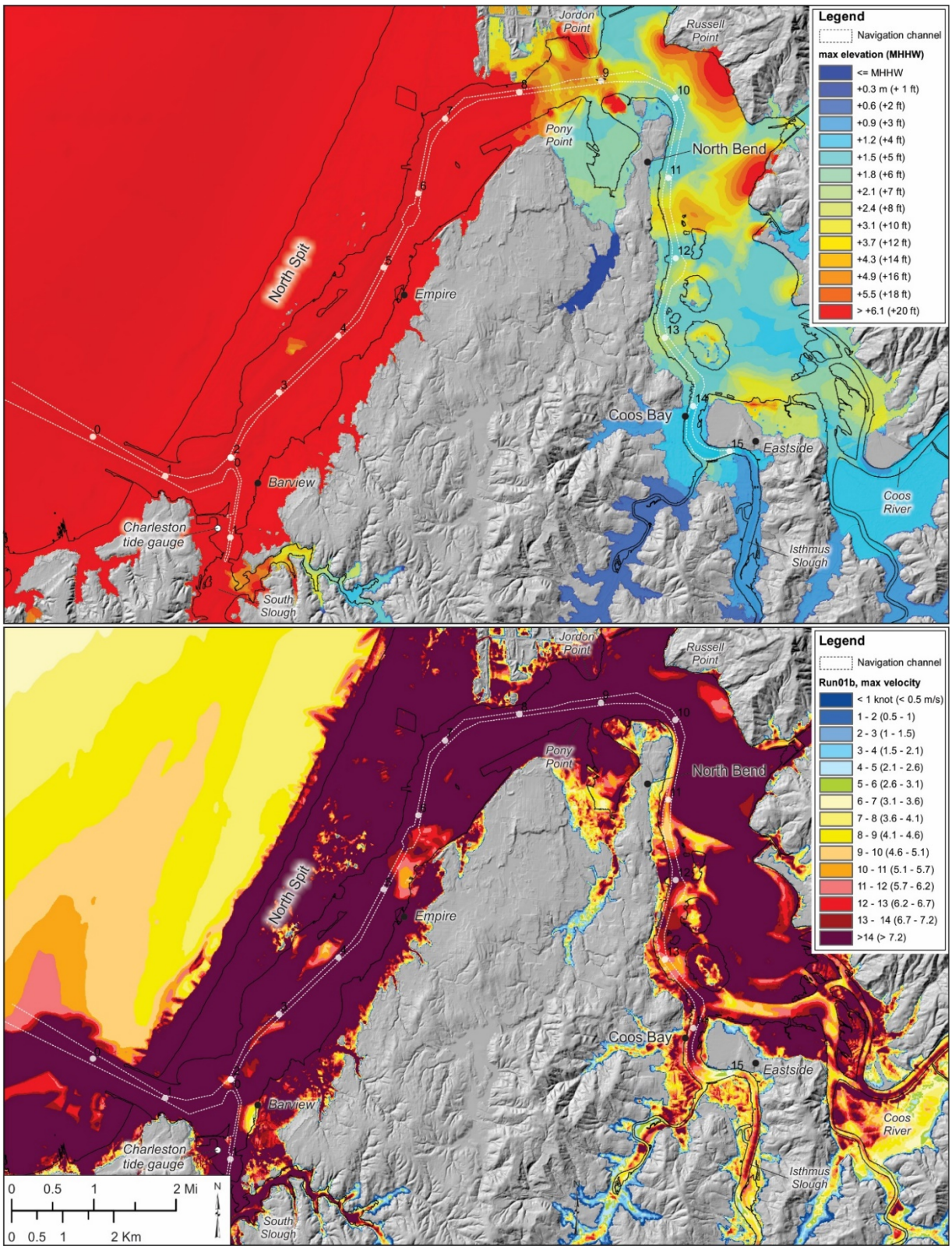

As can be seen in **Figure 12**, the largest tsunami waves are concentrated just inside the MCB. Dispersive effects cause the tsunami waves to begin to decrease in height upon entering the estuary. Nevertheless, the tsunami water levels remain very high along much of the channel between Barview and Empire. Upriver of Empire, the propagation of the tsunami becomes complicated as the tsunami traveling northeast along the navigation channel interacts with tsunami waves crossing from the west over the North Spit. These effects likely account for localized peaks in the tsunami water levels apparent near Empire and at Jarvis Turn (**Figure 12**). East of Jarvis Turn, tsunami water levels begin to decrease in height as the channel morphology widens and the tsunami encounters the broad low-lying area of Pony Slough, immediately east of the Coos airport. However, the most significant transformation in the tsunami water levels occurs upriver of Jordon Point, where the estuary opens up and the waves are dispersed over a broad, shallow area that makes up the upper Coos estuary (**Figure 12**). Localized smaller peaks in tsunami water levels adjacent to Jordon Point are a function of the tsunami once again combining with the main tsunami now directed toward Jordon Point. Upriver of Jordon Point, the tsunami first strikes Russell Point (north side of Conde B. McCullough Memorial Bridge [near RM10]), where the wave is then reflected southward toward Coos Bay. Localized peaks in tsunami water levels between RM11 and RM14 (i.e., from the Mill Casino to Coos Bay, **Figure 12**) are a function of complicated interactions as tsunami waves reflects off various sections of the upper estuary followed by subsequent encounters with additional waves reverberating around the upper estuary. The tsunami waves continue past Coos Bay, traveling along Isthmus Slough and up the Coos and Millicoma Rivers.

Figure 12. Maximum tsunami water levels interpolated along the Coos estuary navigation channel for XXL1 using the original DEM and static tidal elevation (Run01a), and with the updated DEM (Run01b). RM is river mile.

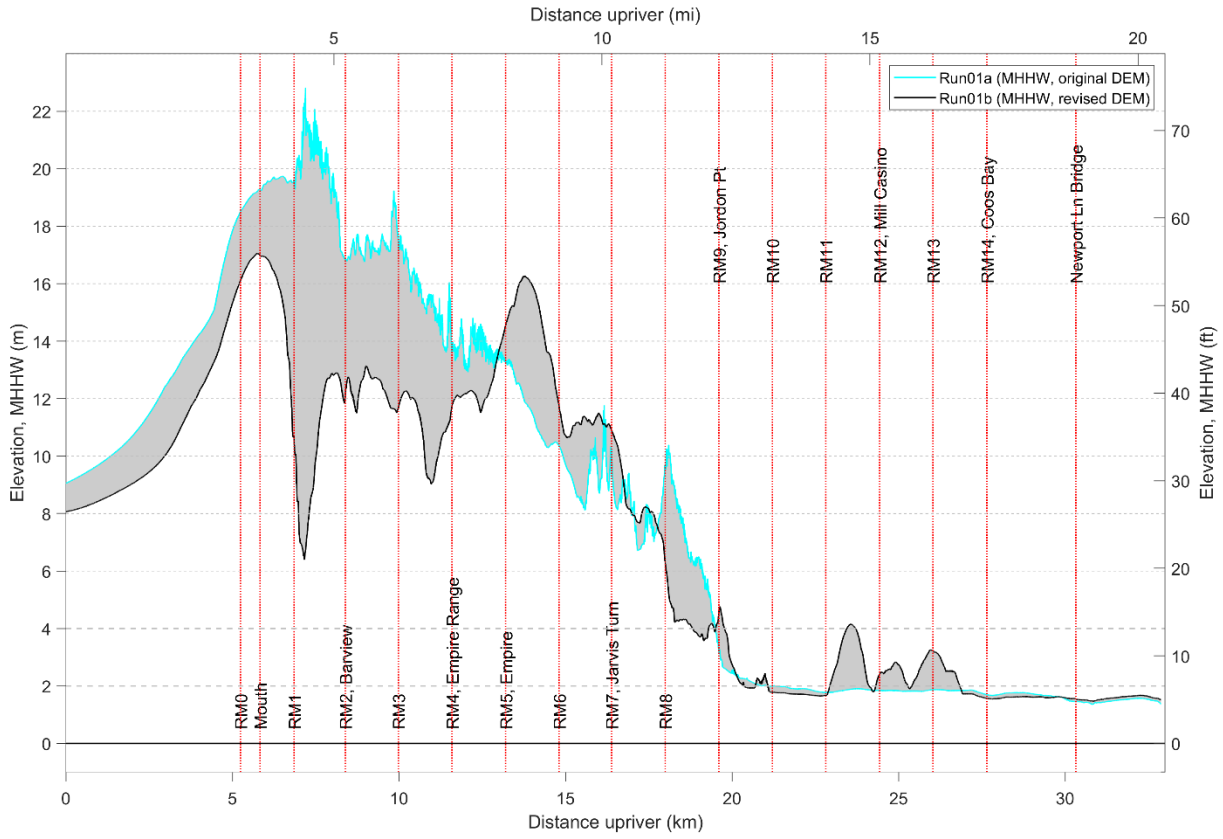

4.2 Dynamic-Tide Results

4.2.1 Tidal effects: flood versus ebb conditions

The addition of dynamic tides introduces a great deal of complexity into the results, due to the nonlinear interaction between tides and tsunamis in the Coos estuary. The predicted maximum velocity exhibits more local extrema along the coast and within the lower estuary, especially near the mouth where the interaction is found to be strongest due to powerful currents and shoaling of tsunami waves (compare **Figure 13** with **Figure 11**). Large differences between the old and new modeling are also observed in the navigation channel, where recent bathymetric changes have been captured (**Figure 14**). Figure 14 shows differences in current velocities between the original modeling (Run01b) compared with the latest results (Run05a), which incorporate dynamic (flood) tide conditions and friction. Velocities less than −0.5 knots (cool colors) indicate that the flood (Run05a) currents dominate, while currents greater than 0.5 knots (warm colors) indicate that original (Run01b) conditions dominate. The region between ±0.5 knots denotes little difference between the simulations.

As can be seen in **Figure 14**, large parts of the estuary (especially on land and in the inter-tidal area of the upper estuary) are characterized with warm colors, which indicate a significant reduction in the overall current velocity. This change is almost entirely a function of the incorporation of friction in our latest modeling (especially on land). **Figure 14** also highlights areas where bathymetric changes have occurred. For example, cooler colors in the navigation channel indicate stronger current velocities associated with the latest simulation effort. This may be attributed to DEM improvements in defining the navigation channel and inter-tidal area between the MCB and the Coos airport. Similarly, warmer colors in the upper estuary (upriver of Jordon Point) indicate that the original modeling produced stronger currents in that region. Thus, improvements in defining areas of shallow bathymetry, especially the inter-tidal area of the upper estuary, cause a general slowing of tsunami currents.

Tsunami wave patterns are highly dependent on the tidal phase at which the tsunamis arrive. The conventional understanding is that tsunamis arriving with a flood spring tide are generally more damaging compared with other tidal stages. To understand these differences we generate a difference map (**Figure 15**), which allows us to compare tsunami currents at ebb stage (Run06a) compared with flood stage (Run05a). In the case of Coos Bay, our analyses confirm the assumption that tsunamis arriving with a flood spring tide are generally more damaging compared with other tidal stages. From **Figure 15** (bright blue colors), this is generally true along the estuary shore between Barview and Empire, as well as parts of the navigation channel (e.g., near Pony Point). Not surprisingly, flood conditions lead to greater inundation on land, evident by the abundant light blue in areas such as the North Spit, at Barview and Empire, along the shore between North Bend and Coos Bay, and in lowland areas adjacent to the Coos River. This difference is almost entirely due to the tidal elevation difference.

The situation becomes very complex in the shallow waters of the lower estuary, where tsunamis arriving at ebb and flood slack are usually more energetic (compare **Figure 15** [ebb], **Figure 16** [flood slack], and **Figure 17** [ebb slack]). As can be seen in **Figure 15**, strong currents dominate the ebb phase (Run06a) offshore the MCB, on the north side of the navigation channel between Barview and Jarvis Turn, near Russell Point, and in the shallower areas of the upper estuary, east of North Bend and Coos Bay. The presence of rings of strong currents southwest of the MCB probably reflects the formation of gyres as the tsunami interacts with a series of rocky reefs near the coast. Strong currents are also observed immediately offshore the North Spit. Tsunamis arriving at flood slack reveal generally stronger current velocities relative to the flood stage across much of the Coos estuary (**Figure 16**), particularly when compared with the generally larger differences (and stronger currents) that characterize flood/ebb tide

conditions (**Figure 15**); see **Figure 2** for an illustration of these different tidal stages. Strong current velocities are apparent even during an ebb slack (**Figure 17**), with our simulation indicating very strong current velocities on the west side of the navigation channel. Ebb slack also contributes to generally stronger currents in the vicinity of Charleston harbor and offshore of the MCB, when compared with a tsunami arriving during flood tide.

Figure 13. Maximum tsunami velocities (in knots) generated for the XXL1 (Run05a) simulation, modeled using dynamic tides, average river flow and friction. Note: timing of the wave arrival coincides with a flood tide at Charleston. Numbers on map are U.S. Army Corps of Engineers river mile locations.

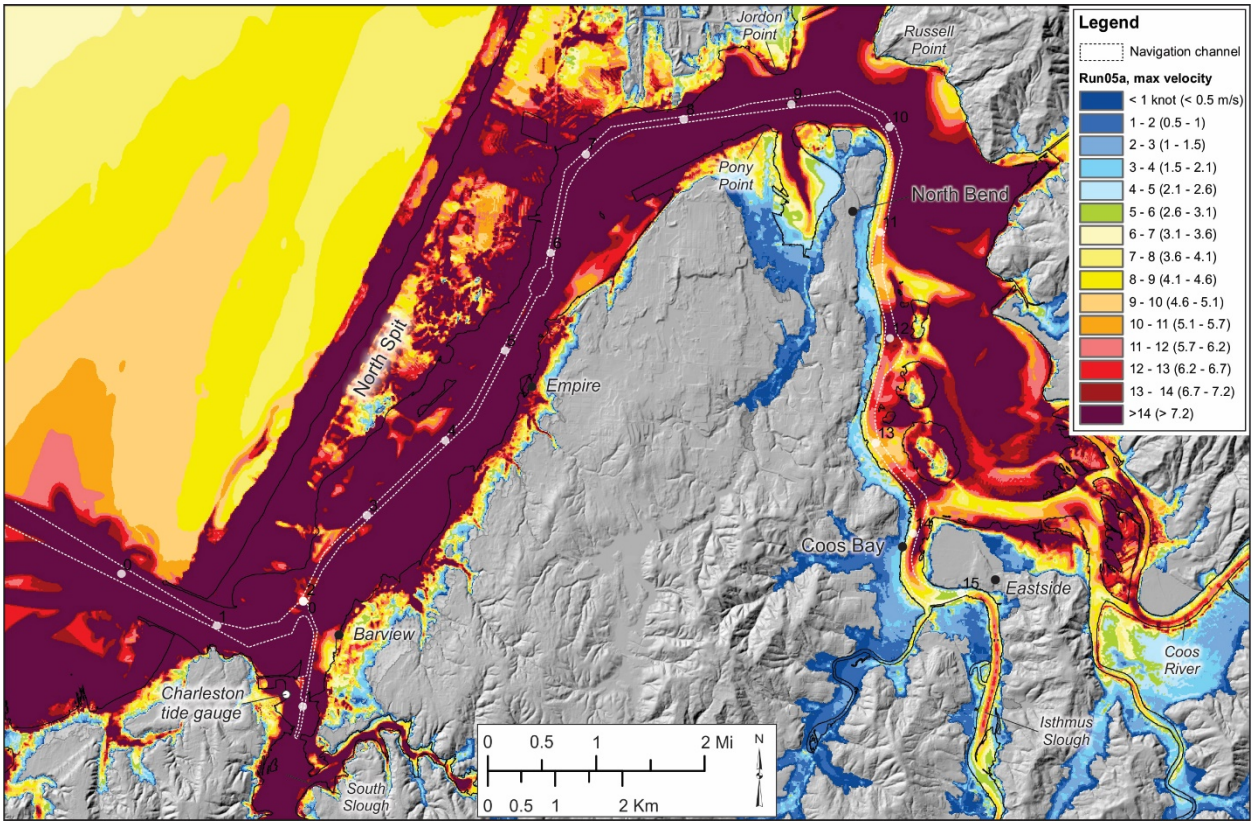

Figure 14. Maximum tsunami velocities (knots) expressed as the difference between original modeling (Run01b) compared with recent modeling (Run05a) that incorporate average river flow and friction. Velocity differences < 0 knots indicate Run05a currents dominate, while velocities > 0 knots indicate that Run01b currents dominate.

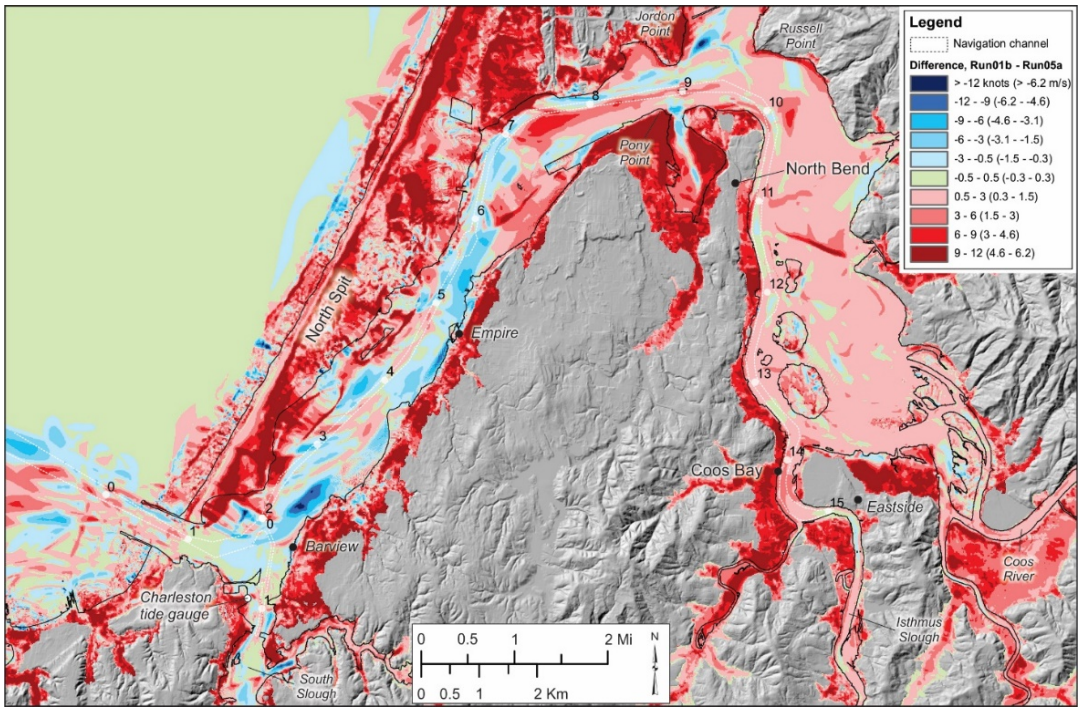

Figure 15. Maximum tsunami velocities (in knots) expressed as the difference between ebb (Run06a) and flood (Run05a) simulations assuming average river flow and friction. Velocity differences < 0 knots indicate Run05a currents dominate, while velocities > 0 knots indicate that Run06a currents dominate.

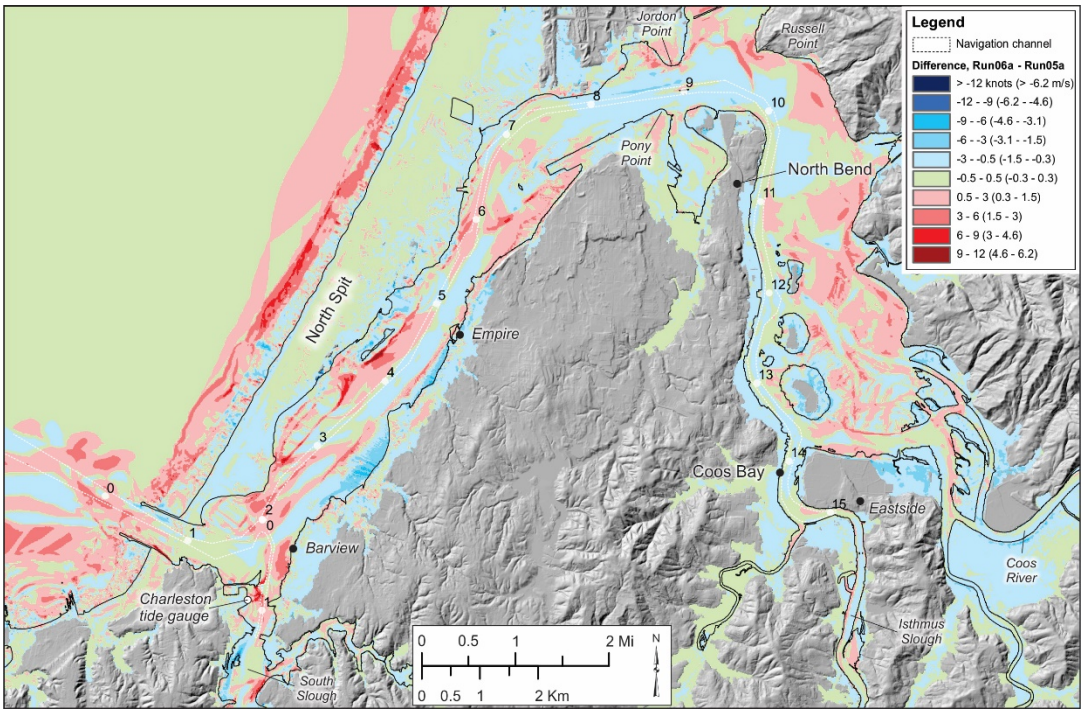

Figure 16. Maximum tsunami velocities (in knots) expressed as the difference between flood slack (Run07a) and flood (Run05a) simulations, average river flow and friction. Velocity differences < 0 knots indicate Run05a currents dominate, while velocities > 0 knots indicate that Run07a currents dominate.

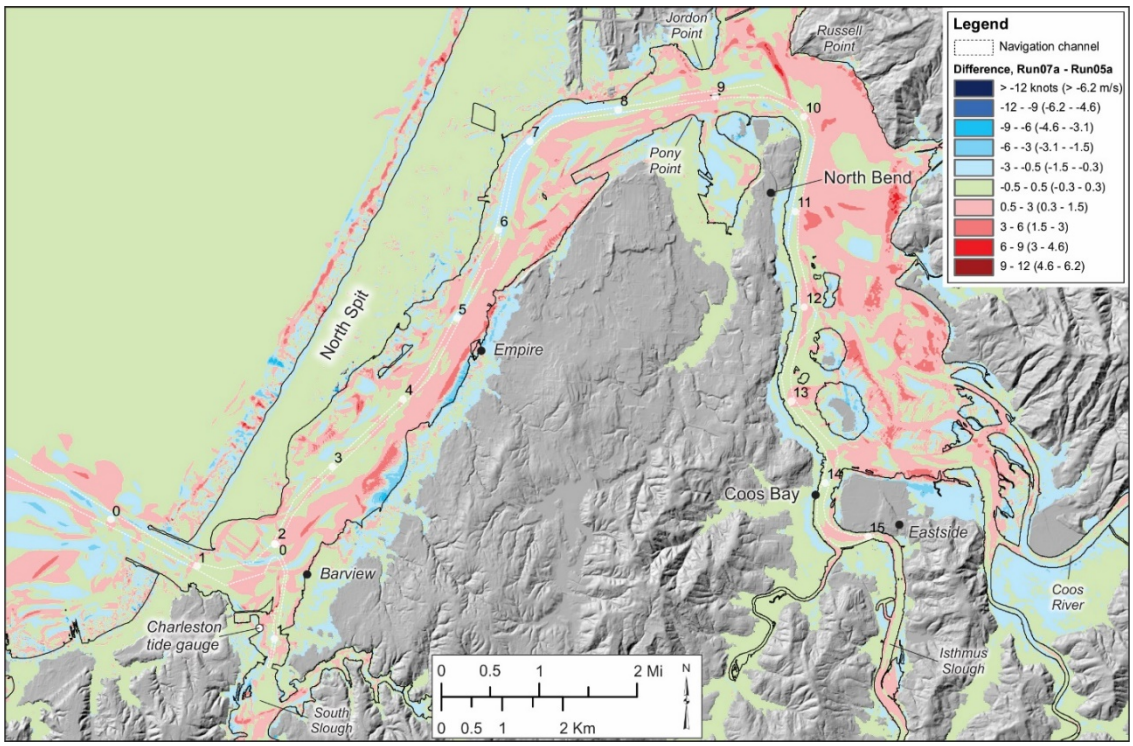

Figure 17. Maximum tsunami velocities (in knots) expressed as the difference between ebb slack (Run08a) and flood (Run05a) simulations, average river flow and friction. Velocity differences < 0 knots indicate Run05a currents dominate, while velocities > 0 knots indicate that Run08a currents dominate.

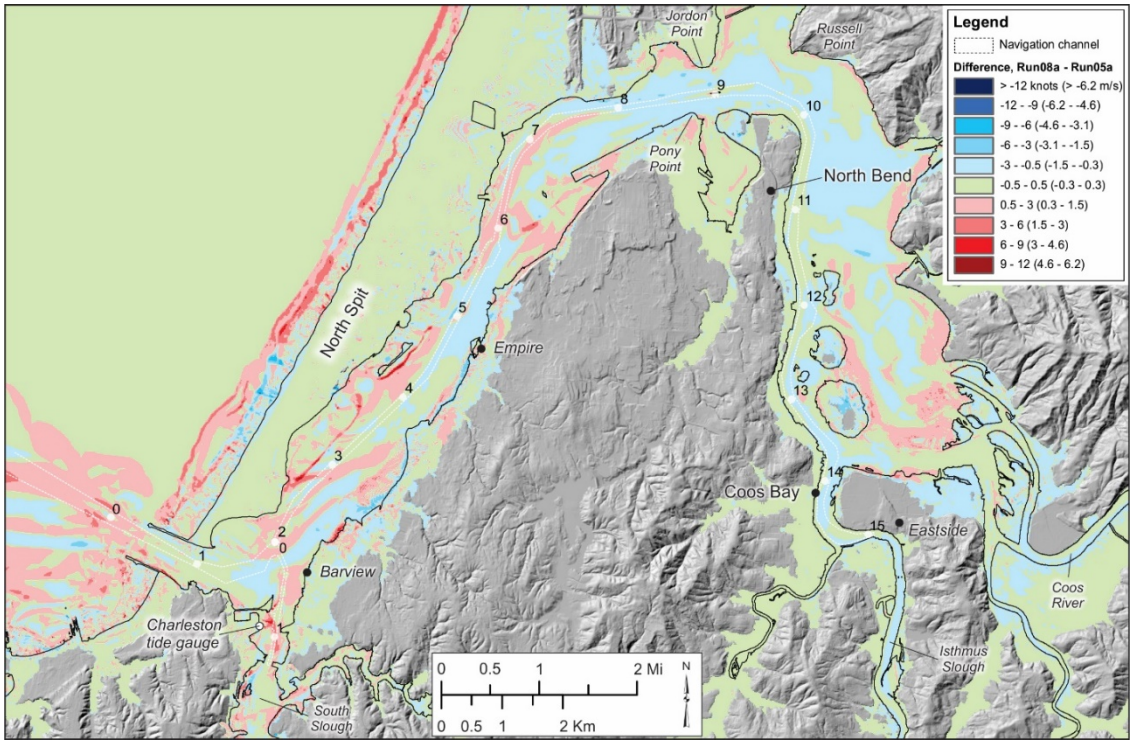

The violent collision between the tidal and tsunami currents at the MCB makes the ebb scenarios especially dangerous for ships of all sizes. **Figure 18** and **Figure 19** present time series information of tsunami currents and water levels for two sites in the Coos estuary: MCB (6) and near Pony Point (15, station locations are identified in **Figure 4**). Unlike our findings at the mouth of the Columbia River (Allan and others, 2018), time series data from Coos Bay suggest there is little difference in the generated tsunami current velocities associated with ebb and flood conditions, at least for the initial tsunami. However, once the first wave has passed, current processes become extremely complex at the mouth as subsequent incoming tsunami waves interact with the drawdown and offshore directed flows associated with the preceding tsunami wave, and with strong outgoing tides. As a result, our results suggest that ebb conditions tend to dominate in later-arriving waves. This is evident in the first major drawdown (t = 0.5) and at t = ~1.5. After 3 hours, the ebb conditions become especially dominant. Upriver near Pony Point, it is evident from **Figure 19** that flood conditions are the predominant force, producing the strongest current velocities. Differences between Coos Bay and the Columbia River are likely to be due to the smaller tidal prism (tidal volume) operating through the Coos estuary, highly irregular channel geometry and morphology, and possibly as a result of significantly lower river discharge.

Unlike current velocities, the water level time series results reveal the opposite response, with the flood scenario exceeding the ebb. As noted previously, this response is entirely due to the different tidal stages on which the tsunamis are arriving. At Jordon Point, the response is a little more complicated due to the outgoing tide coupled with an initial drawdown caused by the approaching tsunami (**Figure 19**). The first peak current during the ebb is slightly lower initially compared with the flood, but subsequent incoming waves result in ebb currents exceeding the flood conditions as water piles up in the estuary. Even at the MCB site, the velocity from the ebb scenario (**Figure 18**, *top*) is actually comparable to the flood case despite the maximum wave heights being noticeably lower (**Figure 18**, *bottom*). This finding can be attributed to the collision of the tsunami waves against opposing currents. Of importance, these collisions appear to prolong the period of strong currents for almost 4 hours. We find similar patterns characterizing the other two earthquake scenarios (L1 and AKMax) modeled in this study.

Figure 18. Time series for Run05a (flood) and Run06a (ebb) showing the modeled *(top) u* and *v* tsunami currents and *(bottom)* water levels at water level station 6 located at the mouth of Coos Bay simulated on an average river flow. Note: positive *u* indicates eastward directed currents, while negative *u* denotes westward directed currents; positive *v* indicates northward directed currents, while negative *v* denotes southward directed currents. Note also how rapidly currents reverse direction and water levels change in the first few hours.

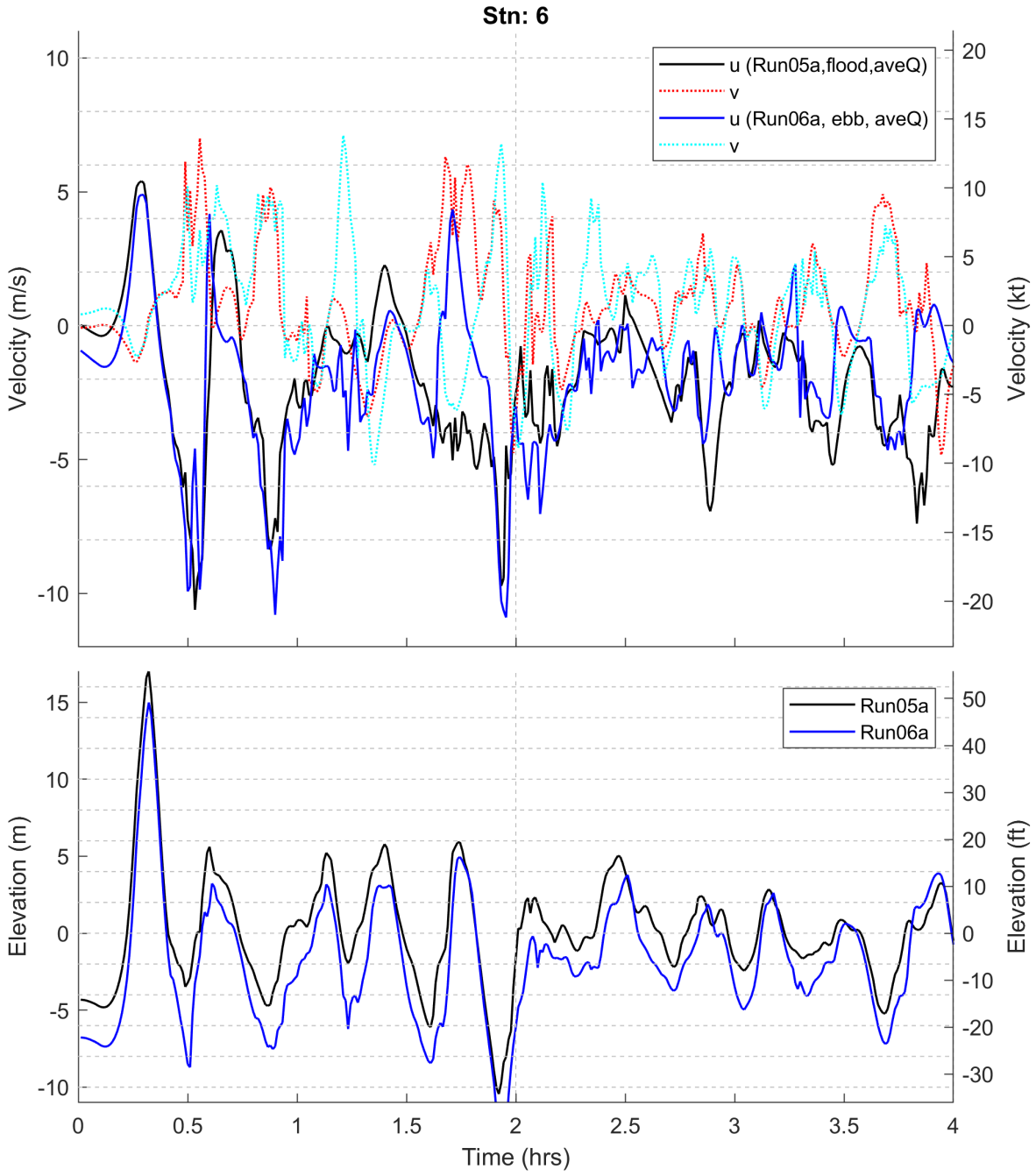

Figure 19. Time series for Run05a (flood) and Run06a (ebb) showing the modeled *(top) u* and *v* tsunami currents and *(bottom)* water levels at water level station 15 located adjacent to Pony Point simulated on an average river flow. Note: positive *u* indicates eastward directed currents, while negative *u* denotes westward directed currents; positive *v* indicates northward directed currents, while negative *v* denotes southward directed currents. Note also how rapidly currents reverse direction and water levels change in the first few hours.

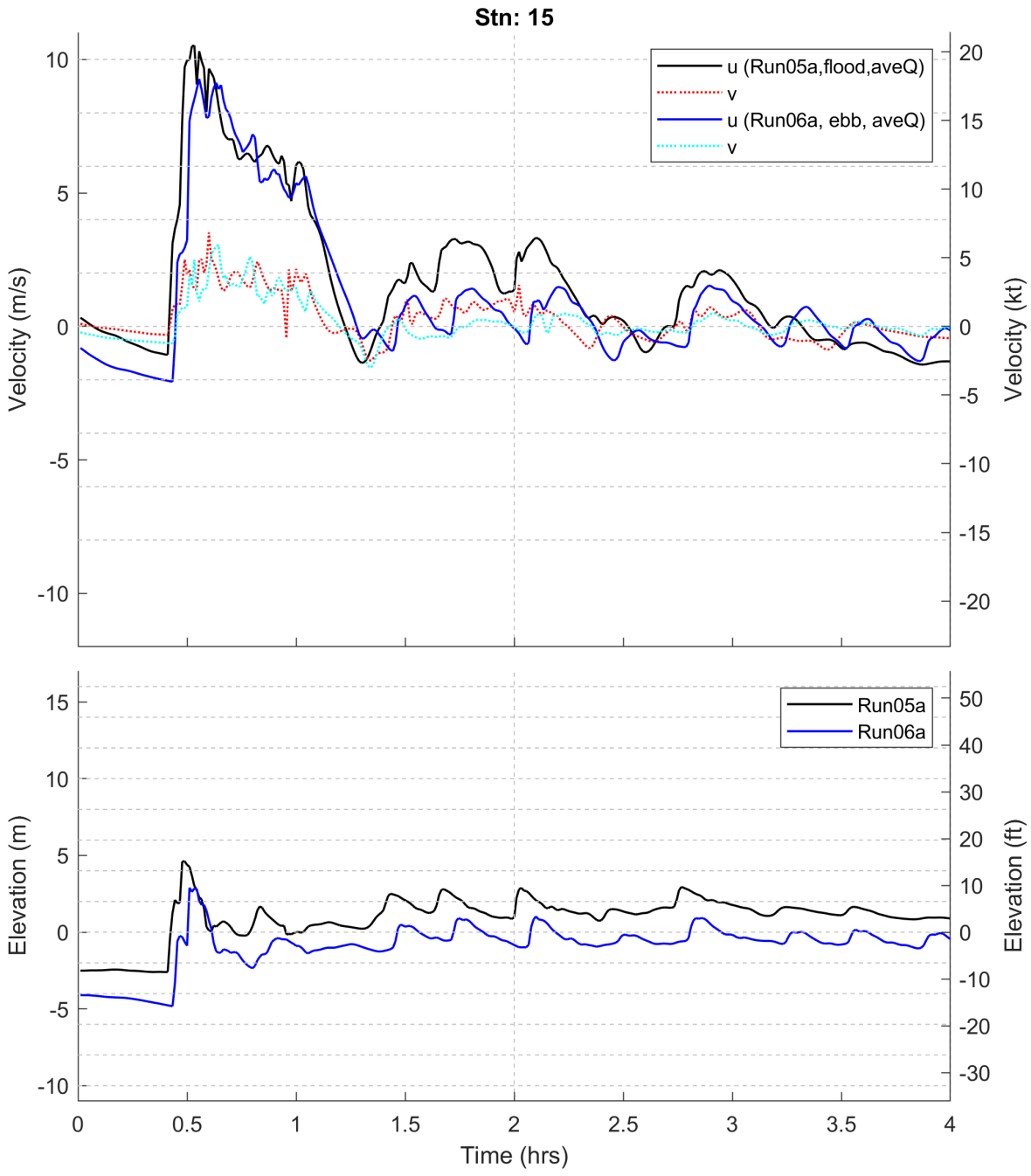

4.2.2 Effects from riverine flows: average and high flow conditions

Figure 20 compares the modeled tsunamis arriving during a high (Run04a) river flow scenario with conditions modeled using the average flow (Run05a), with the tsunami arriving at flood stage in both scenarios. As can be seen from **Figure 20**, our simulation indicates that the high river flow condition actually reduces the tsunami currents across much of the Coos estuary. The exception is a small area on the western side of the navigation channel, between Barview and Empire (RM2 to ~RM6). Seaward of the mouth, tsunami current velocities associated with the high flow (Run04a) scenario are enhanced, producing strong offshore directed jets of currents on both sides of the mouth. This can be attributed to stronger outflows associated with the river flood. Associated with a decrease in overall current velocities, the high river flow regime was found to suppress the maximum tsunami water levels generated. This is discussed further in section 4.3.1. Overall, we conclude that the higher river regime does have an impact on the incoming tsunami waves, suppressing both the generated currents and water levels. Nevertheless, overall we conclude that the tidal component is the primary force affecting both the simulated tsunami currents and water levels observed for this relatively low-flow system.

Figure 20. Maximum tsunami velocities (in knots) expressed as the difference between flood and high river flow (Run04a) and flood (Run05a) simulations. Velocities < 0 indicate Run05a currents dominate, while velocities > 0 indicate that Run04a currents dominate. Numbers on map are U.S. Army Corps of Engineers river mile locations.

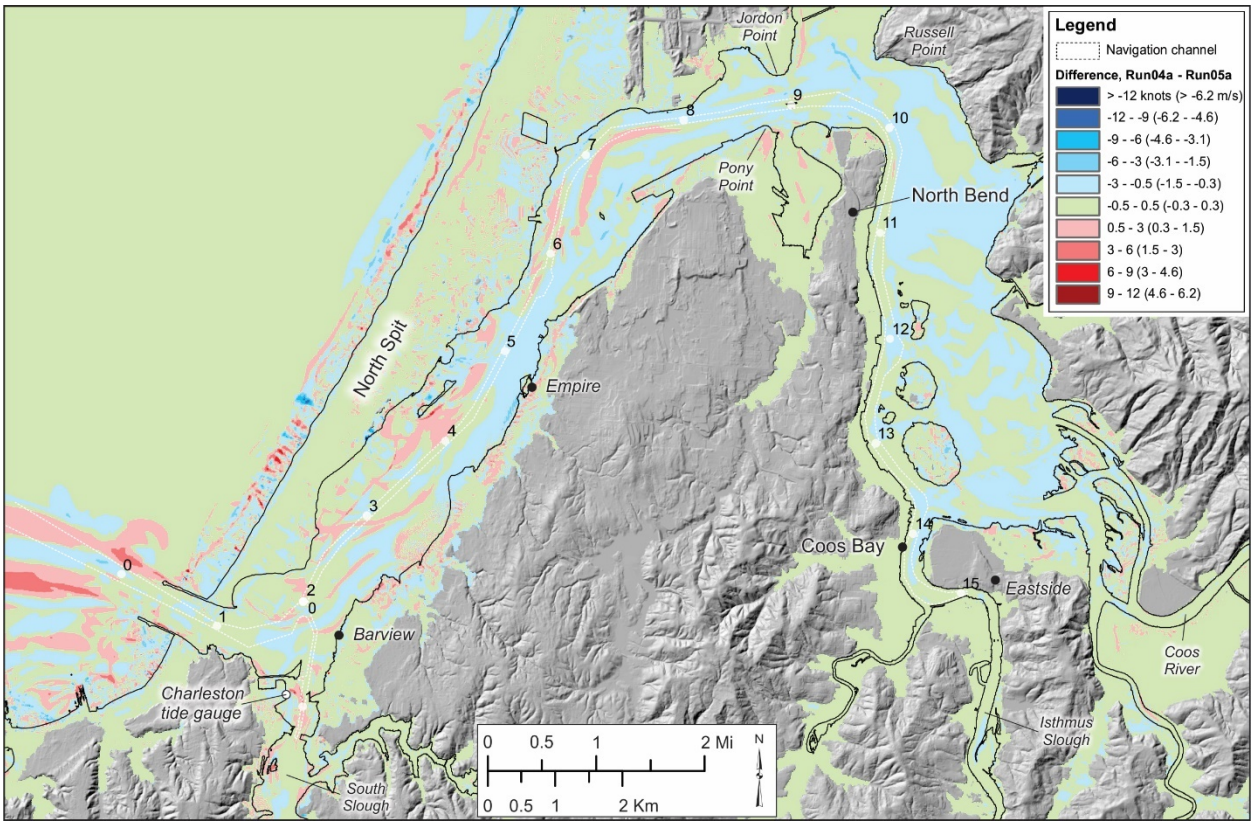

4.3 Wave Arrival Times

Knowledge of tsunami wave arrival times is vital to both terrestrial and maritime evacuation planning, because arrival times determine how much time the public will have to respond. In defining the tsunami arrival times along the Coos estuary, we examined the water level time series determined for a number of key stations within the system, the locations of which are presented in **Figure 4**. Tsunami wave arrivals were defined on the basis of three criteria:

1. An initial wave arrival time, which reflects the moment at which the water level begins to depart from the normal background tidal signal;
2. The time at which the maximum water level is reached for the first wave; and
3. The time associated with the peak water level.

The reason for the latter is that although the first wave generally produces the highest water level, several upriver sites (e.g., Coos Bay) were identified where the maximum water level occurred later.

4.3.1 Local Cascadia tsunami wave arrival times

Figure 21 presents the XXL1 wave arrival times for select sites along the Coos estuary, while **Figure 22** shows an ensemble of the maximum tsunami water levels determined from the various simulations along the length of the navigation channel; a detailed description of the final ensemble maps is provided in section 5. Included in the latter figure are the expected wave arrival times at various locations along the river channel.

As can be seen in **Figure 21** and **Figure 22**, the largest tsunami waves are concentrated at the MCB, where the tsunami waves reach ~17 m (55 ft) in height. Between the mouth and RM2, there is a noticeable decrease in the tsunami water levels (**Figure 22**). This can attributed to a combination of the abrupt change in channel configuration in this area (east-west at the mouth, before changing to a north-south channel orientation), the tsunami having reflected away from the community of Barview, and the reflection of the tsunami away from the open coast beaches and bluffs causing an offshore directed drawdown. Water levels remain high for most scenarios until approximately RM8 (**Figure 22**). A secondary peak near Empire (RM5) can be attributed to the tsunami in the navigation channel (now directed northward) combining with the westward arrival of the tsunami as it crosses the North Spit.

Between RM8 and RM10 (i.e., near Jordon Point) the maximum tsunami water levels fall significantly, dropping from ~6–9 m high (20–30 ft) to about 1–2 m (3–6 ft) in the upper estuary. As noted earlier, the decrease in the tsunami water levels reflects the change in estuary morphology, beginning at Pony Slough, before opening up even more into the larger upper estuary. These changes can thus be explained in terms of the meandering shape of the estuary channel, which helps dissipate the tsunami energy, as well as the general shallowing in the upper estuary upriver of Jordon Point. Our results confirm also that the flood scenario (Run05a) produces the farthest upriver penetration of the tsunami, which extends well up the Coos River (not shown). Finally, flatlining of the tsunami water levels near Coos Bay (**Figure 22**, Run06a and Run08a) is caused by a combination of the strength of the ebb flow and attenuation of the tsunami by the sinuous channel morphology upriver of Jordon Point, which essentially wipes out all tsunami energy. As a result, the maximum water level elevation in these areas is mostly determined by the river flow, which induces a small surface slope and thus the flatline.

The local tsunami arrives at the MCB ~7 minutes after the start of earthquake shaking, while the peak wave arrives some 12 minutes later. Thus, the tsunami maxima at the mouth occurs about 19 minutes following the onset of shaking (**Figure 21**); all times shown in Figure 21 are relative to the start of earthquake shaking. Initial wave arrivals at Barview and Charleston are 13 and 16 minutes, respectively.

Having entered the estuary, the tsunami takes an additional 4–8 minutes to reach its maximum. At Jarvis Turn (RM7) the initial tsunami arrival is about 1 minute faster compared with at Empire. This is because of the tsunami arriving across the North Spit compared with the wave propagating north up along the channel. The tsunami reaches Jordon Point at 25 minutes, and 14 minutes later the tsunami begins to inundate Coos Bay (**Figure 21** and **Figure 23**). As can be seen at several upper estuary stations, the time to the maximum tsunami wave is not necessarily the first wave. For example, the maximum water levels are reached at Coos Bay some 2.3 hours after the start of earthquake shaking, while farther up the Coos River maximum water levels occur 2.5 hours after the start of earthquake shaking.

Figure 21. Tsunami wave arrival times defined for XXL1 (local) for discrete locations along the Coos estuary. Times reported are in minutes. Red numbers correspond to the initial wave arrival (the point at which the water level begins to depart from normal), while black numbers reflect the time at which the maximum wave arrives. Background image reflects the integration of the maximum water levels determined from all XXL1 model simulations to form an "ensemble" result of maximum water levels. Example water level time history plot is for station 6 at the mouth of the Coos Bay (MCB).

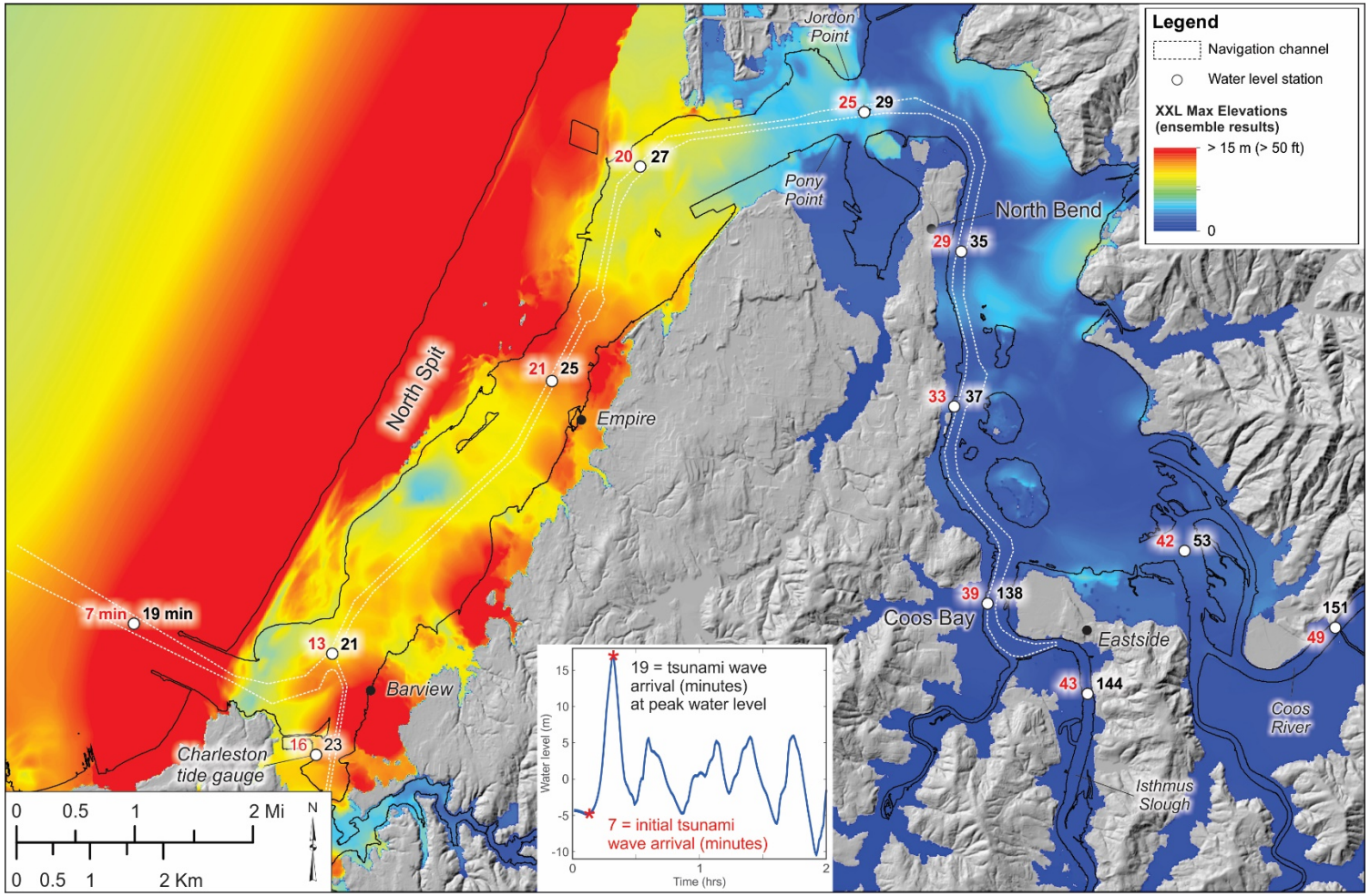

Figure 22. Maximum tsunami water levels interpolated along the Coos estuary navigation channel for various XXL1 (local) simulations. Gray shading covers the spectrum of responses associated with various tidal stages modeled using an average river flow. RM is river mile.

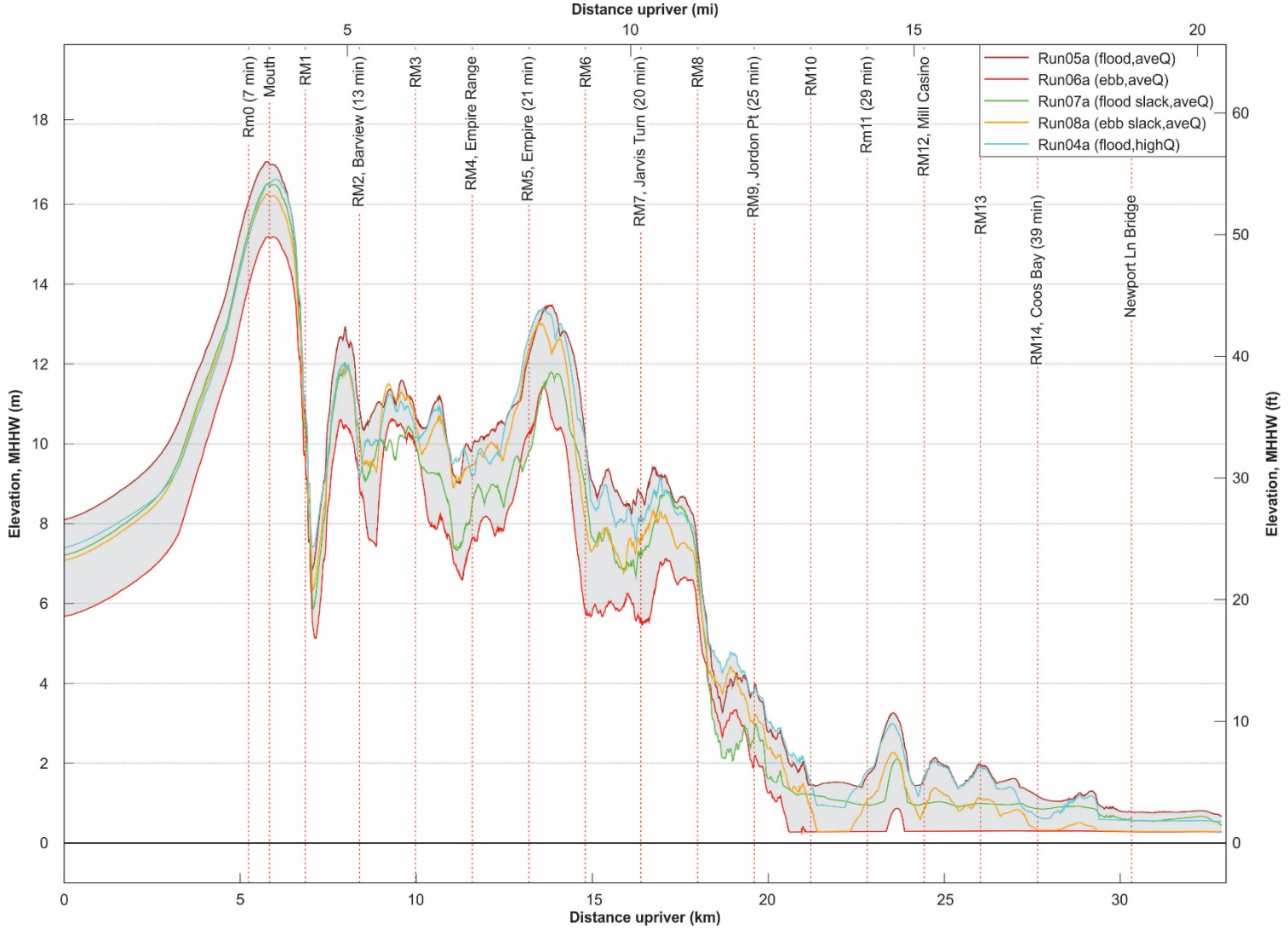

To better understand the timing of the tsunami wave sequence travel and arrival at sites upriver from MCB, we performed a wavelet analysis[10] (e.g., Torrence and Compo, 1998) of the tsunami frequency bands for selected sites along the Coos estuary. This approach allows for a more rigorous assessment of differences in the power within the tsunami time series (essentially the time-varying frequency content of the tsunami signal), allowing us to more definitively track the tsunami as it travels. As noted by Torrence and Compo (1998), converting a time series of water levels into time-frequency space allows one to determine the dominant modes of energy variability and, further, how those modes change over time. Essentially, the approach allows one to track the dominant energy signal of the tsunami as it propagates upriver.

Figure 23 presents the results of the wavelet analysis for two sites in the Coos estuary: Jarvis Turn (RM7, station 13) and the upper Coos River (station 29). The plots indicate that most of the power in the tsunami signal is concentrated in the tsunami band for periods ~2 hours (the left y-axis), with some energy also present at both higher and lower frequencies. The change in the tsunami power over time is captured on the x-axis (time in hours), which shows the signal over 24 hours (the length of the model simulation). The shaded regions on either end (shaped like the keel of a boat) indicate the "cone of influence (COI)," where edge effects become important and errors are introduced from the analyses. The latter occurs because the approach assumes the time series is cyclic. As a result, below the COI line, the results are not considered to be significant.

At Jarvis Turn, the initial peak signal in the time domain occurs at ~27 minutes and is consistent with the peak wave arrival time for Jarvis Turn presented in **Figure 21**. Additional peaks occur at 43 minutes and at 2, 2.6, and 4.1 hours (**Figure 23**) as additional tsunami waves arrive at the site. Of importance, the dominant energy signal at Jarvis Turn is strongest during the first 5–7 hours after the earthquake, with the bulk of the energy expended by hour 10, and negligible by hour 15. In the upper Coos River, the peak signal occurs ~ 1 hour after the earthquake, and there is significantly less energy in the signal compared with the Jarvis Turn station.

[10] https://noc.ac.uk/business/marine-data-products/cross-wavelet-wavelet-coherence-toolbox-matlab

Figure 23. Wavelet analysis of the XXL1 (local, Run05a) tsunami water level time series at Jarvis Turn (RM7) and in the upper Coos River. Hot colors indicate significant energy; shaded regions on either end indicate the "cone of influence," where edge effects become important; solid contour is the 95% confidence level. Time (x axis) in hours is after the earthquake.

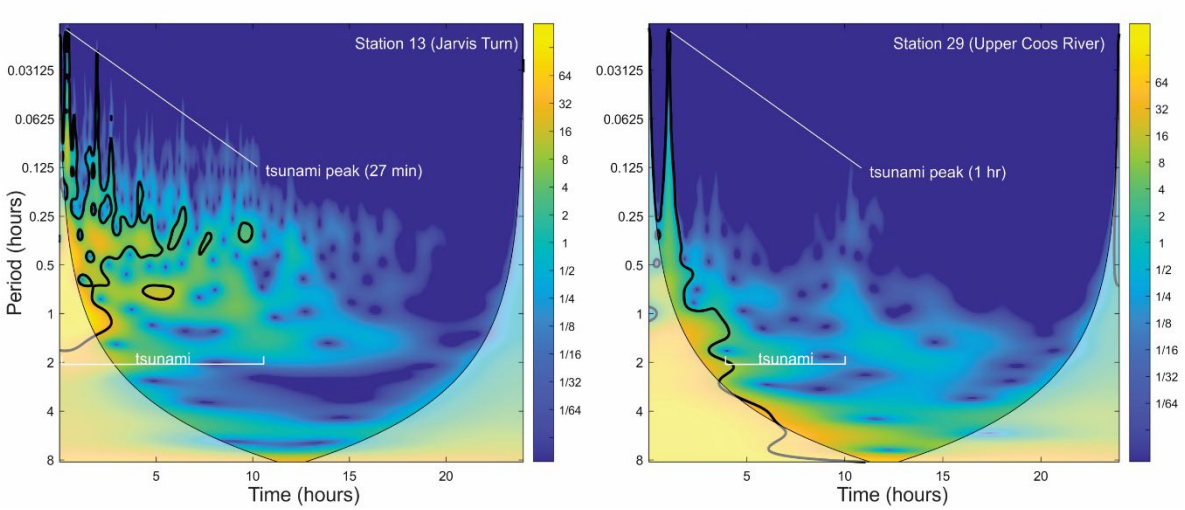

4.3.2 Distant (AKMax) tsunami wave arrival times

The AKMax distant tsunami reaches the MCB ~4 hours after the earthquake, with the wave maximum occurring ~11 minutes later after the water levels began to rise (**Figure 24**). Within the Coos estuary, the initial peak tsunami wave is typically reached ~6–9 minutes after the wave begins to arrive. Longer wave arrival times for the maximum wave are evident in the upper estuary at Coos Bay (e.g., 7 hours after the earthquake) that are caused by later arriving tsunami waves.

Figure 25 shows the maximum tsunami water levels for the various simulations along the length of the navigation channel. Included in the figure are the expected wave arrival times at various locations along the river channel. We also include results from the 1964 Alaska tsunami (solid black line) because this event represents the largest distant event to have impacted the Oregon coast in modern history.

As can be seen in **Figure 25**, the largest tsunami waves are concentrated at the MCB, where the eastern Aleutian tsunami reaches ~5.8 m (19 ft) in height. Between the mouth and RM2, there is a noticeable decrease in the tsunami water levels similar to what we saw for the local XXL1 scenario (**Figure 22**). This is caused by a combination of the abrupt change in channel configuration in this area (east-west at the mouth, before changing to a north-south orientation in the channel), the tsunami having reflected away from the community of Barview, and the reflection of the tsunami away from the open coast beaches and bluffs causing an offshore directed drawdown. Water levels remain high for most scenarios until approximately RM8 (**Figure 25**). Upriver of RM8, maximum water levels decrease significantly.

Apparent in **Figure 25**, ebb tide conditions dominate the tsunami, effectively muting its effect throughout much of the Coos estuary, the exception being the open coast and at the MCB. This strongly suggests that any distant tsunami arriving during an ebb tide is unlikely to cause significant flooding and accompanying damage. The exception will be the area in the vicinity of Charleston harbor and the harbor itself.

Figure 24. Tsunami arrival times defined for AKMax (distant) for discrete locations along the Coos estuary. Times reported are in minutes and are relative to the initial (4 hr) wave arrival at the mouth of Coos Bay (MCB). Red numbers correspond to the initial wave arrival (the point at which the water level begins to depart from normal), while black numbers reflect the time at which the maximum wave arrives. Background image reflects the integration of the maximum water levels determined from all AKMax model simulations to form an "ensemble" result of maximum water levels. Example water level time history plot is for virtual water station 6 at the MCB.

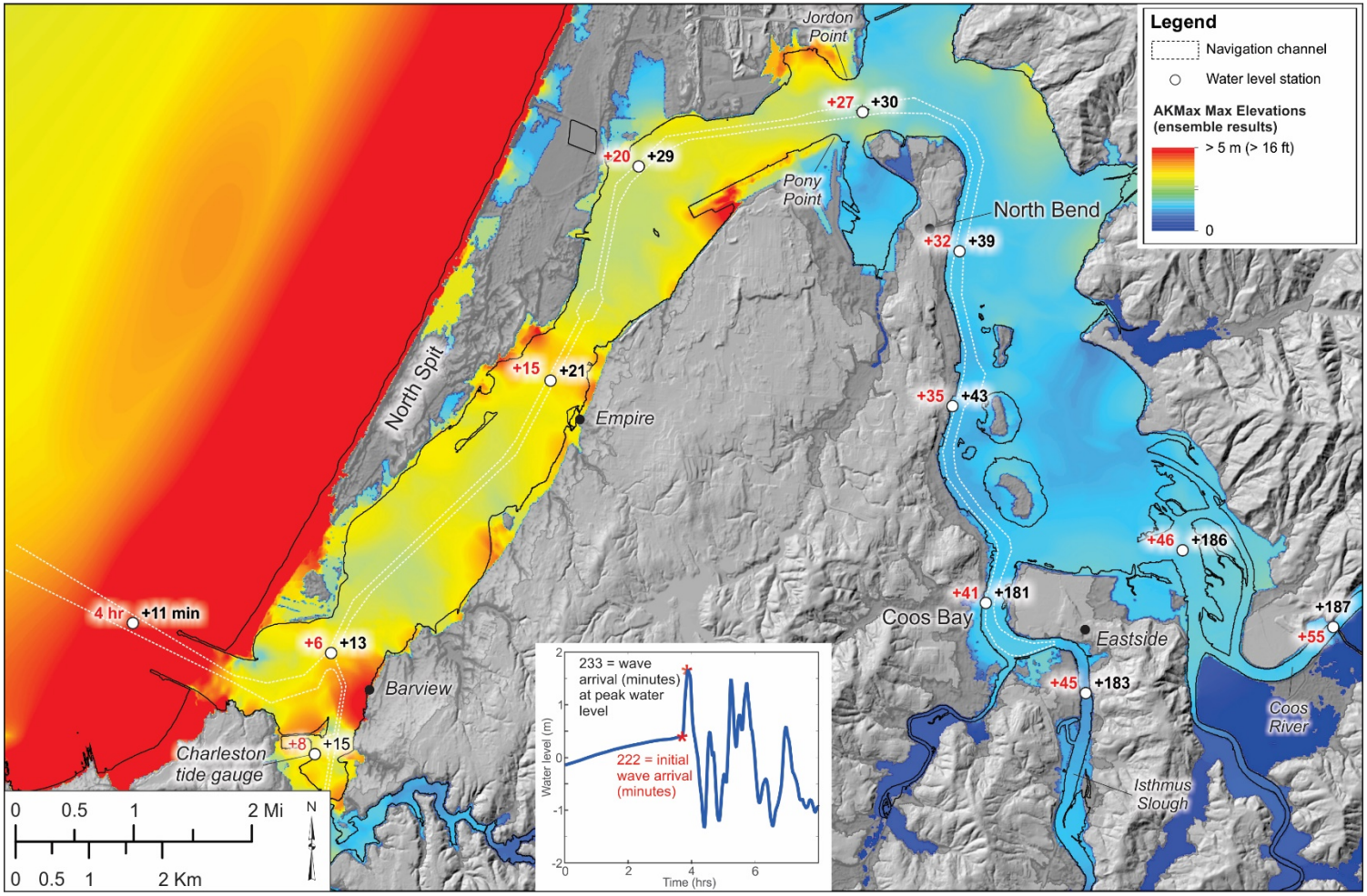

Figure 25. Maximum tsunami water levels interpolated along the Coos estuary navigation channel for various AKMax simulations. Included in the plot are the expected wave arrival times. Gray shading covers the spectrum of responses associated with various tidal stages modeled using an average river flow. RM is river mile.

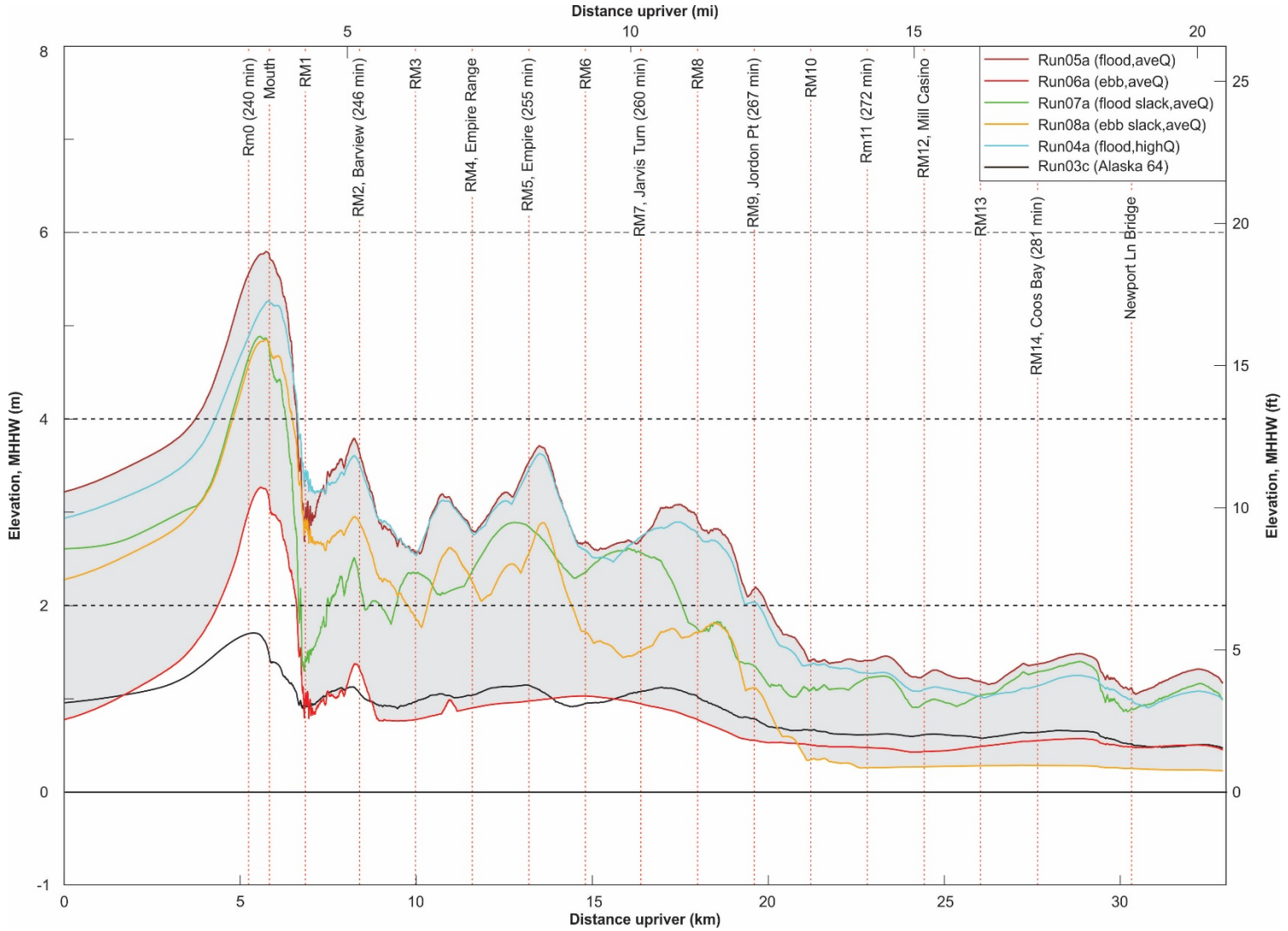

As noted previously, the initial tsunami reaches Coos Bay in ~4 hours (**Figure 24** and **Figure 25**). The tsunami can be tracked up the Coos estuary using wavelet analysis as shown in **Figure 26.** At Jarvis Turn, the tsunami may be identified by an initial peak, indicating the tsunami arrives at ~268 minutes, followed by several other ensuing peaks. Overall, the tsunami persists for at least 10 hours (highlighted by the bright yellow shading at a period of 1 hour in Figure 26). A second period of tsunami activity occurs later between 15 and ~18 hours. The period in between hour 10 and 15 coincides with low (ebb) tide such that the incoming tsunami waves are effectively dampened. However, with the transition to high tide, the tsunami is once again able to penetrate easily up the estuary. This effect is even more apparent at station #29 located well up the Coos River, at the juncture between the Millicoma and Coos River south fork. Nevertheless, by hour 15, there is effectively little energy left and the distant tsunami can be effectively ignored upriver of this station.

Figure 26. Wavelet analysis of the AKMax (distant, Run05a) tsunami water levels time series at Jarvis Turn (RM7) and in the upper Coos River. Hot colors indicate significant energy; shaded regions on either end indicate the "cone of influence," where edge effects become important; solid contour is the 95% confidence level. Time (x axis) in hours is after the earthquake.

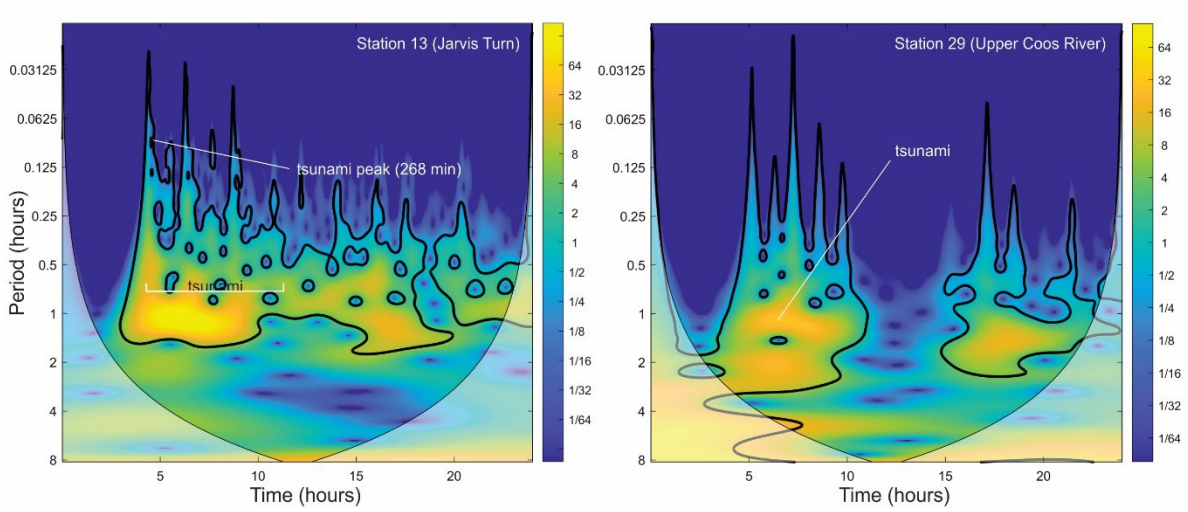

5.0 ENSEMBLE MODEL RESULTS

Due to uncertainties in the timing of a local or distant tsunami event, coincident with different tidal stages and Coos River flow regimes, we derive "ensemble" modeling results for each earthquake source. The approach effectively combines maximum water levels, currents, vortices, and minimum water levels for each scenario into a single merged raster for each of these parameters. This allows us to incorporate the uncertainty characterized by the range of tsunami/tide/flow combinations, providing a more conservative model estimate of the tsunami effect for incorporation into appropriate response guidance. To generate the ensemble product, we produced individual rasters for each model simulation in Esri ArcGIS® and for each of the previously mentioned parameters. We then created the ensemble raster by using the ArcGIS "mosaic to new raster" tool with the maximum value defined for each grid cell; for the minimum flow depth, we used the minimum value assigned to the grid cell.

5.1.1 Local (XXL1 and L1) tsunami ensemble results

5.1.1.1 XXL1 and L1 water levels

Figure 27 presents the merged water levels for both an XXL1 and an L1 local event. The plots demonstrate two contrasting responses: the extreme water levels that will be experienced along the open coast (hot colors), and the generally much lower water levels (cool colors) upriver of Jordon Point. Between these two areas is a large region in which the water levels are expected to be highly variable (varying shades of yellow to red), with localized peaks at Barview (~ 11 m [36 ft] in the channel) decreasing to 4 m (13 ft) at Pony Point, relative to MHHW for an XXL1 size event. Although high tsunami water levels will also be experienced during the L1 event, it is evident from **Figure 27** (*bottom*), the effects are not as extreme when compared to the maximum considered XXL1 event. Overall, L1 water levels tend to be ~4 m in the channel at Barview, before decreasing to ~3 m near Pony Point. Both figures highlight several sites at the shore where tsunami flooding (and hence damage) is likely to be extreme (red colors), including Charleston and the section of shore between Barview and Empire. Catastrophic conditions will characterize both scenarios, especially adjacent to the MCB, while damaging waves and strong currents will affect much of the area within the Coos estuary, especially between the MCB and Pony Point (**Figure 27**).

Figure 27. Ensemble model results of the maximum tsunami water levels (flow depth–depth) generated by a *(top)* XXL1 and *(bottom)* L1 Cascadia subduction zone (local) earthquake. Cartoon showing water level time history and attributes is for virtual water station 6 at the mouth of Coos Bay (MCB). Numbers on map are U.S. Army Corps of Engineers river mile locations.

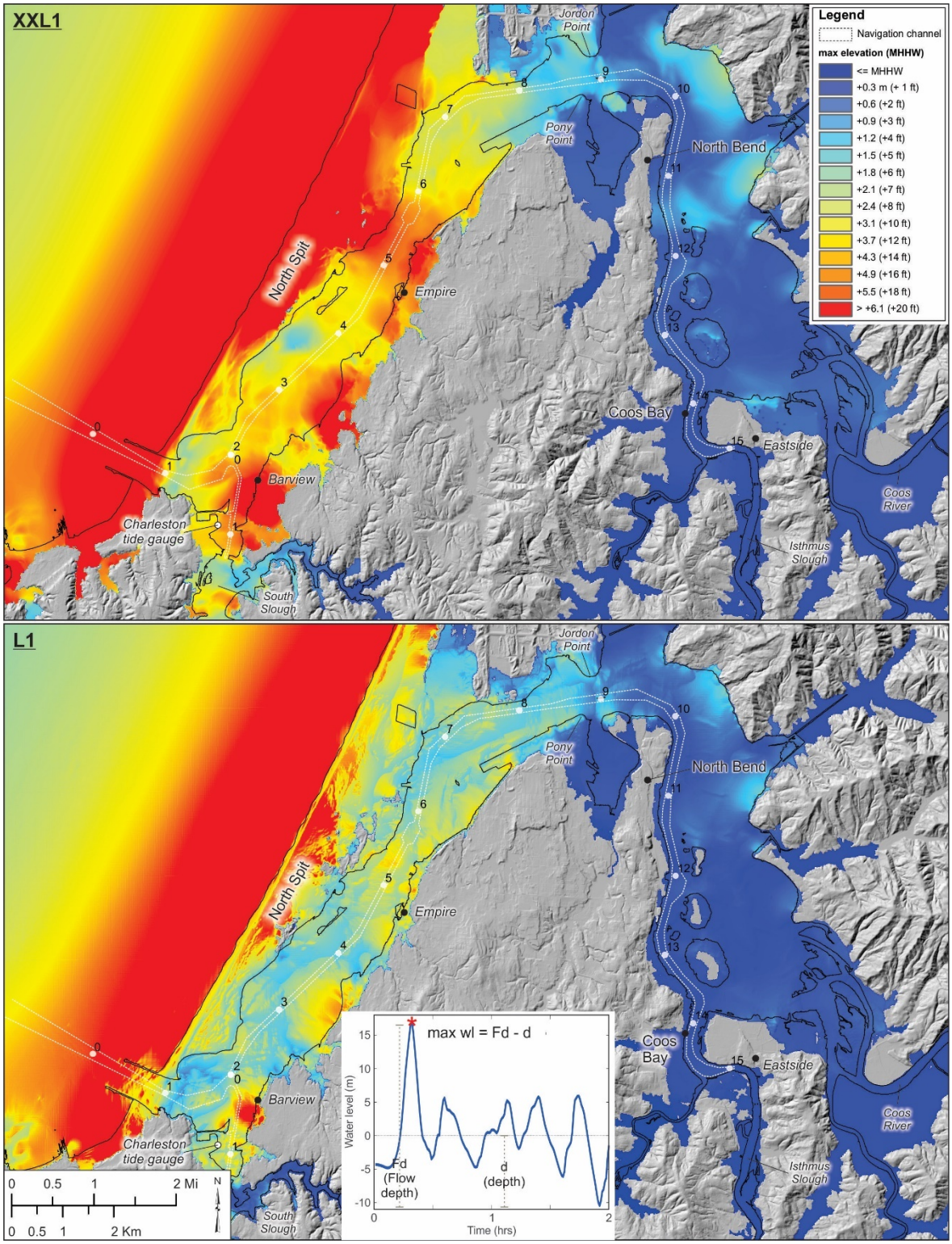

Time series information for select stations along the river is presented in **Figure 28** (XXL1) and **Figure 29** (L1). These data have been truncated to span the first 12 hours of the simulations, providing improved insight into the variability and range of modeled water levels, while the datum used is MHHW. The gray shading in each plot defines the envelope (range) of variability from the combined suite of simulations. Differences in the y-axis scales shown in Figure 28 and Figure 29 are indicative of differences in the magnitude of the tsunami generated by the XXL1 and L1 scenarios. Both time series highlight the extreme nature of the tsunami waves at the MCB (station 6), which decreases rapidly by the time the tsunami reaches Pony Point (station 15). At Coos Bay (station 31), the tsunami wave reflects a large bore (~ 2.5 m [8 ft] high) with a steep wave front with water levels remaining high for at least 6 hours before subsiding. However, as indicated previously, tsunami waves will continue to impact the area for at least 10 to 15 hours after the event before subsiding.

Figure 28. Time series showing the modeled water levels (flow depth–depth) for two simulations of a Cascadia subduction zone tsunami (XXL1) traveling along the navigation channel from the mouth of Coos Bay (MCB) to the town of Coos Bay. Gray shading denotes the envelope of variability in the water levels from all simulations. Stn is virtual water level station.

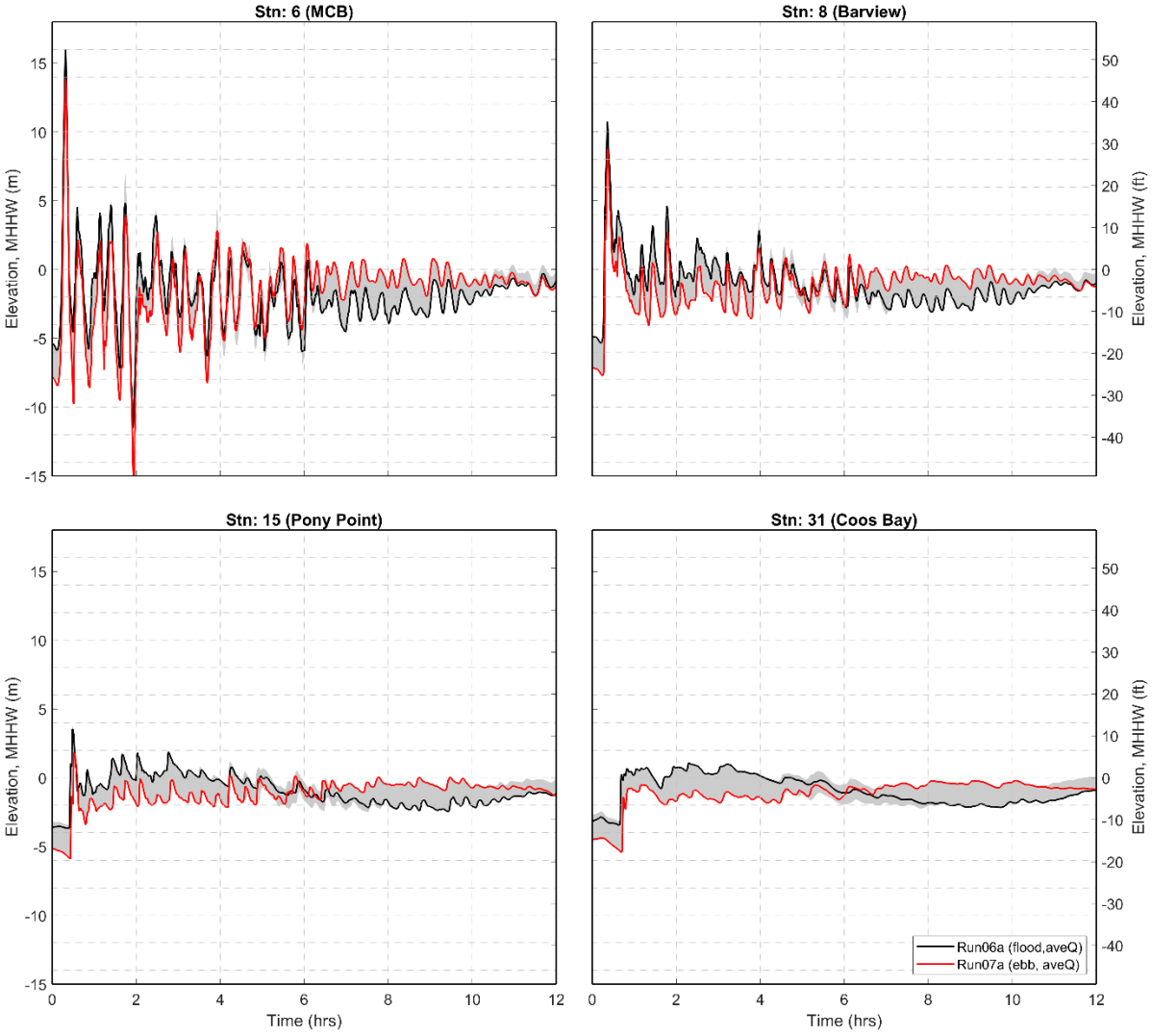

Figure 29. Time series showing the modeled water levels (flow depth–depth) for two simulations of a Cascadia subduction zone tsunami (L1) traveling along the navigation channel from the mouth of Coos Bay (MCB) to the town of Coos Bay. Gray shading denotes the envelope of variability in the water levels from all simulations. Stn is virtual water level station.

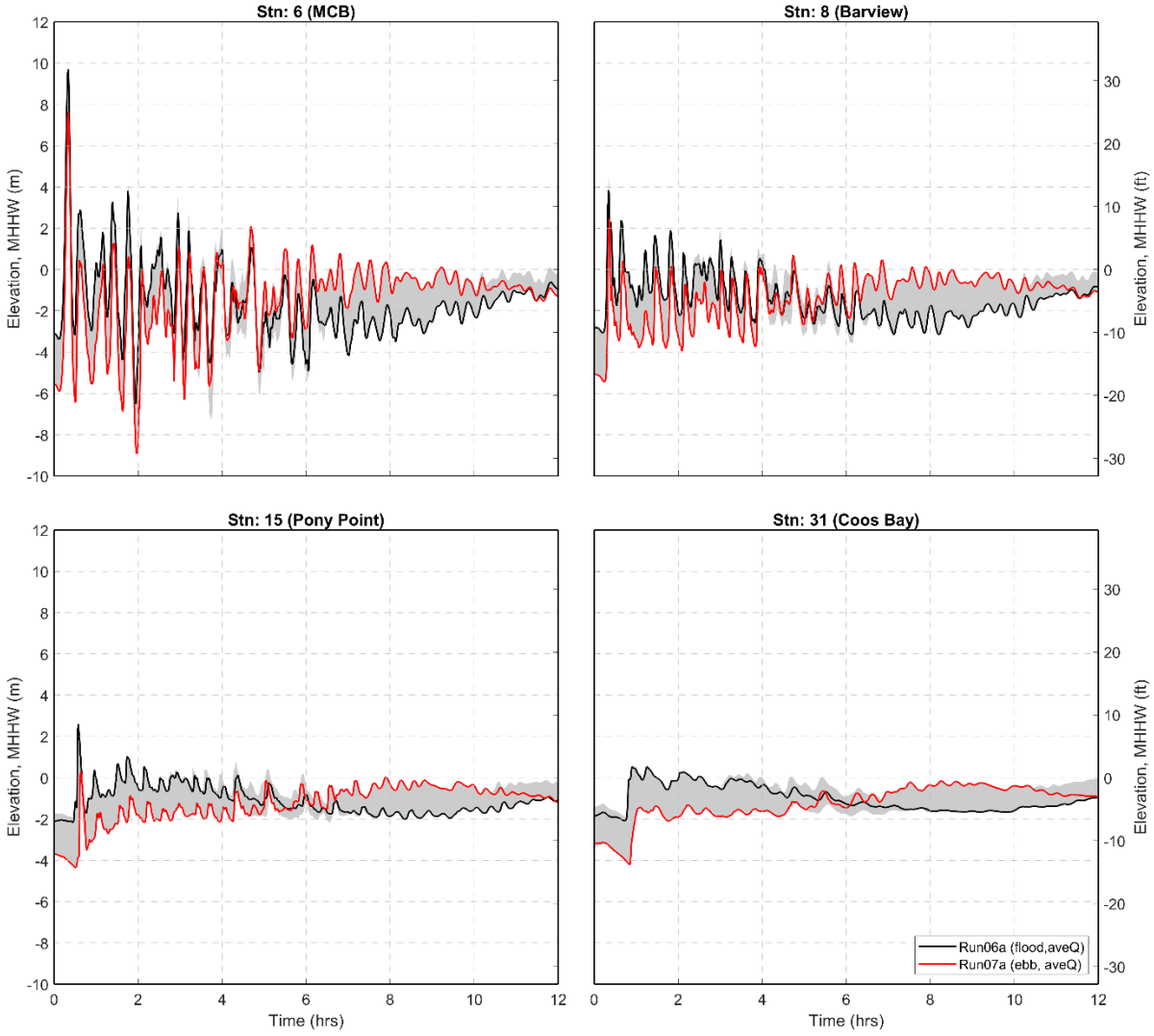

5.1.1.2 XXL1 and L1 tsunami currents

Figure 30 presents the modeled currents for the Coos estuary. For the purposes of assisting with maritime guidance, we have binned the current velocities into five categories consistent with the work of Lynett and others (2014). In general, current velocities exceeding 4.5 m/s [> 9 knots] were found to result in extreme damage to ports and harbors, while little to no damage was found to occur at velocities < 1.5 m/s [< 3 knots].

Modeling of the tsunami currents for an XXL1 event indicates catastrophic conditions will predominate across much of the Coos estuary (**Figure 30**, *top*). In this scenario, extreme currents (> 4.5 m/s [> 9 knots]) will affect all major ports in the estuary and damage is expected to be catastrophic. Damaging currents generated by the L1 scenario are not as severe as with the maximum considered XXL1 event. For the L1 scenario we find that extreme currents (> 4.5 m/s [>9 knots]) will also impact much of the estuary. Although damaging currents are expected to be observed in the vicinity of the town of Coos Bay, our modeling indicates that under the L1 scenario the tsunami currents are likely to be mainly in the range of 1.5 to 4.5 m/s [3 to 9 knots] (**Figure 30**, *bottom*).

Differences in the simulated current velocities become most apparent when one compares the time series of modeled currents for both XXL1 (**Figure 31**) and L1 (**Figure 32**). As can be seen for both figures, strong currents decrease rapidly upriver of the MCB due to the meandering shape of the estuary channel, which helps to dissipate the tsunami energy, in response to collisions with tsunami crossing over the North Spit from the west, the presence of numerous bars and islands (especially near Coos Bay) and the general shallowing in the upper estuary. In particular, there is a significant decrease in the current velocities in both scenarios upriver of the town of Coos Bay, where the currents drop to ~ 1.5–2 m/s [3–4 knots]. Farther up the Coos River, conditions improve significantly. For example, at the confluence of the Millicoma and Coos River south fork, the modeled XXL1 currents fall below the critical 1.5 m/s [3 knot] threshold (**Figure 31**); the modeled L1 currents are almost entirely below that threshold (**Figure 32**).

Figure 30. Ensemble model results of the maximum tsunami currents generated by a *(top)* XXL1 and (*bottom)* L1 Cascadia subduction zone earthquake. Numbers on map are U.S. Army Corps of Engineers river mile locations .

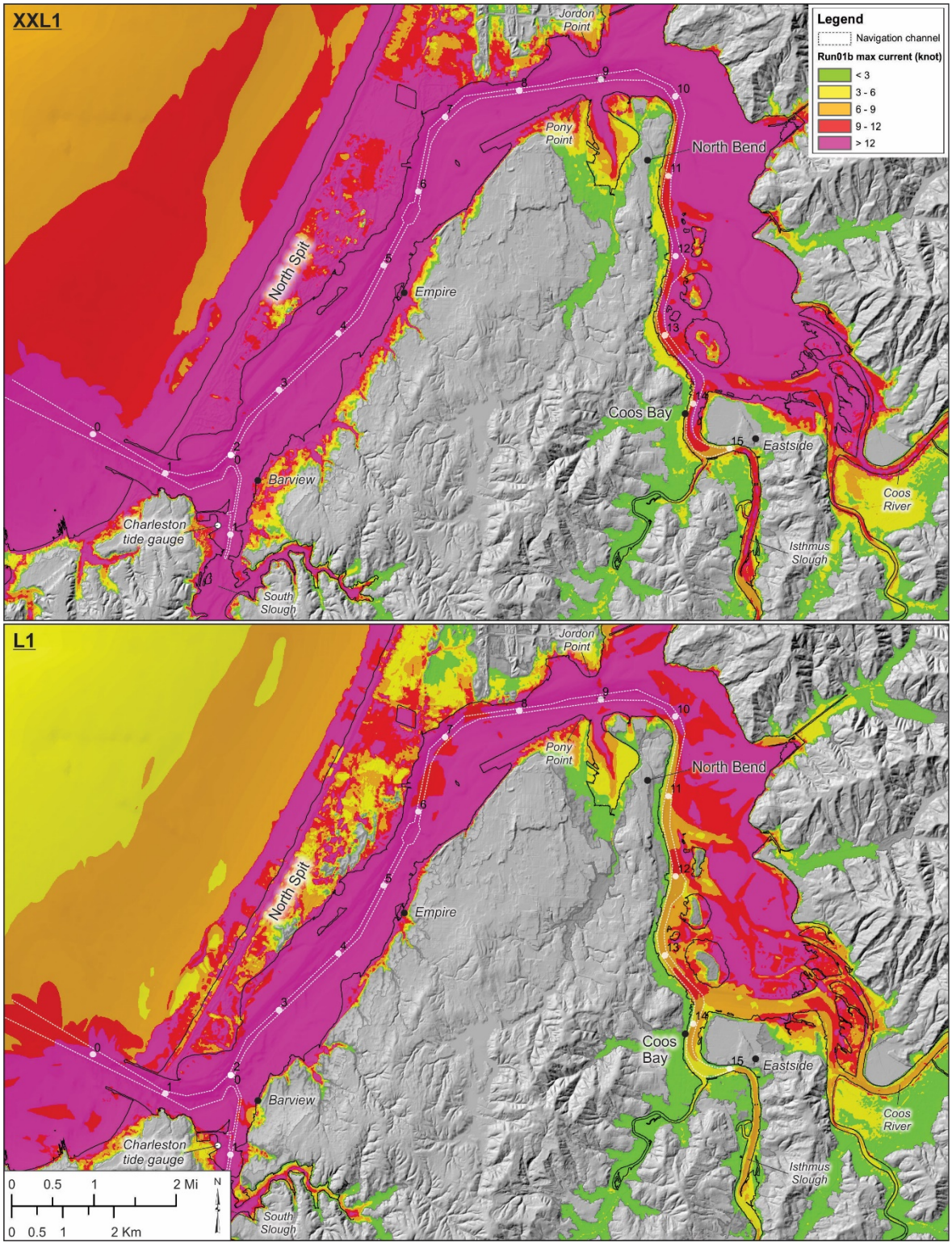

Figure 31. Time series showing the modeled currents generated for two simulations of a Cascadia subduction zone tsunami (XXL1) traveling along the navigation channel from the mouth of Coos Bay (MCB) to the town of Coos Bay. Gray shading denotes the envelope of variability in the tsunami currents from all simulations.

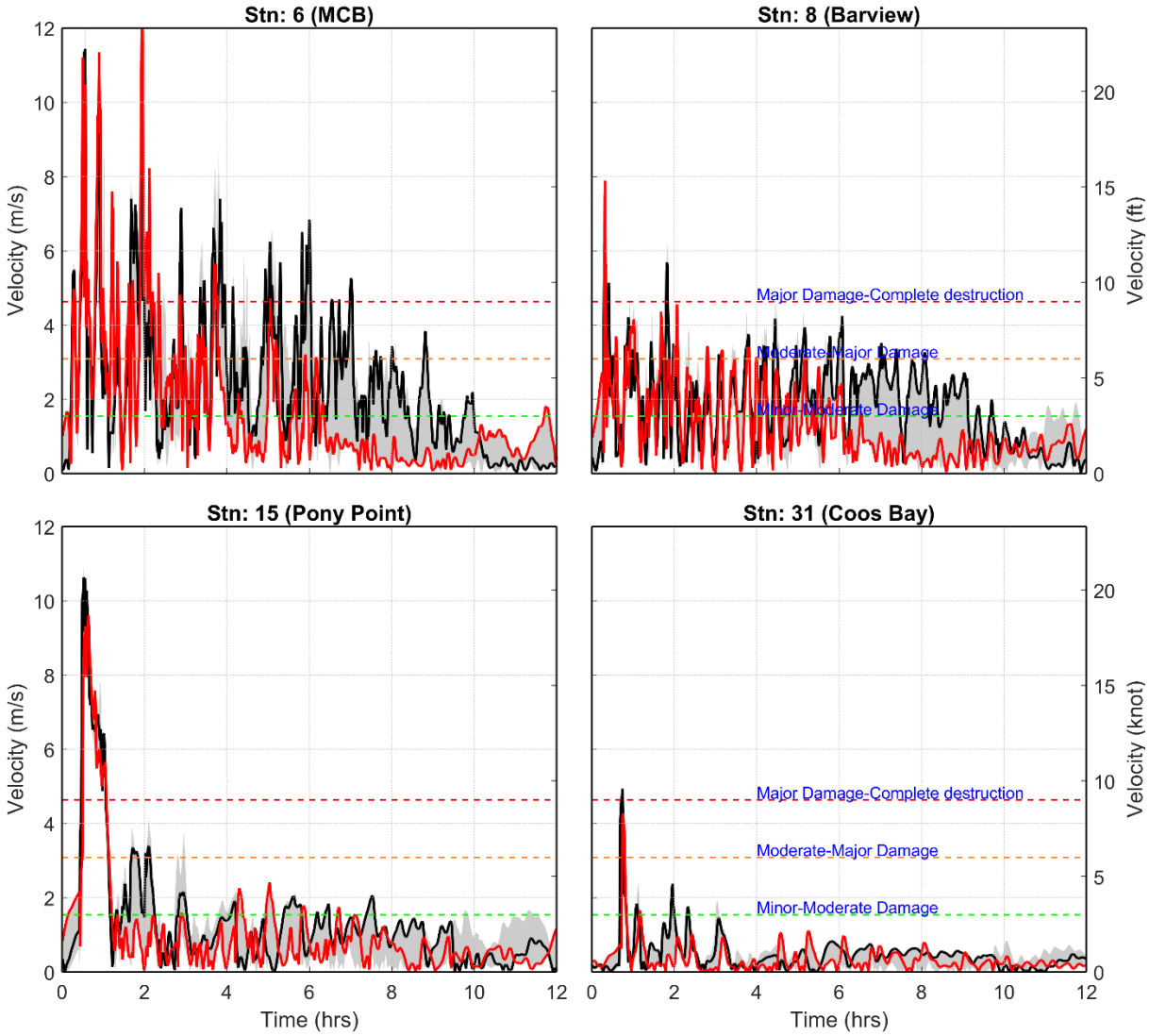

Figure 32. Time series showing the modeled currents generated for two simulations of a Cascadia subduction zone tsunami (L1) traveling along the navigation channel from the mouth of Coos Bay (MCB) to the town of Coos Bay. Gray shading denotes the envelope of variability in the tsunami currents from all simulations.

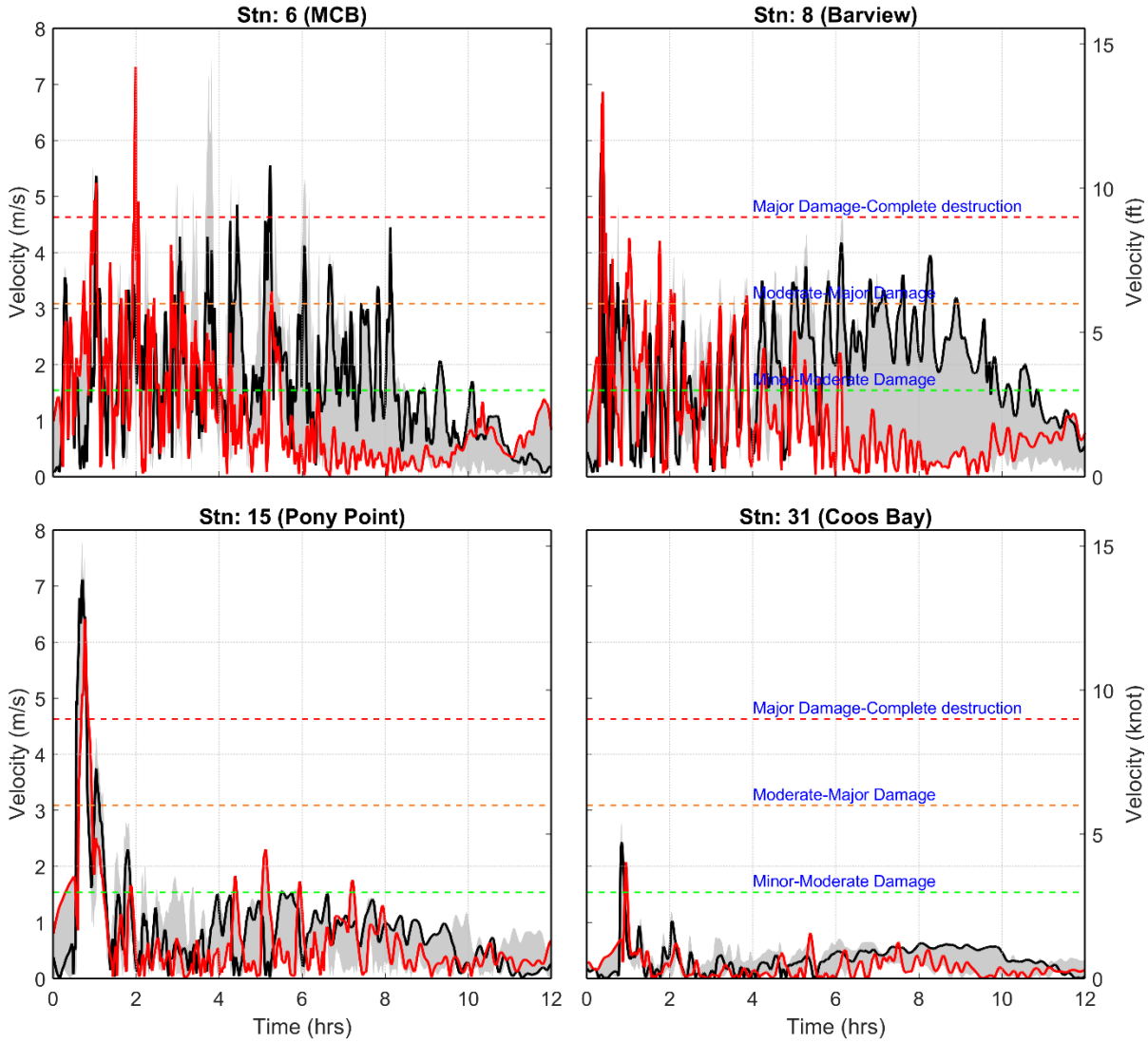

Knowing how long strong currents can be expected to persist following a CSZ earthquake is also important to mariners and emergency officials. Because performing such analyses is computationally demanding, developing ensembles of these types of results is not practical. Instead, we focus on evaluating the current durations for just the estuary and offshore region and the two most important model simulations: flood (Run05a) and ebb (Run06a) conditions. The approach used involves querying the full simulation data using a Fortran script to extract the first 12 hours of model data for every grid node; we ignored data after hour 12 because the tsunami is largely over by then. These data are subsequently processed in MathWorks MATLAB® and converted to Esri form using a python script. For our purposes, we use the following velocity thresholds to distinguish the duration of the currents: 1.5 m/s [3 knots], 3 m/s [6 knots], and 4.5 m/s [9 knots].

The duration of each of the current velocity bins (1.5–3 m/s [3–6 knots] and 3–4.5 m/s [6 to 9 knots]) is presented in **Figure 33**; we have chosen not to include the results for currents > 4.5 m/s [9 knots] because their effect is confined largely to the estuary mouth. Flood conditions are shown on the left side of the figure, while ebb conditions are on the right. Not surprisingly, currents lasting up to one hour in the 1.5–3 m/s [3–6 knot] range affect the entire estuary; this pattern is repeated for the ebb scenario (Figure 33C). Downriver of Jordon Point in the lower Coos estuary these currents are expected to persist for up to 4 hours, especially in the navigation channel. West of the mouth of Coos Bay, currents between 1.5 and 3 m/s [3–6 knots] can be expected to persist for 1–4 hours, up to 4.5 km (2.8 mi) from the mouth, making this area a potential high hazard area. The patterns shown for the ebb scenario (Figure 33C) are broadly similar to the flood scenario. The main difference is the duration of the tsunami currents identified for ebb, which are much shorter when compared with flood. This is particularly obvious for currents in the 3–4.5 m/s [6–9 knot] range, where durations of 1-2 hours dominate (Figure 33D), compared with durations of 2–4 hours for flood (Figure 33B). Hence, these findings reinforce our earlier findings that suggest ebb conditions at Coos Bay have a moderating effect on the tsunami velocities.

Figure 33. Duration of Cascadia subduction zone XXL1 tsunami current velocities for *(left)* Run05a (flood) and *(right)* Run06a (ebb). A) Run05a, 1.5–3 m/s [3–6 knots]; B) Run05a, 3–4.5 m/s [6–9 knots]; C) Run06a, 1.5–3 m/s [3–6 knots]; and D) Run06a, 3–4.5 m/s [6–9 knots].

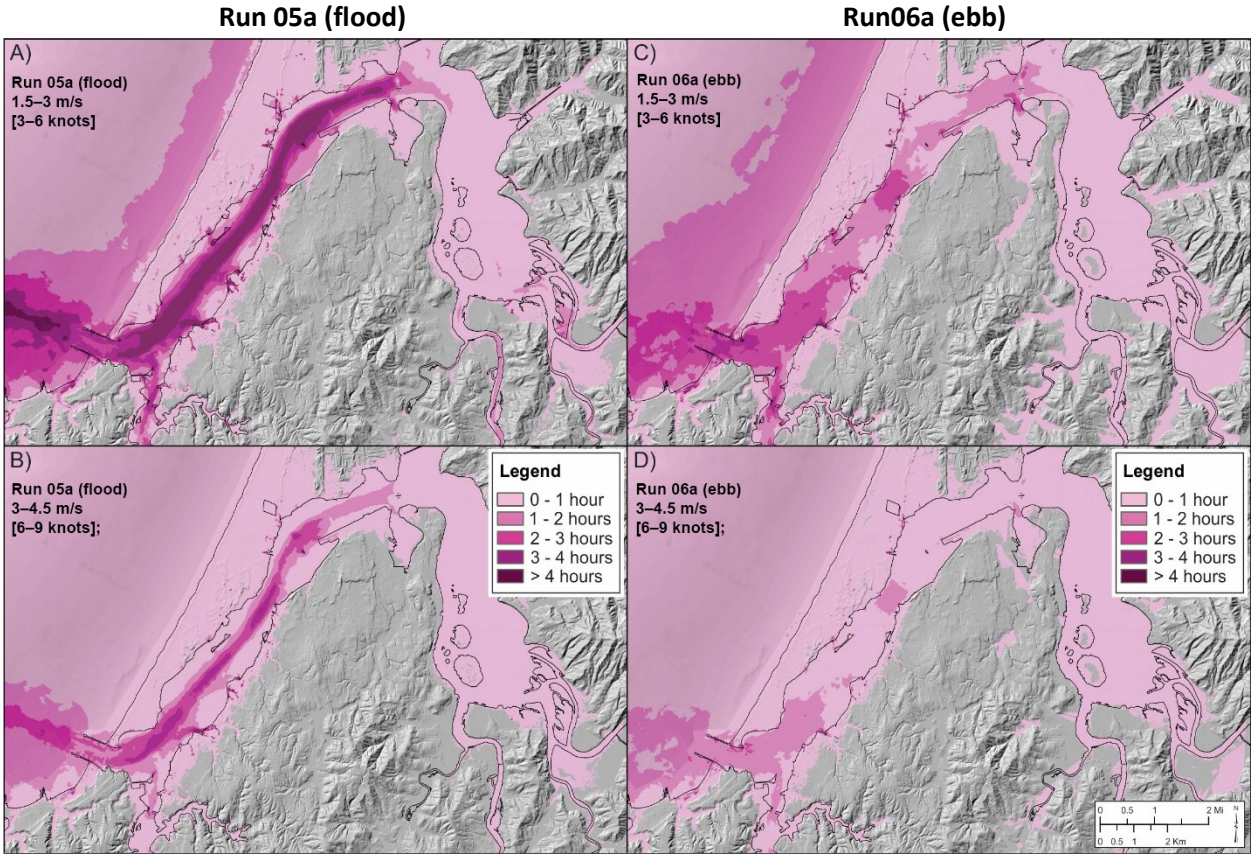

5.1.1.3 XXL1 and L1 vorticity

The occurrence of vorticity or rotation is a process that leads to the development of gyres and whirlpools. These effects can be a major factor affecting maritime operations, particularly for the ability of a vessel to maintain headway. Vorticity is defined as:

$$\text{Vorticity} = \left|\frac{\partial v}{\partial x} - \frac{\partial u}{\partial y}\right| \quad (2)$$

where ∂v is the change in north velocity, ∂u is the change in east velocity, ∂x is the change in distance east, and ∂y is the change in distance north. In general, values greater than 0.1 (0.01 units of 1/sec = velocity changing 1 m/sec over 100-m distance) are akin to very strong shear. **Figure 34** presents the calculated vorticity generated by both the XXL1 and L1 tsunami scenarios. Not surprisingly, our modeling reveals large areas subject to strong rotation potential, with the strongest signal (> 0.1/sec) evident in the nearshore ocean (within ~1 mile of the shoreline). Very strong rotation is also evident at the MCB, particularly adjacent to the jetties and spit tip; within Bastendorff Beach (south of the Coos jetty), especially in the narrow channel at Charleston harbor and near Jarvis Turn. These same areas are also subject to strong rotation generated under the L1 scenario.

Figure 34. Ensemble model results of the maximum vorticity generated by a *(top)* XXL1 and *(bottom)* L1 Cascadia subduction zone tsunami. Numbers on map are U.S. Army Corps of Engineers river mile locations and values.

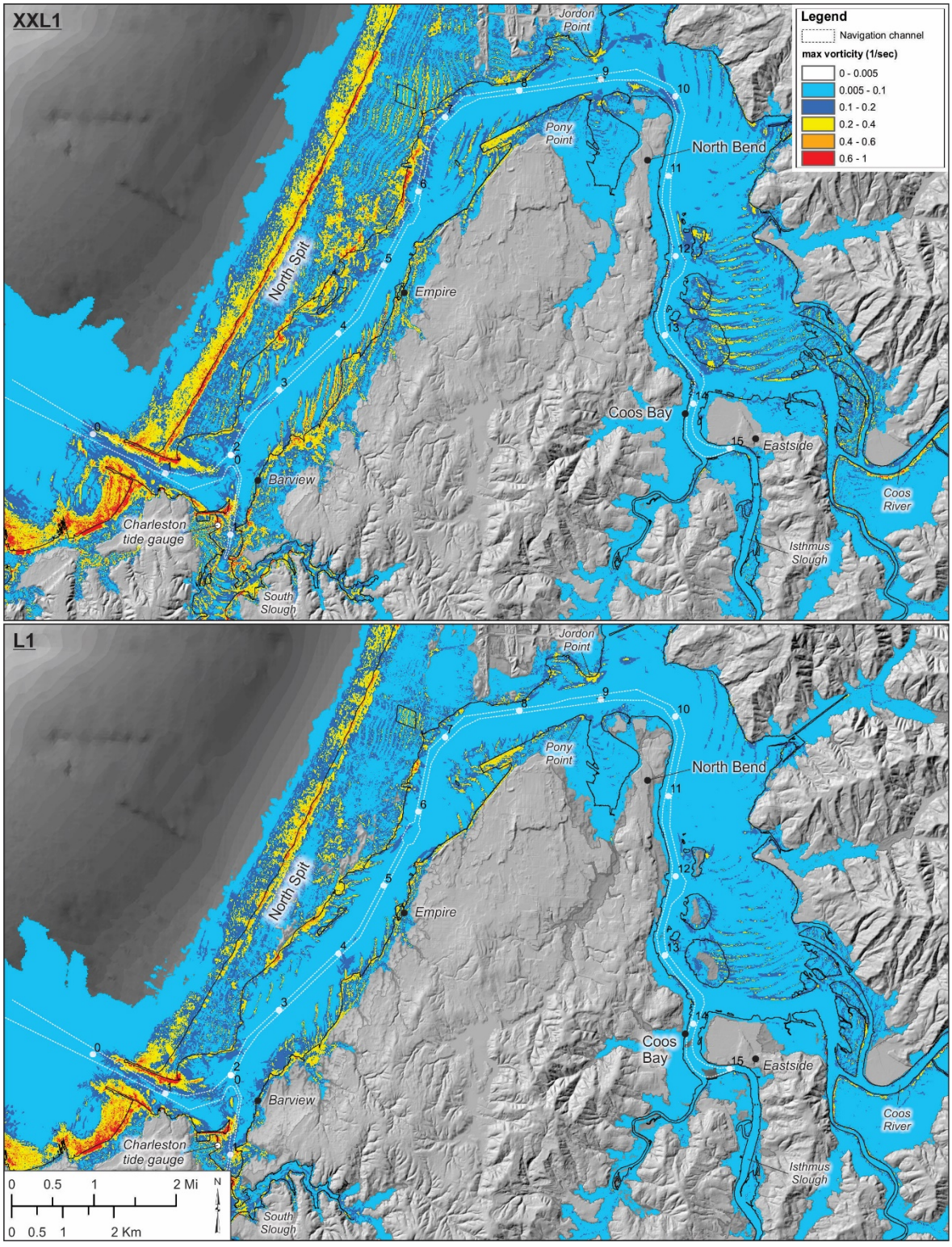

5.1.2 Distant (AKmax) tsunami ensemble results

5.1.2.1 AKMax Water Levels

Figure 35 presents the merged maximum water levels and currents for the maximum considered eastern Aleutian Island (AKMax) distant tsunami event. As with the local scenarios, the highest tsunami water levels are observed along the open coast, especially offshore the North Spit. Dangerous conditions are also observed at the MCB, Charleston, Barview, by the Coos airport, and near Jordon Point. Not surprisingly, the simulated water levels for the AKMax tsunami are considerably lower than those observed for the local scenarios (compare **Figure 35** *top* with **Figure 27**).

Time series information for select stations along the river is presented in **Figure 36**. As with the local scenarios, these data have been truncated to span the first 12 hours of the simulations, providing improved insight into the variability and range of modeled water levels; the datum used is MHHW. The gray shading in each plot defines the envelope (range) of variability from the combined suite of simulations. As can be seen, the time series data highlight the extreme nature of the tsunami waves at the MCB (station 6) and at Barview (station 8). However, upriver of Barview the simulated water levels decrease rapidly, with maximum water levels of about 2 m [6 ft] observed near Pony Point (station 15). Interestingly, unlike the local scenarios, the distant tsunami at Coos Bay remains fairly significant, with varying waves of about 1.5 to 2 m [4.9 to 6 ft] height. With the transition to ebb conditions at ~10 hours the tsunami waves become increasingly attenuated. Nevertheless, the tsunami waves continue to impact the area for at least 10 to 15 hours after the event before fully subsiding.

5.1.2.2 AKMax currents

More telling are the modeled tsunami currents, which indicate potentially dangerous currents occurring within the MCB (**Figure 35**, *bottom* and **Figure 37**). Strong currents exceeding 9 knots are prevalent in the MCB navigation channel and in the narrows between Charleston and Barview, near the south end of the Coos airport, and in the area around Jordon Point (**Figure 35** *bottom*). Of major concern will be the interaction of the incoming tsunami waves with opposing currents generated during an ebb tide coupled with seaward directed tsunami drainage, which will likely contribute to the amplification of wind waves occurring in the vicinity of the mouth (Allan and others, 2018).

Within the estuary, the ensemble results indicate that large parts of the estuary would be affected by currents in the 1.5–4.6 m/s [3–9 knot] range (**Figure 35**, *bottom*). Currents of this magnitude are likely to cause moderate to major damage to facilities located in the ports and harbors (see **Table 4**). For ships and boats operating in the navigation channel (e.g., between the MCB and Jordon Point) and in the harbors, currents of this magnitude will likely necessitate ship operators adding additional drag anchors to larger vessels and or mooring ropes. Evacuation upriver toward Coos Bay may also be feasible depending on how long it takes a ship to get underway (a conservative estimate is about 1 hour for large ships [Dan Jordan, Columbia River Bar Pilots, oral commun., July 2018]), the size of the vessel, and the speed at which a vessel can travel.

Figure 37 presents the modeled AKMax tsunami currents for the same stations defined previously. As noted earlier, the modeled currents are strongest at the MCB (station 6) and rapidly weaken as the tsunami progresses upriver (**Figure 37**). By the time the tsunami reaches the Port of Coos Bay (station 31), the currents fall below the 1.5 m/s [3 knot] damage index threshold. As a result, because of the combination of relatively small tsunami waves and low currents observed at Coos Bay, our simulations suggest that maritime operations upriver from RM13 are unlikely to be significantly impacted by a maximum considered distant tsunami.

The duration in which tsunami currents are expected to exceed 1.5 m/s [3 knots] is presented in Figure 38 for both the flood (Run05d, *left plots*) and ebb (Run06d, *right plots*) scenarios. Longer current durations again characterize the flood scenario, especially along the navigation channel in the lower estuary where currents in the 1.5–3 m/s [3–6 knot] range are expected to last for more than 4 hours (Figure 38A). During ebb conditions, the AKMax tsunami currents are suppressed (Figure 38B), though current durations on the order of 2-3 hours prevail in several key areas including between Empire and Jordon Point, and in parts of the upper estuary (Figure 38C). At the higher velocity of 3–4.5 m/s [6–9 knots], our results indicate that strong tsunami currents arriving on a flood tide will persist for up to 3 hours in the navigation channel downstream of Jordon Point (Figure 38B), but is more muted (mostly < 2 hours) during ebb conditions (Figure 38D). These results suggest that different maritime planning responses may be warranted for flood and ebb conditions when dealing with a distant tsunami event. Overall, these results confirm that a tsunami arriving at flood tide will generally produce stronger currents for longer durations compared with the same event arriving at ebb tide.

5.1.2.3 AKMax vorticity and minimum flow depth

Figure 39 (*top*) presents the calculated vorticity potential, while **Figure 39** (*bottom*) shows the water depth below the minimum trough of the tsunami. The former provides insights as to areas subject to strong rotation, while the latter is important with respect to the grounding of vessels. As with the local scenarios, areas of cool to hot colors indicate potential for rotation and the development of gyres and whirlpools (**Figure 39,** *top*). These areas include the entire nearshore ocean, and areas around the MCB, especially within the entrance to the estuary; the port of Charleston will also be severely impacted by strong incoming and outgoing currents, leading to shear and the formation of whirlpools. The issue of grounding (**Figure 39,** *bottom*) is largely confined to the shallower harbors, such as Charleston, Jarvis Turn, and in the vicinity of Jordon Point. Our analyses suggest that within the navigation channel the effects of passing tsunami troughs are likely to cause grounding issues in most areas of the estuary. This is evident in **Figure 39** (*bottom*) along the navigation channel, which shows simulated minimum water depths ranging from 8 to 12 m (26 to 39 ft), while minimum depths at Coos Bay could decrease significantly.

Figure 35. Ensemble model results of the maximum tsunami *(top)* water levels and *(bottom)* currents generated by a maximum considered distant earthquake and tsunami (AKMax) occurring on the eastern Aleutian Islands. Cartoon showing water level time history and attributes is of station 6 at the mouth of Coos Bay (MCB). Numbers on map are U.S. Army Corps of Engineers river mile locations .

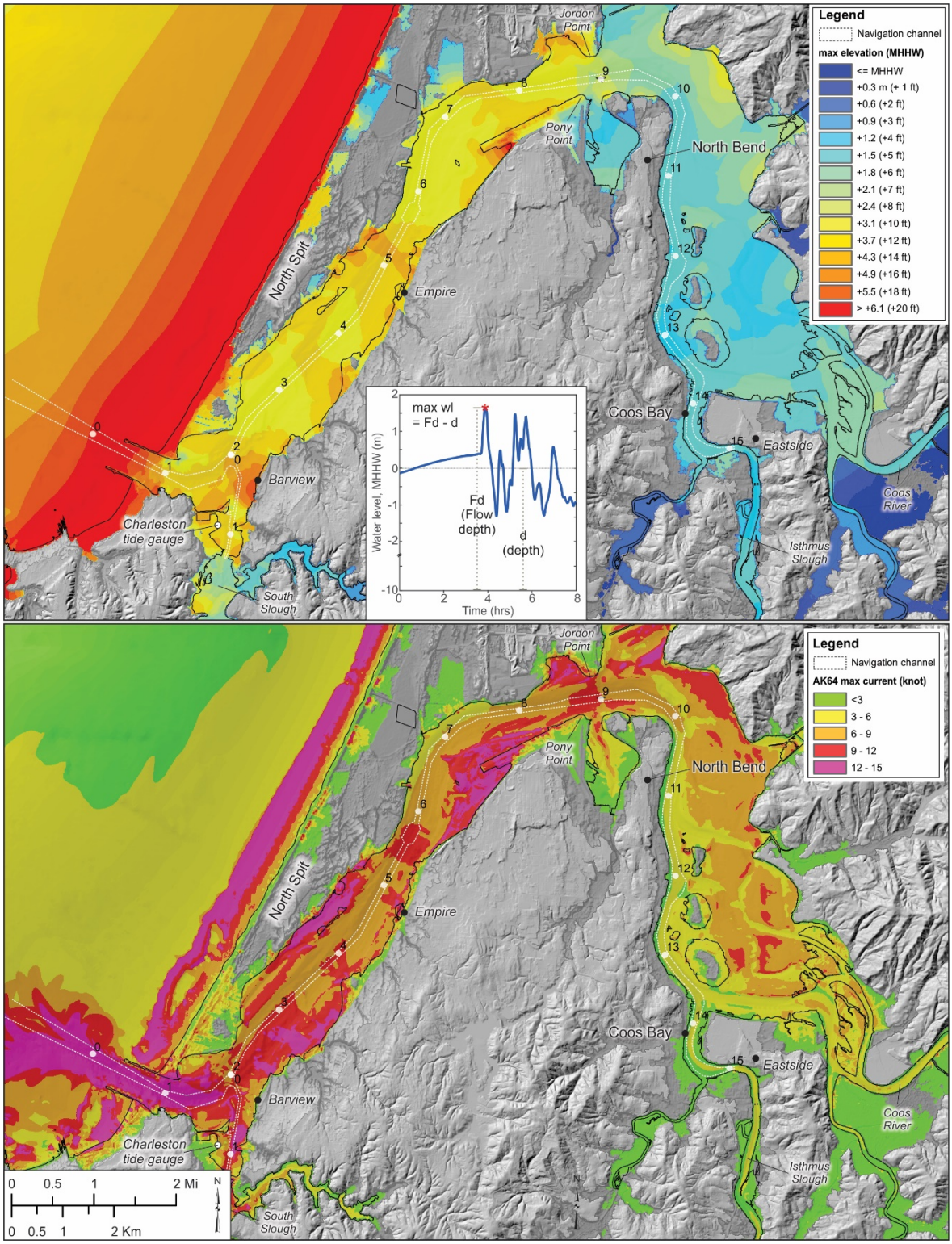

Figure 36. Time series showing the modeled water levels (flow depth–depth) for the AKMax tsunami traveling along the navigation channel from the mouth of Coos Bay (MCB) to the town of Coos Bay. Gray shading denotes the envelope of variability in the water levels from all simulations.

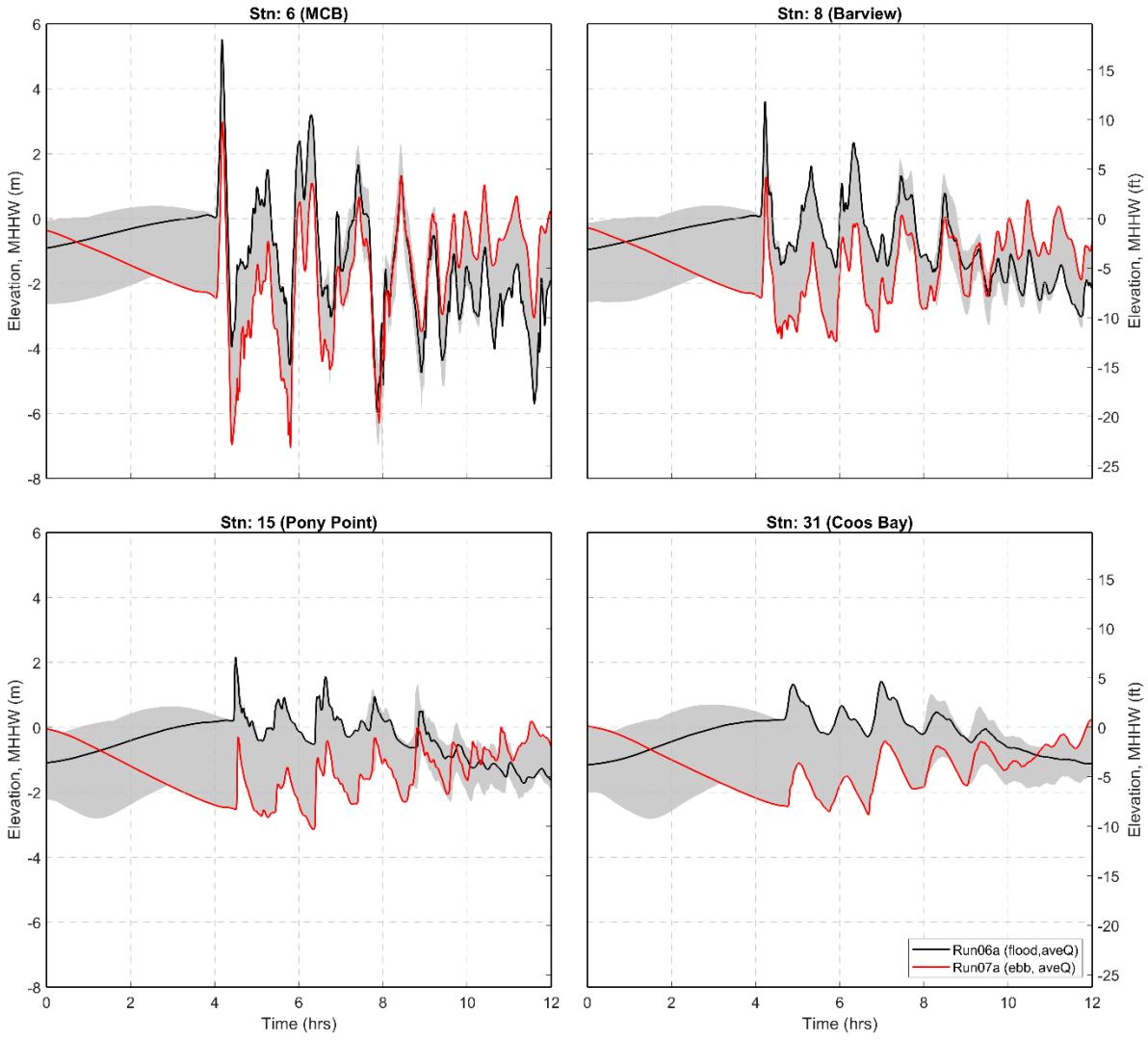

Figure 37. Time series showing the modeled currents for the AKMax tsunami traveling along the navigation channel from the mouth of Coos Bay (MCB) to the town of Coos Bay. Gray shading denotes the envelope of variability in the tsunami currents from all simulations.

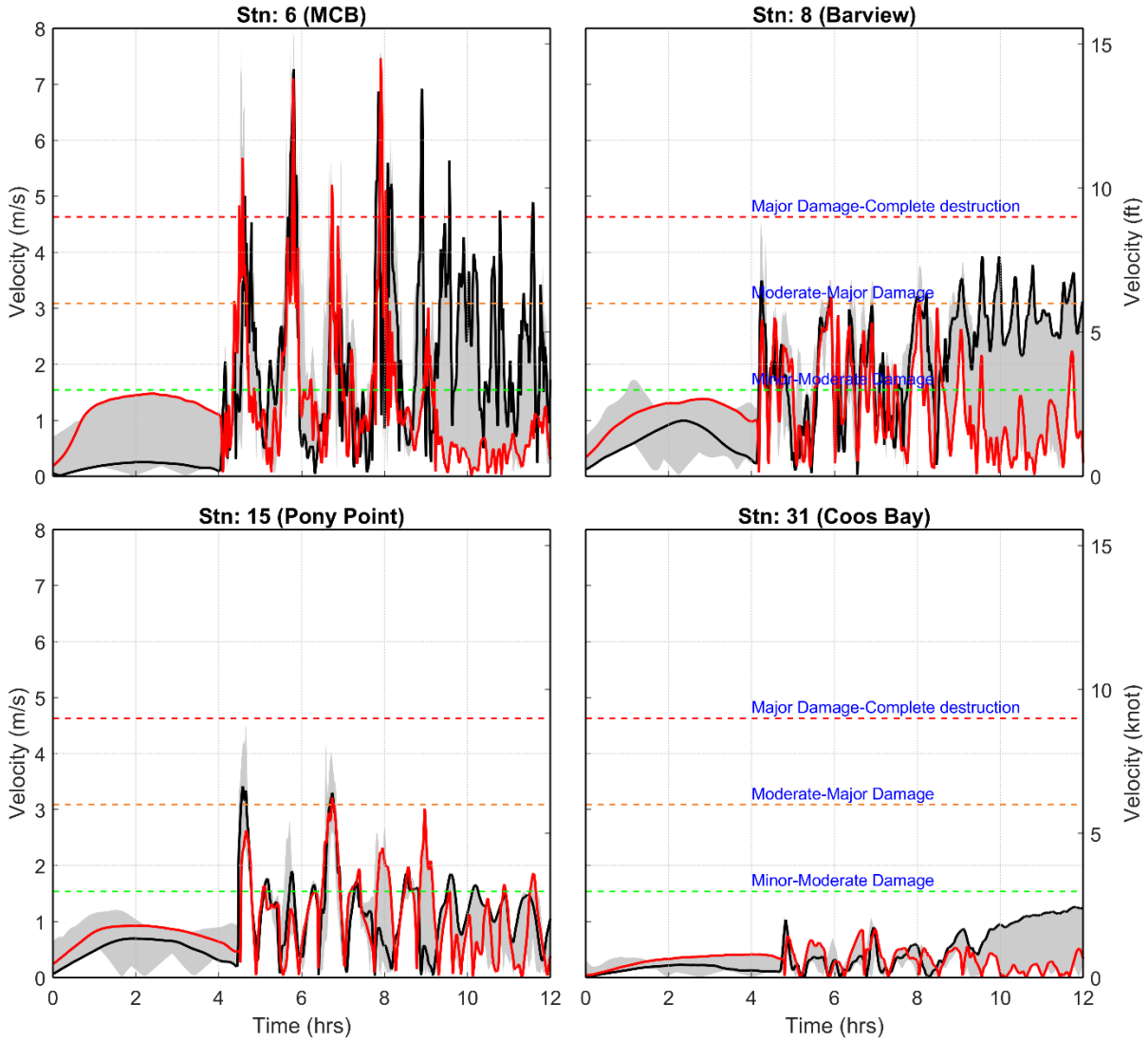

Figure 38. Duration of AKMax tsunami current velocities for *(left)* Run05d (flood) and *(right)* Run06d (ebb). A) Run05d, 1.5–3 m/s [3–6 knots]; B) Run05d, 3–4.5 m/s [6–9 knots]; C) Run06d, 1.5–3 m/s [3–6 knots]; and D) Run06d, 3–4.5 m/s [6–9 knots].

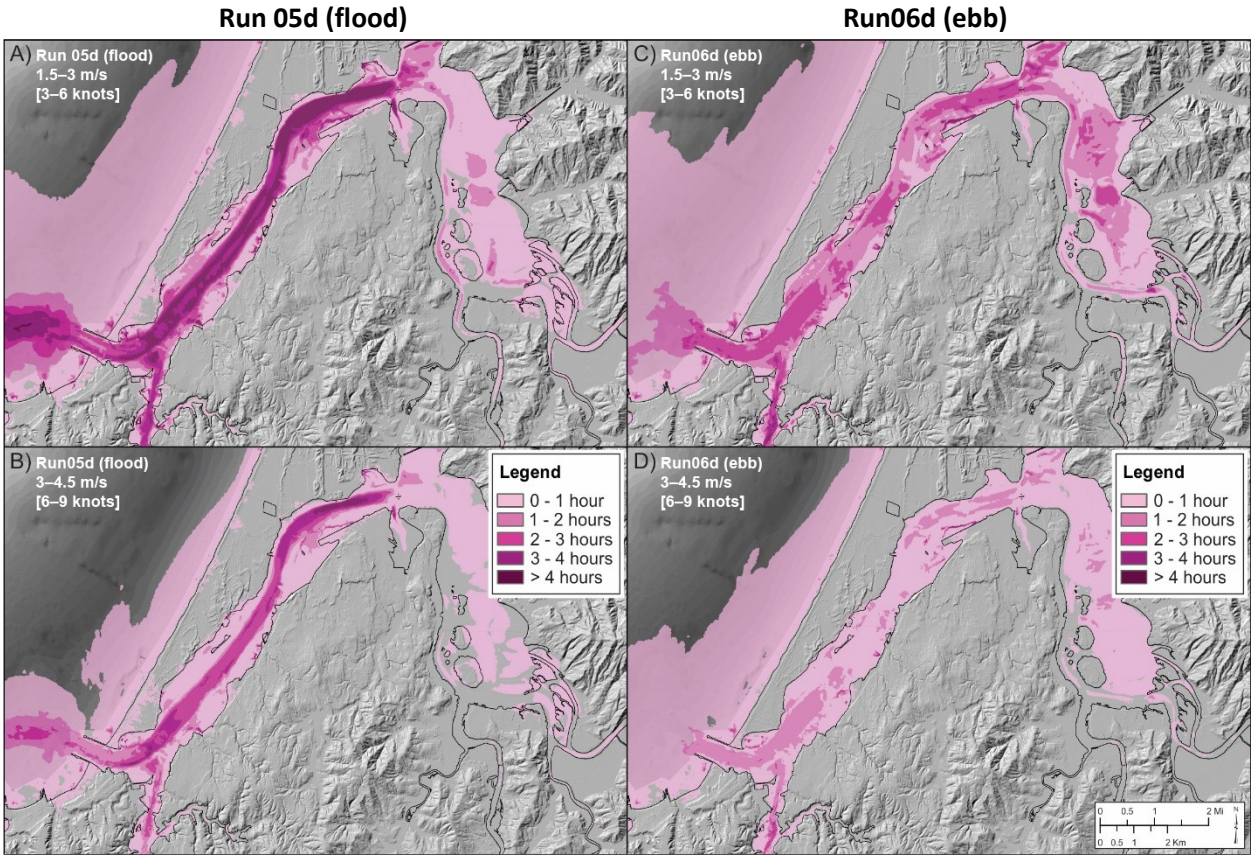

Figure 39. Ensemble model results of the *(top)* maximum vorticity and *(bottom)* minimum water depths generated by a maximum considered distant earthquake and tsunami (AKMax) occurring on the eastern Aleutian Islands. Cartoon showing water level time history and attributes is of station 6 at the mouth of Coos Bay (MCB). Numbers on map are U.S. Army Corps of Engineers river mile locations.

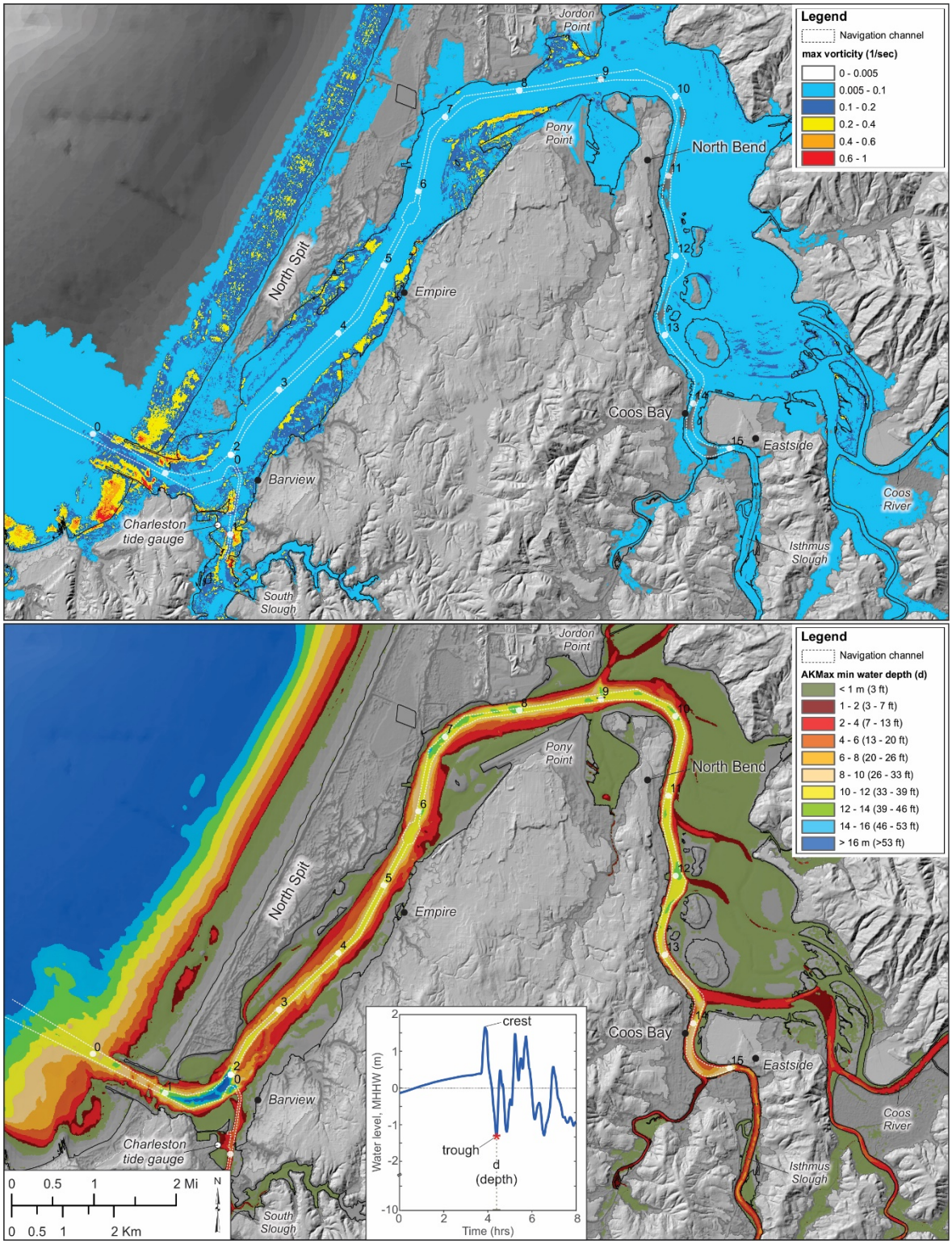

6.0 COOS CHANNEL DEEPENING EFFECTS

In order to accommodate larger ships traversing the Coos estuary, a proposal has been developed by the Port of Coos Bay to both widen and deepen the navigation channel. Hence, it is of interest that a comparison be undertaken in order to evaluate if such modifications could affect the hydrodynamics of tsunami waves as they enter the estuary and travel up the navigation channel. To perform such an evaluation, we first modified the tsunami model grid based on the information included in **Table 1**. In general, the revised grid reflected an increase to the channel depth of 3.3 m (10 ft) near the mouth to a fixed depth of 17.4 m (57 ft), while the rest of the channel was deepened by ~2.4 m (8 ft) to a fixed depth of 13.7 m (45 ft) (Oregon International Port of Coos Bay, 2019). We chose to use the L1 CSZ earthquake scenario in order to evaluate possible changes in estuary hydrodynamics. As a reminder, the L1 scenario accounts for 95% of the possible earthquake scenarios (based on the geologic record) that have impacted the Oregon coast in the last 10,000 years.

Figure 40 shows differences in the simulated maximum tsunami water levels (*top*) and currents (*bottom*) between the modified channel configuration (Run05c-L1) and the existing configuration (Run05a-L1). As can be seen for the maximum water levels, the bulk of our model domain (no color shading) indicates that the difference between the two grids is ± 0.25 m (± 0.8 ft). Nevertheless, our analyses indicate two areas of broad differences: at the mouth of Coos Bay (between RM1 and RM2), and adjacent to the Coos airport runway (**Figure 40**). In these two areas we find that the deepened channel configuration results in marginally higher (+0.25 to +0.5 m [+0.8 to + 1.6 ft]) tsunami water levels; there are also small patches at the MCB where the original channel configuration produces higher tsunami water levels. More telling are the difference results associated with the simulated tsunami currents. These data are presented in **Figure 40** (*bottom*). Overall, our modeling indicates that there is generally little difference (pale green shading) in the generated currents between the two configurations, especially upriver of Jordon Point. Conversely, between the MCB and Jordon Point we find that either configuration is capable of generating localized areas of slightly stronger currents; in almost all cases differences in the currents are typically < ± 1.5 m/s (< ± 3 knots). Evident from **Figure 40** (*bottom*), the largest current differences occur from seaward of the MCB to RM2. Such a response is probably due to the deeper channel, which results in an increase in estuary volume (more water is able to be accommodated by the deeper configuration) such that during tsunami drawdown accompanied by later outgoing tides, the deeper channel produces slightly stronger currents offshore the MCB; the simulated currents are typically < ± 1.5 m/s (< ± 3 knots).

Finally, **Figure 41** (water levels) and **Figure 42** (tsunami currents) present a series of four plots associated with our virtual water level stations located along the navigation channel. As can be seen in **Figure 41**, the largest difference in the water levels generated by the two simulations occurs at the MCB. As with **Figure 40**, positive values indicate that the original configuration dominates, while negative values indicate that the deepened channel is dominant. Not surprisingly, the largest differences occur in the navigation channel between the MCB and Pony Point, where modifications to the channel are made. As can be seen from the figures, these differences are most apparent at station 6 (MCB) and 8 (Barview) for both water levels and currents. With progress up the estuary, differences between the two simulation results become increasingly smaller. At the town of Coos Bay there is effectively no difference between the two configurations; this is repeated in the tsunami current velocity plots. From these results we conclude that deepening the navigation channel will not significantly modify Coos Bay tsunami hydrodynamics.

Figure 40. ***(top)*** **Changes in the maximum tsunami water levels expressed as the difference between the existing model grid (Run05a-L1) compared with the deepened navigation channel (Run05c-L1) for a Cascadia subduction zone tsunami. Values less than zero indicate Run05a water levels dominate, while values greater than zero indicate that Run05c dominates.** ***(bottom)*** **Maximum tsunami velocities (in knots) expressed as the difference between the original modeling (Run05a_L1) compared with results from the deepened navigation channel (Run05c). Velocities less than 0 indicate Run05a currents dominate, while velocities greater than 0 indicate that Run05c currents dominate. Both runs incorporate average river flow and friction. Numbers on map are U.S. Army Corps of Engineers river mile locations.**

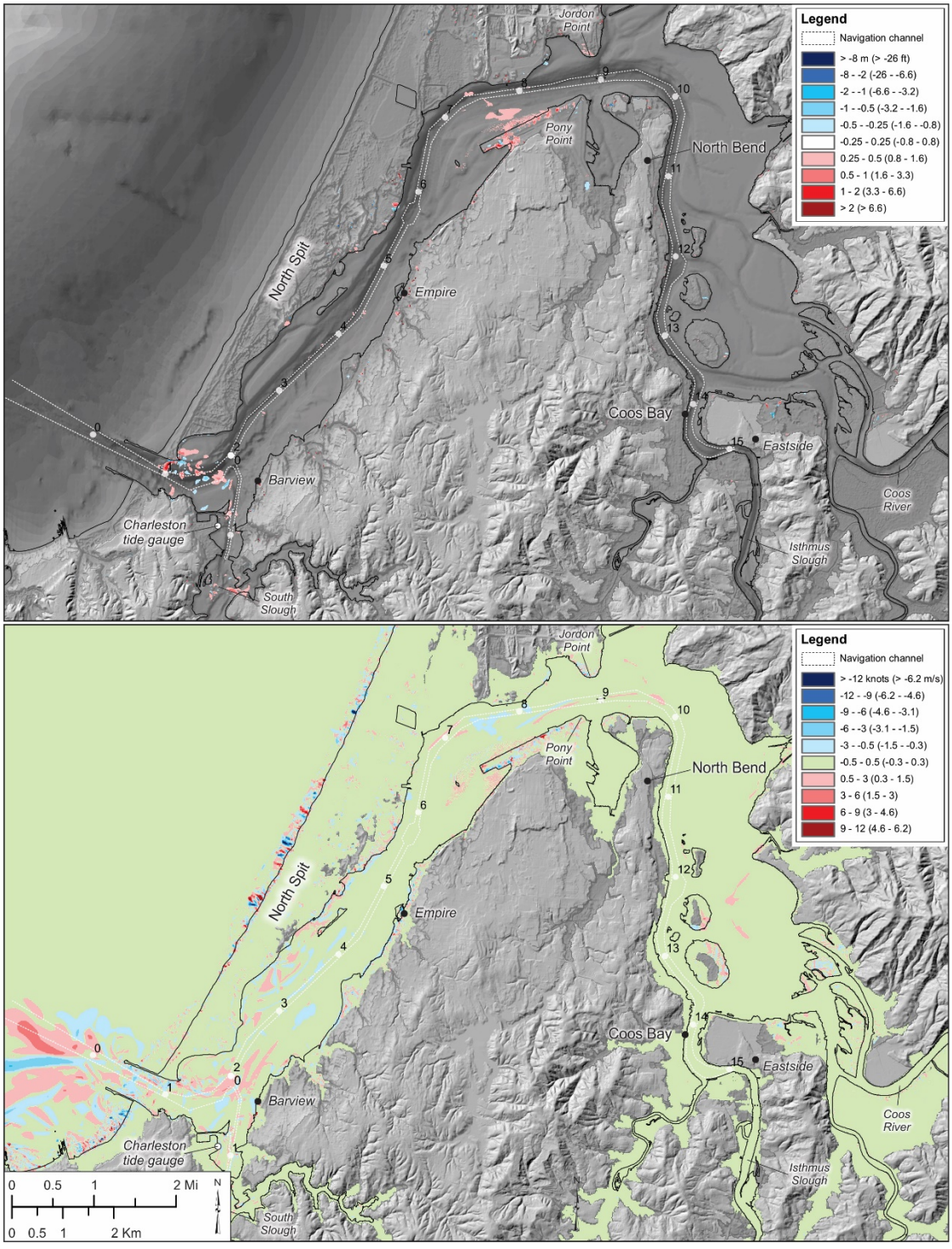

Figure 41. Time series showing differences in the modeled water levels (Run05c versus Run05a) for the L1 Cascadia subduction zone tsunami traveling along the navigation channel from the mouth of Coos Bay (MCB) to the town of Coos Bay. Note: positive values indicate that the original channel configuration dominates, while negative values indicate that the deepened channel is dominant.

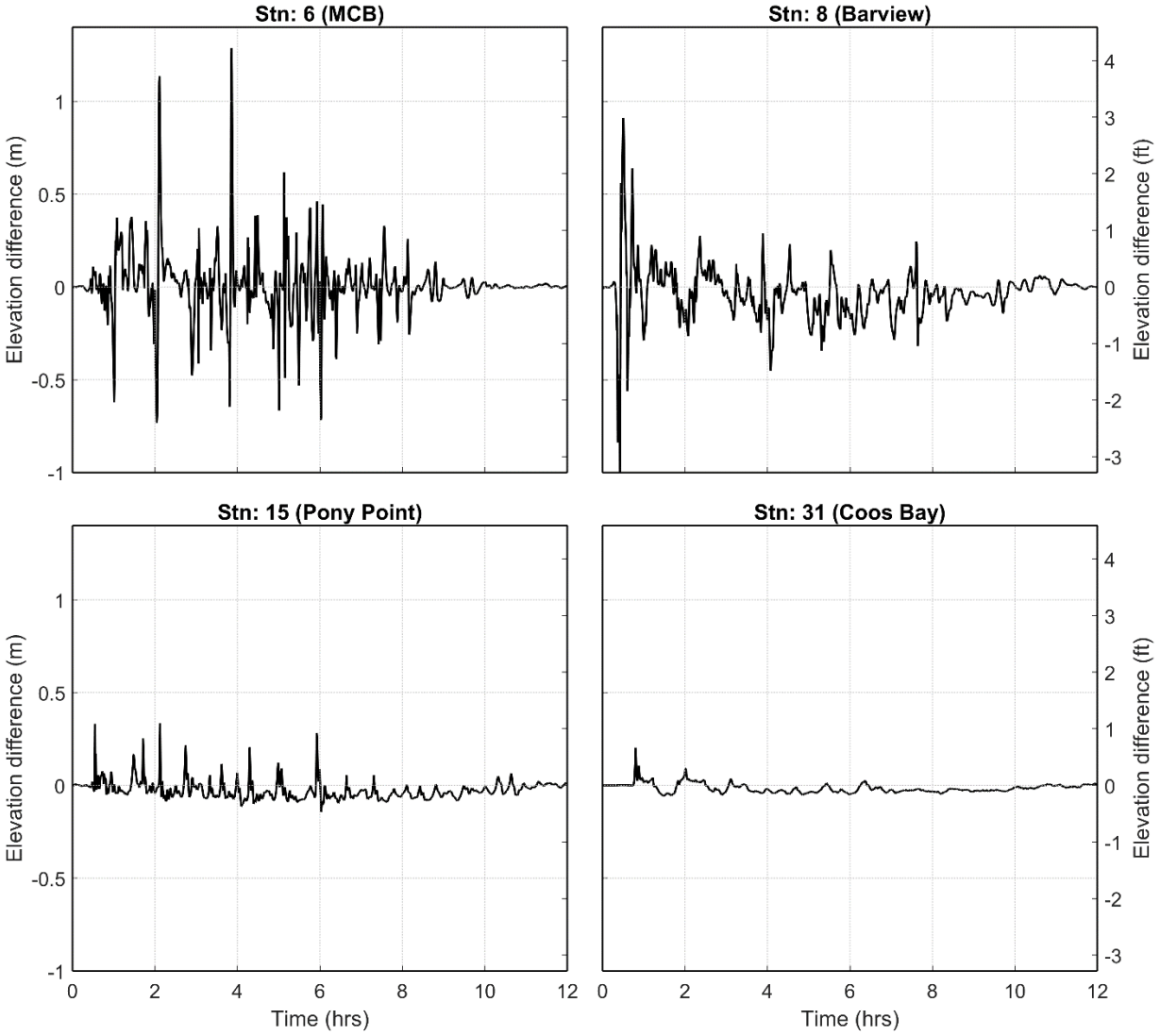

Figure 42. Time series showing differences in the modeled tsunami currents (Run05c versus Run05a) for the L1 Cascadia subduction zone tsunami traveling along the navigation channel from the mouth of Coos Bay (MCB) to the town of Coos Bay. Note: positive values indicate that the original channel configuration dominates, while negative values indicate that the deepened channel is dominant.

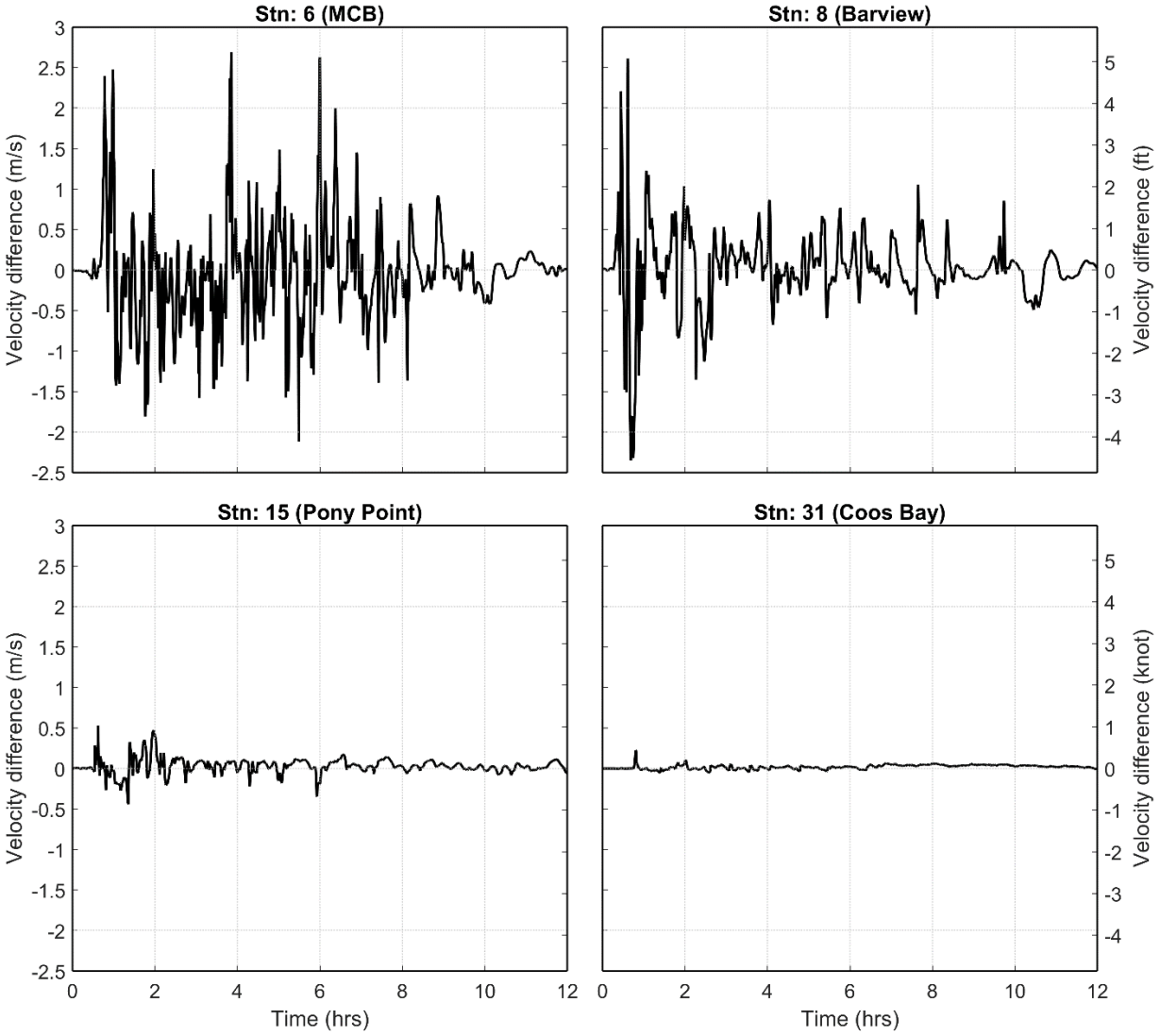

7.0 COOS ESTUARY MARITIME GUIDANCE

Our review of the scientific literature indicates that tsunami-generated currents pose a potential threat to the maritime community, especially within ports and harbors (Borrero and others, 2015; Lynett and others, 2014; Uslu and others, 2010). There is general agreement in the scientific literature that damage from tsunami within ports and harbors begins to occur at velocities ~1.5–2 m/s [3–4 knots]. However, the same cannot be said for the effects of currents generated by a tsunami on boats operating out on the ocean. Vessel vulnerability to open ocean currents is difficult to assess because it depends not only on the strength of the currents but, importantly, on the size of the vessel and its cargo load and on prevailing antecedent conditions (wave heights and winds). An additional factor is the ability of smaller boats to cope with being in some cases tens of kilometers from the coast for potentially extended periods. All these factors have implications for where to best send mariners in the event of a tsunami.

Lynett and others (2014) attempted to address the issue of offshore tsunami evacuation by comparing the maximum-simulated currents with depth for a distant tsunami affecting Crescent City, California. They noted that maximum currents of ~0.5 m/s [1 knot] are expected at a depth of 180 m (100 fathoms), while large variations in the currents exist near shore to a depth of 45 m (25 fathoms). They concluded that depths of ~55 m (30 fathoms) would generally be safe for most vessels (**Table 5**). In Japan, Suppasri and others (2015) noted that Japanese fishermen have practiced offshore evacuation (known as "oki-dashi") for generations, although prior to 2011 such a response was not recommended by the national government. This is because steering a boat toward a tsunami is considered to be dangerous and difficult, requiring expert knowledge of the offshore conditions as well as luck. Nevertheless, Japan's Fisheries Agency (2006 in Suppasri and others, 2015) indicated in its guidelines that boats should evacuate to a depth of at least 50 m (27 fathoms) in response to a tsunami warning (**Table 5**).

Since 2011, the Japanese have initiated a variety of recommendations for offshore tsunami evacuation. For example, Aomori Prefecture developed rules for offshore evacuation, such that in the case of a 5-m (16 ft) tsunami warning, the required sea depth for evacuation was 50 m (27 fathoms), which increased to 150 m (82 fathoms) for a 10-m (33 ft) tsunami warning (Suppasri and others, 2015). In the Tokushima Prefecture, a 4-m (13 ft) tsunami warning requires evacuation to 70-m (38 fathom) water depth, while evacuation to 110-m (60 fathom) water depth is recommended for a 6-m (20 ft) tsunami (**Table 5**).

Although the focus in Japan is on a locally generated tsunami, the same rules appear to apply for a distant tsunami. Most recently, however, Iwate Prefecture officials indicated that they would no longer recommend offshore maritime evacuation for a local tsunami (Dr. Anawat Suppasri, written commun., March 2018).

In the United States, considerable modeling and mapping efforts undertaken by National Tsunami Hazard Mitigation Program (NTHMP) state programs have led to the development of maritime guidance recommendations for each state. These recommendations include a range of potential depths for maritime evacuation purposes covering both local and distant scenarios (NTHMP, 2017). For Oregon, the currently recommended minimum depth is 55 m (30 fathoms) for the maximum-considered distant tsunami (DOGAMI, 2014); for the local XXL1 tsunami, the recommended depth for evacuation is 183 m (100 fathoms). For the distant event, the distances to safety range from a low of 2 km (1.2 mi) in Douglas County to as much as 16 km (10 mi) offshore from Lane County and requiring as little as 11 min to as much as 130 min to reach safety assuming a mean boat speed of 2–3 m/s [4–6 knots]. In contrast, distances to safety for an XXL1 event increase significantly and range from 30 to 66 km (19–41 mi) depending on position along the Oregon coast. These distances place boaters a long way from the shore in potentially hazardous seas (Allan and others, 2018).

After evaluating the tsunami currents, their durations, and water depths, Allan and others (2018) proposed a tri-zone hazard region for both distant and local tsunamis affecting the Oregon coast. For an XXL1 event, they identified a high hazard zone (depths < 150 m [82 fathoms]) where strong, dangerous currents would predominate. Between 150 and 250 m (82–109 fathom) water depth, Allan and others (2018) defined a moderate hazard region where the simulated tsunami currents ranged from 2 to 2.6 m/s [4 to 5 knots]. However, within this region the duration in which the current velocities exceed 2 m/s [4 knots] was found to be < 1 minute north of Stonewall Bank, increasing to 1.5–5.5 minutes south of the bank. Thus, it may be possible for a vessel to be moving through the moderate hazard area at the time of the event and, provided the vessel is able to maintain a westward direction and speed, the chance of survival improves. At depths > 250 m (137 fathoms), the tsunami currents fall below 2 m/s [4 knots]. For the AKMax scenario, Allan and others (2018) recommended that vessels north of Stonewall Bank evacuate to depths > 45 m (25 fathoms); strong, dangerous currents can be expected at depths < 28 m (15 fathoms).

Table 5. Maritime tsunami evacuation depths previously identified.

Location	Scenario	Tsunami Height (m)	Tsunami Height (ft)	Depth (m)	Depth (ft)	Depth (fathoms)	Reference
Crescent City	distant			55	180	30	Lynett and others (2014)
Japan's Fisheries Agency	local			50	164	27	Suppasri and others (2015)
Japan, Aomori Prefecture	local	5	16	50	164	27	Suppasri and others (2015)
	local	10	33	150	492	82	
Japan, Tokushima Prefecture	local	4	13	70	230	38	Suppasri and others (2015)
	local	6	20	110	360	60	
Japan, Iwate Prefecture	local**						
Oregon, USA	distant			55	180	30	DOGAMI (2014), NTHMP (2017)
Oregon, USA	local			183	600	100	DOGAMI (2014), NTHMP (2017)
Oregon, USA	distant			45	150	25	Allan and others (2018)
Oregon, USA	local			250[#]	820	137	Allan and others (2018)
				350[##]	1150	200	

Note: **Offshore evacuation for a local tsunami is prohibited (A. Sappasri, written commun., 2018).

[#] All coastal counties except Curry County;

[##] Curry County

In an examination of new tsunami model data generated for the Columbia River estuary, Allan and others (2018) recommended that vessels seaward of the MCR evacuate to depths greater than 46 m (25 fathoms/150 ft) for a distant tsunami event. They noted further that dangerous currents (> 2.6 m/s [5 knots]) caused by such a tsunami are expected to occur at depths shallower than 27 m (15 fathoms/90 ft). For a local CSZ event, Allan and others (2018) recommended that vessels seaward of the MCR evacuate to depths greater than 146 m (80 fathoms), specifically identifying Astoria Canyon as a potential staging area.

7.1 Maritime Guidance for a Local Tsunami

Given that initial wave arrival for a locally generated tsunami is expected to occur at the MCB in ~ 7 min, with a peak wave at 19 minutes, there is insufficient time for mariners moored in ports and harbors within Coos Bay or along the navigation channel to respond to this event other than to evacuate by foot to high ground. Hence, maritime evacuation planning for a locally generated tsunami is generally limited to those vessels already operating out on the open ocean. For vessels west of the MCB, the most effective strategy is to evacuate immediately toward deeper water and, accordingly, toward decreasing tsunami-generated currents. However, steering a vessel toward an approaching tsunami is dangerous and difficult and should only be attempted if land-based evacuation is impossible (Allan and others, 2018). In this scenario, there will be little to no warning for operators out on the ocean. Telltale signs of an earthquake and approaching tsunami may include a background ocean roar, changes in boat motions, stronger ocean currents, and/or muddier water. Vessels located closer to shore may witness clouds of dust appearing along the coastline and in the hills, where landslides may be occurring.

As previously mentioned, Allan and others (2018) completed a comprehensive analysis of tsunami currents generated by both local and distant events for the Oregon coast, and they proposed a tri-zone hazard region for maritime evacuation based on certain thresholds of tsunami currents. Using this approach at Coos Bay, we find that the most extreme and dangerous currents (> 2 m/s [> 4 knots]) generated by a local tsunami occur in water depths < 146 m (80 fathoms). Nearer to shore, wind generated waves and swell may be greatly amplified by strong opposing tsunami currents.

Tsunami generated currents were found to fall below 2 m/s [< 4 knots] at ~183 m depth (100 fathoms), while the safest area to stage vessels occurs in water depths > 274 m (150 fathoms); the latter is where currents fall below 1.5 m/s [3 knots]. Thus, for a maximum considered XXL1 tsunami, the safest staging area would place vessels some 13 to 14.5 nautical miles west of the MCB. However, given the extreme (and rare) nature of an XXL1 event, we identified an intermediate area of low currents based on the L1 scenario. This latter line was found to occur at ~128 m depth (70 fathoms) and occurs ~10 nautical miles west of the MCB. As a result of these data, we define a Coos Bay maritime evacuation zone for a local tsunami hazard zone beginning at ~146 m depth (80 fathoms, pale shaded region in **Figure 43**) and extending westward to depths > 274 m (150 fathoms, bright yellow region in **Figure 43**). Safety improves significantly with additional westward travel as tsunami generated currents will continue to fall with increasing water depth. The preferred staging area is in depths greater than 100 fathoms (600 ft) located 13.4 nautical miles west of the mouth of Coos Bay.

In these circumstances, mariners should prepare to potentially remain offshore for days due to the likelihood that navigation within the lower estuary could be dangerous if not impossible for some time. This is because of a combination of expected changes to bay hydraulics due to the likely failure and destruction of the Coos Bay jetties, changes in the locations of sandbanks, side channel collapse and infilling of the navigation channel, and the presence of debris throughout the estuary. More importantly, in this scenario all ports in the lower estuary are likely to be heavily damaged. As a result, vessel operators should develop plans to evacuate to potentially safe ports located to the south of Cape Mendocino on the California coast.

Figure 43. Offshore maritime evacuation zones for the Coos Bay study area. Map identifies the minimum distance to the DISTANT (orange) and LOCAL (yellow) maritime tsunami evacuations zones offshore the coast. These zones define the region where tsunami currents fall below 4 knots. Maritime safety from tsunami generated currents improves with farther westward travel. Note: bathymetric contours on the map are fathoms (1 fathom = 6 ft).

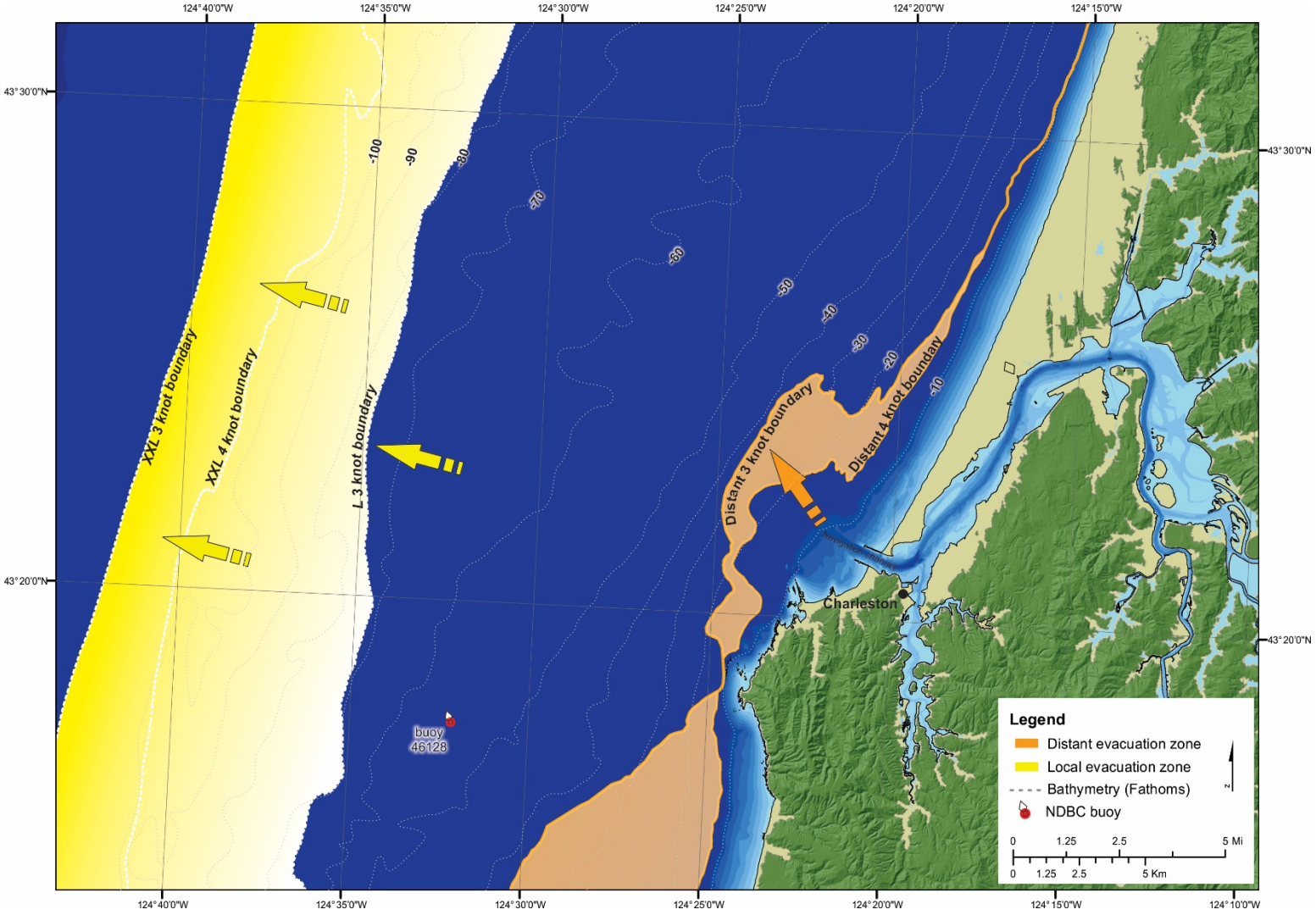

For vessels operating within the Coos estuary, the options are limited. Wave arrival times and water levels are presented in **Figure 21** and **Figure 22** for multiple sites along the river. Maritime operators should be aware of these arrival times and, if caught out on the estuary, attempt to evacuate to the nearest point of high ground and evacuate uphill. Depending on proximity to the MCB, this may be feasible for operators in smaller, faster boats.

For large ships operating in the navigation channel or in port, the options are limited. Modeling indicates that tsunami waves caused by a local CSZ event could reach 6–13 m (20–43 ft) above the tide, with the largest wave being the first wave. Extreme tsunami wave heights are expected to persist for at least 10 hours after the initial event. Accompanying the initial peak wave will be dangerous currents that are expected to reach ~4.6 m/s [~9 knots]. Strong currents in the 2 to 3.6 m/s [4–7 knot] range will persist for at least 6 hours after the event before gradually subsiding. In all likelihood, ships within the Coos lower estuary at the time a CSZ event occurs will be transported farther up the estuary (e.g., toward Russell Point) or eastward, where they will become grounded. Although tsunami waves and currents become more dispersed with progress upriver, vessels moored near Coos Bay will also be severely impacted by strong currents and shear; vessels will also be subject to grounding.

7.2 Maritime Guidance for a Distant Tsunami

For the maximum-considered distant (AKMax) tsunami scenario, our modeling indicates that the tsunami reaches the Coos estuary at ~ 4 hours after the start of earthquake shaking; for distant events occurring in Japan the tsunami will take ~9-10 hours to arrive. For the AKMax scenario, a tsunami warning will be issued by the U.S. Tsunami Warning Center[11] based out of Palmer, Alaska, as well as via channel 16 from the U.S. Coast Guard (USCG). In this scenario, maritime operators will have some time to respond. If vessels are already on the water, we advise operators to check with the USCG before taking any action. If offshore evacuation is advised by USCG, a maritime operator should consider the size of the vessel relative to the prevailing (and forecast) ocean conditions, and the vessel and operator's ability to remain offshore for a potentially extended period of time.

We recommend that vessels seaward of the MCB evacuate to depths greater than 46 m (25 fathoms), identified in **Figure 43** by the orange zone. This distant maritime evacuation zone depicts where the tsunami currents are expected to fall respectively below 2 m/s (4 knots - landward edge) and 1.5 m/s (3 knots - seaward edge). This region of lower currents is located ~2.5 nautical miles northwest of the mouth of Coos Bay (2.4 nautical miles north of the Cape Arago lighthouse). Dangerous currents (>2.6 m/s [5 knots]) are expected to occur at depths shallower than 15 fathoms in this scenario and especially within the MCB (**Figure 35**, *bottom*). If conditions do not permit offshore evacuation, maritime operators should dock their vessels and evacuate on foot out of the distant tsunami evacuation zone.

For vessels operating within the estuary, the model results indicate that large parts of the estuary would be affected by currents in the 3–6 knot range (**Figure 35**, *bottom*). Currents of this magnitude are likely to cause moderate to severe damage to facilities located adjacent to the Charleston harbor. For vessels moored in the harbor, currents of this magnitude could result in significant damage to the boats, including boats breaking their mooring lines, causing the boats to collide with other vessels. For large ships moored at the Port of Coos Bay and elsewhere in the estuary, ship operators may need to add additional mooring lines and/or drag anchors to help stabilize larger vessels. Evacuation upriver toward the Port of Coos Bay may be feasible for some smaller boats and vessels. However, this will depend on how long it takes the vessel to get underway (a conservative estimate is about 1 hour for large ships), the

[11] https://www.tsunami.gov/

availability of river pilots, and the speed at which the ship can travel. **Table 6** identifies the time and distance to safety for select areas in the Coos estuary. These times assume an average transit time of 6 knots and do not account for ocean or riverine conditions that could serve to slow travel times. For example, the distance from Charleston to Coos Bay (where tsunami currents fall below 4 knots) is 11 nautical miles (**Table 6**). For a vessel traveling at 6 knots, this equals ~1 hour 50 minutes travel time. Offshore evacuation is not recommended for vessels moored at the Port of Coos Bay. This is because the distance to the distant tsunami staging area (ORANGE zone) and 15-fathom line offshore the MCB is 14 nautical miles, and a vessel traveling at 6 knots would take ~2 hours 20 minutes to reach areas of expected low currents, providing little buffer between leaving the estuary and the arrival of the tsunami. The latter also assumes that conditions at the MCB are manageable for vessels trying to move out through the mouth into the Pacific Ocean.

Our modeling indicates that the worst conditions generated by the AKMax distant tsunami occur at Charleston, and in the channel between Barview and Jordon Point. Conversely, upriver of the Jordon Point, the height of the tsunami waves decreases to ~1.4 m (~4.6 ft), while the expected maximum tsunami currents are mostly below the 3-knot threshold, with some discrete peaks reaching 4 knots (**Figure 36** and **Figure 37**). Thus, for ships moored upriver of RM12, we recommend that the vessel operators deploy additional drag anchors to further safeguard their vessels.

Table 6. Maritime evacuation times to nearest offshore (where currents fall below 4 knots) and upriver staging destinations for a *DISTANT* tsunami. Evacuation times assume an average vessel speed of 6 knots.

Location	Distance to Offshore Safety (km / NM)	Time to Safety (min)	Distance to Upriver Safety (km / NM)	Time to Safety (min)
Charleston	7.6 / 4.1	40 min	20.4 / 11	1 hour 50 min
Lower Jarvis Range	13.2 / 7.1	1 hour 11 min	12.6 / 6.8	1 hour 8 min
Jordon Point	17.2 / 9.3	1 hour 33 min	8.3 / 4.5	45 min
Port of Coos Bay	26 / 14	2 hours 20 min	NA	NA

km = kilometers. NM = nautical miles.

8.0 CONCLUSIONS

Over the past 160 years, 29 distant (far-field) earthquake events have produced transoceanic tsunamis that struck the Oregon coast (Lander and others, 1993; NGDC, 2017). The majority of these have resulted in negligible effects in ports and harbors located on the Oregon coast. Of these, the largest event was the 1964 Alaska tsunami, which generated water levels that ranged from ~2.5 to 3.7 m (8 to 12 ft) (Schatz and others, 1964; Zhang and others, 2011) with higher wave heights at the open coast. At Coos Bay, the Alaska 1964 event produced estimated runup levels that reached 2.1 m (6.9 ft) near Empire. The most recent tsunami is the March 11, 2011, event that resulted in significant damage to several ports and harbors (e.g., Depoe Bay, Coos Bay, and at Brookings), as well as to recreational and commercial vessels attempting to escape the tsunami (Allan and others, 2018). Accordingly, even modest distant tsunamis like the one in 2011 pose a significant risk within the ports and harbors of Oregon, as well as to the safety of commercial and recreational mariners that operate offshore the coast.

To address the issue of maritime tsunami preparation and safety on the northern Oregon coast, this study has evaluated an entirely new suite of tsunami modeling results completed for both distant and local Cascadia tsunamis for the Coos estuary. The goal of this effort has been to examine the interaction of tsunamis with dynamic tides, different riverine flow regimes, and friction in order to provide an improved understanding of tsunami effects offshore the mouth of Coos Bay and within the estuary. These data are necessary for developing improved maritime guidance for this region. Modeling involved some 19 simulations based around two distant earthquake scenarios: the 1964 Anchorage, Alaska (AK64) event and a maximum considered eastern Aleutian Island (AKMax) earthquake, and two local CSZ scenarios: Large1 (L1) and Extra-extra-large1 (XXL1).

Although the 1964 Alaska event was used to quality control our modeling, results from this event also provide an excellent reference for the effects of the most extreme distant event to strike the northern Oregon coast in the past 160 years; as a result, the Alaska event remains an important benchmark when developing maritime guidance. Thus, for the 1964 scenario (coinciding with a spring flood tide) the modeled maximum tsunami water levels reached 2 m [7 ft] along the open coast (**Figure 8**), while the water levels within the estuary reached ~1.3 m (4.3 ft) at Barview, within the Charleston harbor, and in the vicinity of Empire; near the Coos airport, localized runup levels peaked at ~1.8 m (5.9 ft). However, for much of the navigation channel between the MCB and Pony Point, water levels remained ~1 m (3 ft). Upriver from Pony Point, water levels were ~0.6 m (2 ft), including ship-mooring sites near the Port of Coos Bay. Accordingly, upriver from about Pony Point, the tsunami waves rapidly decrease in height, becoming negligible up Isthmus Slough and east of Eastside. Strongest currents (>6 knots) are observed at the MCB near RM1. Strong currents (3–6 knots) are also observed along the navigation channel downstream of Jordon Point. Elsewhere in the estuary the tsunami current velocities are generally below the 3-knot threshold (**Figure 9**); damage to ports and harbors tends to occur above this threshold.

For the AKMax scenario, our analyses indicate that the initial wave arrival at the MCB occurs ~4 hours after the start of the earthquake (**Figure 24**). From the mouth of Coos Bay the tsunami takes an additional 13 minutes to reach its maxima inundating the community of Barview; 15 minutes to reach Empire; 27 minutes to reach Jordon Point; and ~41 minutes to reach the town of Coos Bay; total travel time to the town of Coos Bay is 4 hours 41 minutes. The tsunami is detectable well beyond the juncture between the Millicoma River and Coos River south fork, although the amount of energy in the tsunami is effectively negligible at this stage.

The simulations demonstrated significant along-coast and in-water variability in maximum tsunami water levels and currents (**Figure 35**), a function of localized bathymetric effects, as well as interactions

with tidal and riverine hydraulics. From a maritime standpoint, the most dangerous conditions will be observed at the MCB, and in the estuary channel between Charleston and Jordon Point (**Figure 35**). Strong currents exceeding 9 knots will dominate the lower estuary downstream of Jordon Point, and ~1.7 miles seaward of the MCB (**Figure 35**, *bottom*). ***For vessels seaward of the MCB, we recommend vessels proceed to a staging area greater than 46 m (25 fathoms/150 ft) (orange zone, Figure 43, located ~2.5 nautical miles northwest of the mouth of Coos Bay [2.4 nautical miles north of the Cape Arago lighthouse]). In this scenario, dangerous currents (> 2.6 m/s [5 knots]) are expected to occur at depths shallower than 27 m (15 fathoms/90 ft)***.

For vessels operating within the Coos estuary, several options are available to maritime operators in the event of a distant tsunami. Offshore maritime evacuation may be feasible for some vessels operating out of Charleston harbor, or in the navigation channel downstream of Jordon Point (**Table 6**). Conversely, smaller vessels upriver of Jordon Point may choose to evacuate farther upriver; seaward evacuation for vessels in the vicinity of Coos Bay is not advised because those vessels might be transiting the mouth at the time when a tsunami arrives. Operators of large ships moored between Jordon Point and Coos Bay could deploy additional drag anchors or mooring ropes to further safeguard their vessels.

In a real distant tsunami event, local officials will have time to work with the National Oceanic and Atmospheric Administration, U.S. Coast Guard, and Oregon Emergency Management to provide guidance tailored to the size of the expected tsunami. Mariners should follow that guidance, if possible.

A locally generated CSZ event will reach the MCB in as little as 7 minutes (**Figure 21**), and will take an additional 18 minutes to reach Jordon Point; the XXL1 local tsunami arrives at Coos Bay ~39 minutes after the start of earthquake shaking. Tsunami water levels and currents along the open coast and offshore the MCB will be catastrophic. Maximum water levels exceeding 17 m (56 ft) at the MCB, and 10 to 13 m (~33 to 43 ft) in the navigation channel downstream of Jordon Point will be observed. Upriver of Jordon Point, the tsunami energy is dispersed across a broad valley and becomes strongly influenced by the shallowing estuary as well as small islands. Maximum tsunami water levels upriver of Jordon Point are generally in the range of 2 to 4 m (7 to 10 ft) (MHHW) depending on the tidal stage (**Figure 27** and **Figure 28**), with localized maxima of up to 6 m (24 ft) in a few areas where the tsunami wave is focused. Extreme currents exceeding 6.1 m/s [12 knots] will be observed across the entire estuary (**Figure 30** and **Figure 31**). These currents will be enhanced during ebb tide conditions (**Figure 15**), which could contribute toward localized amplification of tsunami waves at the MCB. Damage to ports and harbors in this scenario will probably be devastating for all ports in the lower estuary.

Because the tsunamis arrive at the MCB in ~ 7 minutes, there is insufficient time for mariners moored in ports and harbors within Coos Bay or along the navigation channel to respond to this event other than to evacuate by foot to high ground. Thus, maritime evacuation planning for a locally generated tsunami is largely limited to those vessels operating out on the open ocean. For these vessels west of the MCB, the most effective strategy is to immediately evacuate toward deeper water and, accordingly, toward decreasing tsunami-generated currents. ***We recommend a Coos Bay maritime evacuation zone for a local tsunami hazard zone beginning at ~146 m depth (~80 fathoms, pale shaded region in Figure 43) and extends westward to depths > 274 m (150 fathoms, bright yellow region in Figure 43).*** Thus, increasing safety occurs with additional westward travel because tsunami generated currents will continue to decrease with increasing water depth. The preferred staging area is in depths greater than 100 fathoms (600 ft) located 13.4 nautical miles west of the mouth of Coos Bay. Under these circumstances, mariners should prepare to remain offshore for potentially days as the MCB is unlikely to be navigable. Hence, vessel operators should develop plans to evacuate to potentially safe ports located to the south of Cape Mendocino on the California coast.

For vessels caught in the Coos estuary, the options are limited. Given the range of wave arrival times associated with a local tsunami, the best course of action is to head vessels toward the nearest point of high ground and evacuate uphill out of the tsunami inundation zone.

Simulations undertaken as part of this study using dynamic tides and varying river flows have yielded some useful insights, when compared with static models undertaken at MHHW and with no flows. These include:

- The predicted maximum velocities exhibit more local extrema along the coast and within the estuary, especially near the mouth where the interaction is found to be strongest due to powerful currents and shoaling of tsunami waves (**Figure 15** to **Figure 17**);
- The conventional wisdom is that tsunamis arriving with a flood spring tide are usually more damaging. This is generally true in the deep channel downstream of Jordon Point. However, the situation becomes very complex in the shallow waters of the upper estuary, where tsunamis arriving at ebb and flood slack were found to contain considerably energy (**Figure 17** and **Figure 16**);
- The violent collision between tidal and tsunami currents at the MCB makes the ebb scenarios especially dangerous for ships of all sizes (**Figure 17**). Our modeling confirms that tsunami arrival during an ebb phase produces considerably stronger currents when compared with the flood scenario (**Figure 18** and **Figure 19**);
- Conditions generated under the high river flow scenario indicate even stronger currents at the MCB (**Figure 20**);
- Under ebb tide conditions, our simulations demonstrate that a distant (AKMax) tsunami response is strongly affected by the outgoing tidal currents, such that the largest tsunami waves and currents are confined entirely to the MCB and in the immediate channel west of Barview. Upriver of Barview, the effects of a distant tsunami become negligible under ebb tide conditions.
- Simulations that compare the existing channel configuration (Run05a-L1) with a proposed deeper channel (Run05c-L1) indicate nominal impact on estuary hydrodynamics. Impacts were largely confined to two areas: adjacent to the Coos airport and the MCB. Elsewhere the effects are negligible. Of the two identified areas, the largest changes (slightly increased current velocities) are observed at the MCB, where the deeper channel configuration appears to enhance offshore directed currents. This is probably caused by the increased volume associated with the modified estuary channel, allowing more water to penetrate the estuary, with accompanying stronger tsunami drawdown.

9.0 ACKNOWLEDGMENTS

This project was funded under award NA18NWS4670076 by the National Oceanic and Atmospheric Administration (NOAA) through the National Tsunami Hazard Mitigation Program. We thank Richard Dybevik (Chair of the Coos Bay Harbor Safety Committee), Mike Dunning (Director of Maritime Operations, Oregon International Port of Coos Bay), Rick Wilson from the California Geological Survey, and Robert Houston from the Oregon Department of Geology and Mineral Industries for their insightful report reviews and comments. Simulations used in this paper were conducted using the following computational facilities: 1) SciClone at the College of William and Mary, which was provided with assistance from the National Science Foundation, the Virginia Port Authority, Virginia's Commonwealth Technology Research Fund, and the Office of Naval Research; 2) the Extreme Science and Engineering Discovery Environment (XSEDE; grant TG-OCE130032), which is supported by National Science Foundation grant number OCI-1053575; and 3) NASA's Pleiades supercomputer.

10.0 REFERENCES

Allan, J. C., 2020, Maritime guidance for distant source tsunami events: Coos Bay, Coos County, Oregon: Oregon Department of Geology and Mineral Industries Oregon Maritime Tsunami Response Guidance (MTRG) No. 2020-OR-01, 25 p. https://www.oregongeology.org/pubs/mtrg/MTRG-20120-OR-01_Coos-Bay.pdf

Allan, J. C., Komar, P. D., Ruggiero, P., and Witter, R. C., 2012, The March 2011 Tōhoku tsunami and its impacts along the U.S. West Coast: Journal of Coastal Research, v. 28, no. 5, p. 1142–1153. https://doi.org/10.2112/JCOASTRES-D-11-00115.1

Allan, J. C., Priest, G. R., Zhang, Y. J., and Gabel, L. L., 2018, Maritime tsunami evacuation guidelines for the Pacific Northwest coast of Oregon: Natural Hazards, v. 94, no. 1, p. 21–52. https://doi.org/10.1007/s11069-018-3372-2

Atwater, B. F., and others, 1995, Summary of coastal geologic evidence for past great earthquakes at the Cascadia subduction zone: Earthquake Spectra, v. 11, no. 1, p. 1–18. https://doi.org/10.1193/1.1585800

Atwater, B. F., Satoko, M.-R., Satake, K., Yoshinobu, T., Kazue, U., and Yamaguchi, D. K., 2005, The orphan tsunami of 1700—Japanese clues to a parent earthquake in North America: U.S. Geological Survey Professional Paper 1707, 144 p. https://doi.org/10.3133/pp1707

Borrero, J. C., Lynett, P. J., and Kalligeris, N., 2015, Tsunami currents in ports: Philosophical Transactions of the Royal Society A, v. 373, no. 2053, p. 20140372. https://doi.org/10.1098/rsta.2014.0372

Bunya, S., and others, 2010, A high-resolution coupled riverine flow, tide, wind, wind wave, and storm surge model for southern Louisiana and Mississippi. Part I: Model development and validation: Monthly Weather Review, v. 138, no. 2, p. 345–377. https://doi.org/10.1175/2009MWR2906.1

Burla, M., Baptista, A. M., Zhang, Y., and Frolov, S., 2010, Seasonal and interannual variability of the Columbia River plume: a perspective enabled by multiyear simulation databases: Journal of Geophysical Research: Oceans, v. 115, no. C2. https://doi.org/10.1029/2008JC004964

Conroy, T., Sutherland, D. A., and Ralston, D. K., 2020, Estuarine exchange flow variability in a seasonal, segmented estuary. Journal of Physical Oceanography, v. 50, no. 3, 595–613. https://doi.org/10.1175/JPO-D-19-0108.1

Eidam, E. F., Sutherland, D. A., Ralston, D. K., Dye, B., Conroy, T., Schmitt, J., Ruggiero, P., and Wood, J., 2020, Impacts of 150 Years of Shoreline and Bathymetric Change in the Coos Estuary, Oregon, USA. Estuaries and Coasts: 1-19. https://doi.org/10.1007/s12237-020-00732-1

Goldfinger, C., Nelson, C. H., and Johnson, J. G., 2003, Holocene earthquake records from the Cascadia Subduction Zone and Northern San Andreas fault based on precise dating of offshore turbidites: Annual Review of Earth and Planetary Sciences, v. 31, p. 555–577. https://doi.org/10.1146/annurev.earth.31.100901.141246

Goldfinger, C., and others, 2012, Turbidite event history: methods and implications for Holocene paleoseismicity of the Cascadia subduction zone: U.S. Geological Survey Professional Paper 1661-F, 170 p. https://pubs.usgs.gov/pp/pp1661f/

Goldfinger, C., Galer, S., Beeson, J., Hamilton, T., Black, B., Romsos, C., Patton, J., Nelson, C. H., Hausmann, R., and Morey, A., 2017, The importance of site selection, sediment supply, and hydrodynamics: A case study of submarine paleoseismology on the northern Cascadia margin, Washington USA: Marine Geology, v. 384, p. 4–16, 17, 25–46. https://doi.org/10.1016/j.margeo.2016.06.008

González, F., Geist, E. L., Jaffe, B., Kânoğlu, U., Mofjeld, H., Synolakis, C., Titov, V. V., Arcas, D., Bellomo, D., and Carlton, D., 2009, Probabilistic tsunami hazard assessment at Seaside, Oregon, for near-and far-field seismic sources: Journal of Geophysical Research: Oceans, v. 114, no. C11. https://doi.org/10.1029/2008JC005132

Hickey, B. M. and Banas, N. S., 2003. Oceanography of the US Pacific Northwest coastal ocean and estuaries with application to coastal ecology. Estuaries, v. 26, no. 4, 1010–1031. https://doi.org/10.1007/BF02803360

Homer, C. G., Dewitz, J. A., Yang, L., Jin, S., Danielson, P., Xian, G., Coulston, J., Herold, N. D., Wickham, J. D., and Megown, K., 2015, Completion of the 2011 National Land Cover Database for the conterminous United States—representing a decade of land cover change information: Photogrammetric Engineering and Remote Sensing, v. 81, no. 5, p. 345–354.

Hyde, N., 2007. Towards National Estuarine Modeling and Characterization/classification Systems: A Pilot Study for Coos Bay, OGI School of Science & Engineering at OHSU.

Hyndman, R. D., and Wang, K., 1995, The rupture zone of Cascadia great earthquakes from current deformation and the thermal regime: Journal of Geophysical Research, v. 100, no. B11, p. 22,133–22,154. https://doi.org/10.1029/95JB01970

Johnson, J., Satake, K., Holdahl, S. R., and Sauber, J., 1996, The 1964 Prince William Sound earthquake: joint inversion of tsunami and geodetic data: Journal of Geophysical Research, v. 101, no. B1, p. 523–532. https://doi.org/10.1029/95JB02806

Kelsey, H. M., Nelson, A. R., Hemphill-Haley, E., and Witter, R. C., 2005, Tsunami history of an Oregon coastal lake reveals a 4600 yr record of great earthquakes on the Cascadia subduction zone: Geological Society of America Bulletin, v. 117, no. 7/8, p. 1009–1032. https://doi.org/10.1130/B25452.1

Lander, J. F., Lockridge, P. A., and Kozuch, M. J., 1993, Tsunamis affecting the west coast of the United States, 1806–1992: National Oceanic and Atmospheric Administration, National Geophysical Data Center key to geophysical Records Documentation (KGRD) No. 29, 242 p. ftp://ftp.library.noaa.gov/noaa_documents.lib/NESDIS/NGDC/key_to_geophysical_records_documentation/Kgrd-29.pdf

Lynett, P. J., Borrero, J., Son, S., Wilson, R., and Miller, K., 2014, Assessment of the tsunami-induced current hazard: Geophysical Research Letters, v. 41, no. 6, p. 2048–2055. https://doi.org/10.1002/2013GL058680

Lynett, P. J., and others, 2017, Inter-model analysis of tsunami-induced coastal currents: Ocean Modelling, v. 114, p. 14–32. https://doi.org/10.1016/j.ocemod.2017.04.003

McCaffrey, R., Qamar, A., King, R. W., Wells, R. W., Khazaradze, G., Williams, C., Stevens, C., Vollick, J. J., and Zwick, P. C., 2007, Fault locking, block rotation and crustal deformation in the Pacific Northwest: Geophys. J. Int., v. 169, p. 1315–1340.

McCrory, P. A., Blair, J. L., Oppenheimer, D. H., and Walter, S. R., 2004, Depth to the Juan de Fuca slab beneath the Cascadia subduction margin—a 3-D model for sorting earthquakes: U.S. Geological Survey Data Series DS-91. https://pubs.usgs.gov/ds/91

Mitchell, C. E.., Vincent, P., Weldon, R. J., II, and Richards, M. A., 1994, Present-day vertical deformation of the Cascadia margin, Pacific Northwest, United States: Journal of Geophysical Research: Solid Earth, v. 99, no. B6, p. 12,257–12,277. https://doi.org/10.1029/94JB00279

Mori, N., and Takahashi, T., 2012, Nationwide post event survey and analysis of the 2011 Tohoku earthquake tsunami: Coastal Engineering Journal, v. 54, no. 1, 1250001-1–1250001-27. https://doi.org/10.1142/S0578563412500015

Mori, N., Takahashi, T., Yasuda, T., and Yanagisawa, H., 2011, Survey of 2011 Tohoku earthquake tsunami inundation and run-up: Geophysical Research Letters, v. 38, no. 7. https://doi.org/10.1029/2011GL049210

National Geophysical Data Center/World Data Service (NGDC), 2017, NCEI/WDS Global Historical Tsunami Database. NOAA National Centers for Environmental Information. https://doi.org/10.7289/v5pn93h7 [accessed June 2017]

Nelson, A. R., Kelsey, H. M., and Witter, R. C., 2006, Great earthquakes of variable magnitude at the Cascadia subduction zone: Quaternary Research, v. 65, no. 3, p. 354–365. https://doi.org/10.1016/j.yqres.2006.02.009

NTHMP, 2017, Guidance for safe minimum offshore depth for vessel movement for tsunamis: National Tsunami Hazard Mitigation Program. https://nws.weather.gov/nthmp/documents/GuidanceforSafeMinimumOffshoreDepthforVesselMovement.pdf. Accessed July 10, 2017.

Oregon Department of Geology and Mineral Industries (DOGAMI), 2014, Tsunami! What Oregon boat owners need to know. https://www.oregongeology.org/pubs/tsubrochures/TsunamiBrochureMaritime.pdf, 2 p. Accessed August 5, 2017.

Oregon International Port of Coos Bay, 2019, Coos Bay channel modification fact sheet: Ways and Means Subcommittee on Capital Construction, Exhibit 6, HB 5030 Lottery Bond - April 19, 2019, Testimony - Port of Coos Bay, RE: HB 5030, Funding for the Coos Bay Channel Modification Project, p. 8. https://olis.oregonlegislature.gov/liz/2019R1/Downloads/CommitteeMeetingDocument/194475

Priest, G. R., Goldfinger, C., Wang, K., Witter, R. C., Zhang, Y., and Baptista, A. M., 2009, Tsunami hazard assessment of the northern Oregon coast: A multi-deterministic approach tested at Cannon Beach, Clatsop County, Oregon: Oregon Department of Geology and Mineral Industries Special Paper 41. https://www.oregongeology.org/pubs/sp/SP-41.zip

Priest, G. R., Goldfinger, C., Wang, K., Witter, R. C., Zhang, Y., and Baptista, A. M., 2010, Confidence levels for tsunami-inundation limits in northern Oregon inferred from a 10,000-year history of great earthquakes at the Cascadia subduction zone: Natural Hazards, v. 54, no. 1, p. 27–73. https://doi.org/10.1007/s11069-009-9453-5

Priest, G. R., Witter, R. C., Zhang, Y. J., Wang, K., Goldfinger, C., Stimely, L. L., English, J. T., Pickner, S. G., Hughes, K. L. B., Willie, T. E., and Smith, R. L., 2013, Tsunami inundation scenarios for Oregon: Oregon Department of Geology and Mineral Industries Open-File Report O-13-19. https://www.oregongeology.org/pubs/ofr/p-O-13-19.htm

Ruggiero, P., Eshleman, J. L., Kingsley, E., Thompson, D. M., Voigt, B., Kaminsky, G. M., Gelfenbaum, G., 2000, Beach morphology monitoring in the Columbia River Littoral Cell: 1997–2005: U.S. Geological Survey Data Series 260. https://doi.org/10.3133/ds260

Satake, K., Wang, K., and Atwater, B. F., 2003, Fault slip and seismic moment of the 1700 Cascadia earthquake inferred from Japanese tsunami descriptions: Journal of Geophysical Research, v. 108, no. B11. https://doi.org/10.1029/2003JB002521

Schatz, C. E., Curl, H., and Burt, W. V., 1964, Tsunamis on the Oregon coast: Ore Bin, v. 26, no. 12, p. 231–232. https://www.oregongeology.org/pubs/og/OBv26n12.pdf

Suppasri, A., Shuto, N., Imamura, F., Koshimura, S., Mas, E., and Yalciner, A. C., 2013, Lessons learned from the 2011 Great East Japan tsunami: performance of tsunami countermeasures, coastal buildings, and tsunami evacuation in Japan: Pure and Applied Geophysics, v. 170, no. 6–8, p. 993–1018. https://doi.org/10.1007/s00024-012-0511-7

Suppasri, A., Nguyen, D., Abe, Y., Yasuda, M., Fukutani, Y., Imamura, F., and Shuto, N., 2015, Offshore evacuation of fishing boats—Lessons from the 2011 great east Japan tsunami and its future challenge: Tsunami Engineering Technical Report, 32, p. 33–45.

Torrence, C., and Compo, G. P., 1998, A practical guide to wavelet analysis: Bulletin of the American Meteorological society, v. 79, no. 1, p. 61–78. https://doi.org/10.1175/1520-0477(1998)079<0061:APGTWA>2.0.CO;2

Tsunami Pilot Study Working Group (TPSWG), 2006, Seaside, Oregon tsunami pilot study—modernization of FEMA flood hazard maps: Seattle, Wash., U.S. National Oceanic and Atmospheric Administration, Office of Oceanic and Atmospheric Research, Pacific Marine Environmental Laboratory, NOAA OAR special report (Contribution No. 2975), 94 p., 7 appendices. https://www.pmel.noaa.gov/pubs/PDF/tsun2975/tsun2975.pdf

U.S. Army Corps of Engineers (USACE), 2008, HEC-RAS River Analysis System, hydraulic reference manual, v. 4.0, March 2008: Davis, Calif., USACE Hydraulic Engineering Center, Computer Program Documentation CPD-69.

Uslu, B., Eble, M., Titov, V. V., and Bernard, E. N., 2010, Distant tsunami threats to the ports of Los Angeles and Long Beach, California; Tsunami Hazard Assessment Special Series, v. 2: National Oceanic and Atmospheric Administration, Office of Oceanic and Atmospheric Research (OAR) Special Report, 100 p. https://nctr.pmel.noaa.gov/hazard_assessment_reports/02_LA_LB_CA_3532_web.pdf

Wilson, B. W., and Torum, A., 1968, The tsunami of the Alaskan earthquake, 1964: Engineering Evaluation: U.S. Army Corps of Engineers, Coastal Engineering Research Center, Technical Memorandum No. 25.

Wilson, R. I., Admire, A. R., Borrero, J. C., Dengler, L. A., Legg, M. R., Lynett, P., McCrink, T. P., Miller, K. M., Ritchie, A., Sterling, K., and Whitmore, P. M., 2013, Observations and impacts from the 2010 Chilean and 2011 Japanese tsunamis in California (USA): Pure and Applied Geophysics, v. 170, no. 6–8, p. 1127–1147. https://doi.org/10.1007/s00024-012-0527-z

Wiśniewski, B., and Wolski, T., 2012, The safety of the shipping and ports in the aspect of the tsunami events: Maritime University of Szczecin Scientific Journals [Zeszyty Naukowe/Akademia Morska w Szczecinie], v. 30, no. 102, p. 150–157.

Witter, R. C., 2008, Prehistoric Cascadia tsunami inundation and runup at Cannon Beach, Clatsop County, Oregon: Oregon Department of Geology and Mineral Industries Open-File Report O-08-12, 36 p., 3 appendices. https://www.oregongeology.org/pubs/ofr/O-08-12.zip

Witter, R. C., Kelsey, H. M., and Hemphill-Haley, E., 2003, Great Cascadia earthquakes and tsunamis of the past 6700 years, Coquille River estuary, southern coastal Oregon: Geological Society of America Bulletin, v. 115, no. 10, p. 1289–1306. https://doi.org/10.1130/B25189.1

Witter, R. C., Zhang, Y., Goldfinger, C., Priest, G. R., and Wang, K., 2010, Validating numerical tsunami simulations in southern Oregon using late Holocene records of great Cascadia earthquakes and tsunamis [abs.], Seismological Society of America 2010 Annual Meeting, Portland, Oreg.: Seismological Research Letters. v. 81, no. 2, p. 290. https://doi.org/10.1785/gssrl.81.2.284

Witter, R. C., Zhang, Y., Wang, K., Priest, G. R., Goldfinger, C., Stimely, L. L., English, J. T., and Ferro, P. A., 2011, Simulating tsunami inundation at Bandon, Coos County, Oregon, using hypothetical Cascadia and Alaska earthquake scenarios: Oregon Department of Geology and Mineral Industries Special Paper 43, 57 p. https://www.oregongeology.org/pubs/sp/p-SP-43.htm

Witter, R. C., Zhang, Y., Wang, K., Goldfinger, C., Priest, G. R., and Allan, J. C., 2012, Coseismic slip on the southern Cascadia megathrust implied by tsunami deposits in an Oregon lake and earthquake-triggered marine turbidites: Journal of Geophysical Research; Solid Earth, v. 117, no. B10. https://doi.org/10.1029/2012JB009404

Witter, R., Zhang, Y. J., Wang, K., Priest, G. R., Goldfinger, C., Stimely, L. L., English, J. T., and Ferro, P. A., 2013, Simulated tsunami inundation for a range of Cascadia megathrust earthquake scenarios at Bandon, Oregon, USA: Geosphere, v. 9, no. 6, p. 1783–1803. https://doi.org/10.1130/GES00899.1

Zhang, Y. J., and Baptista, A. M., 2008, SELFE: A semi-implicit Eulerian-Lagrangian finite-element model for cross-scale ocean circulation: Ocean Modelling, v. 21, no. 3-4, p. 71–96. https://doi.org/10.1016/j.ocemod.2007.11.005

Zhang, Y. J., Witter, R. C., and Priest, G. R., 2011, Tsunami–tide interaction in 1964 Prince William Sound tsunami: Ocean Modelling, v. 40, p. 246–259. https://doi.org/10.1016/j.ocemod.2011.09.005

Zhang, Y. J., Stanev, E. V., and Grashorn, S., 2016a, Seamless cross-scale modelling with SCHISM: Ocean Modelling, v. 102, p. 64–81. https://doi.org/10.1016/j.ocemod.2016.05.002

Zhang, Y. J., Priest, G. R., Allan, J. C., and Gabel, L., 2016b, Benchmarking an unstructured-grid model for tsunami current modeling: Pure and Applied Geophysics, v. 173, no. 12, p. 4075–4087. https://doi.org/10.1007/s00024-016-1328-6